Electrocatalytic reduction of CO2 and nitrate on immobilized metal porphyrins

Shen, Jing

Electrocatalytic reduction of CO_2 and nitrate on immobilized metal porphyrins

Proefschrift

ter verkrijging van

de graad van Doctor aan de Universiteit Leiden,

op gezag van Rector Magnificus Prof. Mr. C. J. J. M. Stolker,

volgens besluit van het College voor Promoties

te verdedigen op woensdag 9 december 2015

klokke 08.45 uur

door

Jing Shen

geboren te Hunan in 1984

Promotiecommissie:

Promotor:	Prof. Dr. M.T.M. Koper
Co-promotor:	Dr. D. G.H. Hetterscheid
Overige Leden:	Prof. Dr. J. Brouwer (Leiden University)
	Prof. Dr. E. Bouwman (Leiden University)
	Prof. Dr. B. de Bruin (University of Amsterdam)
	Prof. Dr. B. Dam (Delft University of Technology)

A fellowship from the Chinese Scholarship Council (Grant No.2011634090) is kindly acknowledged.

ISBN 978-94-6299-240-5

Printed by: Ridderprint BV, the Netherlands

Table of Contents

Chapter 1

Introduction

1.1. Electrochemical reduction of CO_2

The carbon cycle, along with nitrogen cycle and oxygen (water) cycle, comprises a sequence of events that are key to making the earth capable of sustaining life. However, human activities are altering the carbon cycle by adding more CO_2 to the atmosphere and influencing the ability of natural sinks, like forests and oceans, to remove CO_2 from the atmosphere, which will eventually jeopardize the living environment of humans. The main emission of CO_2 is from the combustion of fossil energy (coal, natural gas and oil) for energy and transportation. Since the industrial revolution, human related CO_2 emission has increased significantly, which is claimed to be one of the major contributors to the green-house effect and will result in a serious global warming issue[1, 2]. As an abundant and problematic source in the atmosphere, we aspire to utilize CO_2. Mimicking natural photosynthesis, we would like to reduce CO_2 to valuable products using renewable energy, like sunlight and wind. Among different kinds of methods, the electrochemical reduction of CO_2 is a promising approach to achieve this goal. CO_2 is a very stable molecule, and its electrochemical reduction generally requires high overpotentials. On the other hand, the hydrogen evolution reaction (HER) is a competing reaction with the electrochemical reduction of CO_2, which leads to H_2 as a dominant product in many cases. In order to overcome these problems, different kinds of catalysts and solvents have been utilized. The equilibrium potential of the formation of each product is listed in Table 1[3].

Table 1: The equilibrium potentials for the formation for various product from the electrochemical reduction of CO_2.

Reactions	E^0 /V vs NHE
$CO_2 + 2H^+ + 2e^- \longrightarrow CO + H_2O$	-0.28
$CO_2 + 2H^+ + 2e^- \longrightarrow HCOOH$	-0.37
$CO_2 + 4H^+ 4e^- \longrightarrow HCHO + H_2O$	-0.24
$CO_2 + 6H^+ + 6e^- \longrightarrow CH_3OH + H_2O$	-0.14
$CO_2 + 8H^+ + 8e^- \longrightarrow CH_4 + 2H_2O$	0.04

As mentioned above, one of difficulties for the electrochemical reduction of CO_2 is the competition with the hydrogen evolution reaction. The hydrogen evolution reaction takes place close to its equilibrium potential of 0 V on many metal electrodes in aqueous electrolytes. Therefore, metal electrodes with high hydrogen overpotential have been utilized for the electrochemical reduction of CO_2 in early years, such as mercury and lead, to inhibit the hydrogen evolution reaction. Eyring and his coworkers showed that $HCOO^-$ is produced with 100% faradaic efficiency from the CO_2 reduction in neutral aqueous electrolyte on a Hg electrode[4]. Later, other metal electrodes have been investigated for the CO_2 electrochemical reduction. Sakata et al. studied the electrochemical reduction of CO_2 on 32 metal electrodes in low-temperature aqueous $KHCO_3$ media. A periodic table for CO_2 reduction based on the dependence of reduction products on various metals, suggests the existence of a systematic rule for the electrocatalytic reduction of CO_2 on metal surfaces[5]. Hori et al have made comprehensive investigations on the electrochemical reduction of CO_2 on all different kinds of metal electrodes in 0.5 M $KHCO_3$[6]. They found that the purity of the metal electrodes and electrolyte solution significantly affects the product selectivity. They also conducted full chemical analysis of products. Based on the product selectivity from their studies, the metal electrodes have been divided into four groups: (i) formate ion as the major product, such as on Pb, Hg, In, Sn, Cd, Tl and Bi electrodes; (ii) CO formed as the main product, such as on Au, Ag, Zn, Pd and Ga electrodes; (iii) Cu electrode produces CH_4, C_2H_4 and alcohols; (iv) hydrogen is the only

product on electrodes such as Ni, Fe, Pt and Ti. The results from Hori et al have been confirmed later by other researchers[7-11].

From Hori's studies Cu is an exceptional electrode, as it is the only metal producing hydrocarbons and alcohols in a measurable quantity. Therefore, the Cu electrode has attracted intensive studies not only to increase the activity but also to reveal the mechanism for the CO_2 reduction. Recently, Jaramillo et al. observed 16 different products from the CO_2 reduction on Cu electrode, which makes it challenging to propose a mechanism[12]. CO is a widely accepted key intermediate for the formation of hydrocarbons on Cu electrode from the reduction of CO_2[13]. Peterson et al. have studied 41different intermediates on the Cu (211) surface by density functional theory calculations and proposed possible pathways for the electrochemical reduction of CO_2[14]. The adsorbed formate (*OCHO) is an alternative intermediate for the formation of formic acid, which is responsible for the formic acid production at more negative potential (-0.61 V). They also concluded that the key step in the formation of CH_4 and C_2H_4 is the hydrogenation of adsorbed CO to form adsorbed *CHO. The subsequent hydrogenation of *CHO leads to the formation of $*H_2CO$ and $*H_3CO$, which will finally produce CH_4. The formation of ethylene requires of the creation of a C-C bond, which is a non-electrochemical step on the surface. Schouten et al. proposed a new reduction mechanism for CO_2 on Cu electrode[15]. The overall rate-determining step is the first electron transfer to form $CO_{2,ads}^{-}$[16]. $CO_{2,ads}^{-}$ will further react to give CO and formic acid. Formic acid is an dead-end product[16, 17]. CO is the intermediate for the formation of both CH_4 and C_2H_4. The rate-determining step for the formation of CH_4 is the breaking of the C-O bond in formyl intermediate (*CHO), while selectivity-determining step to C_1 and C_2 species is the formation of a CO dimer. Possible mechanistic pathways have been illustrated for the formation of C_1 and C_2 species on transition metals and molecular catalysts, as presented in Figure 1[18].

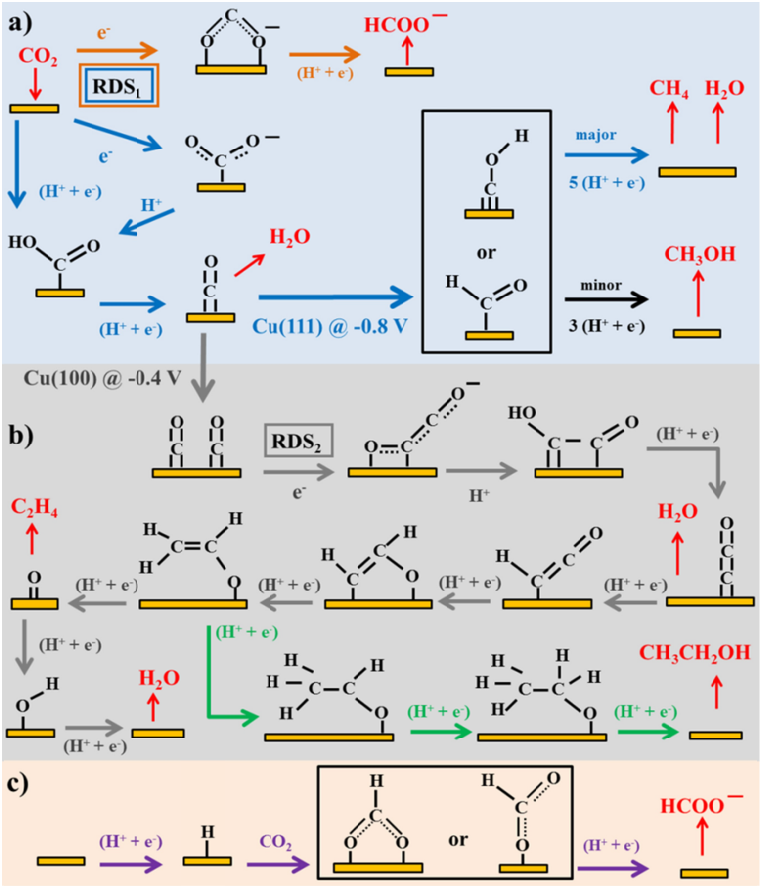

Figure 1. Possible reaction pathways for the electrocatalytic reduction of CO_2 to products on transition metals and molecular catalysts; a) pathways from CO_2 to CO, CH_4 (blue arrows), CH_3OH (black arrows), $HCOO^-$ (orange arrows); b) pathways from CO_2 to ethylene (grey arrows) and ethanol (green arrows); c) pathway of CO_2 insertion into a metal-H bond yielding formate (purple arrows). Species in black are adsorbates, while those in red are reactants or products in solution. Potentials are reported versus RHE, while RDS indicates rate determining steps and ($H^+ + e^-$) indicate steps in which either concerted or separated proton-electron transfer takes place. Reprinted from Ref.18.

Molecular electrocatalysts are the other promising class of catalysts for the electrochemical reduction of CO_2. Molecular catalysts are primarily utilized as homogeneous catalysts, but they are more applicable when mobilized on an inert electrode acting as heterogeneous catalyst. The 2-electron transfer product CO is produced on a

cobalt porphyrin modified electrode from the electrochemical reduction of CO_2, such as a $Co^{II}TPP$ (TPP= 5,10,15,20-tetraphenyl-21H, 23H-porphine) modified glass carbon electrode (with current efficiency of 92%)[19], and 5,10,15,20-tetrakis (4-methoxyphenyl) porphyrinato cobalt(II) (CoTMPP) modified nanoporous activated carbon fiber electrode (with current efficiency up to 70%)[20]. Formic acid is the other 2-electron transfer product formed on carbon-nanotubes supported iron-porphyrin (FeP) electrode[21] and a cobalt- and nickel-phthalocyanine (CoPc and NiPc) coated graphite electrode[22-24]. Sende et al. have found that up to 87% formaldehyde, which is a 4-electron transfer product, is produced on a $[Cr(4\text{-v-tpy})_2]^{2+}$ (v-tpy = vinyl-terpyridine) film, which is higher than that of Co and Fe complexes, which produce 39% and 28% , respectively[25].

In order to suppress the hydrogen evolution reaction and increase the concentration of CO_2 in the electrolyte, non-aqueous solvents have been utilized for the CO_2 electrochemical reduction. Various solvent have been used, such as acetonitrile (AN), dimethylformamide (DMF), dimethyl sulfoxide (DMSO) and propylene carbonate (PC). Ito and coworkers have investigated various metal electrodes for the electrolysis of CO_2 in PC with tetraethylammonium perchlorate (TEAP) as the electrolyte[26]. The water content was 300 ppm. Metal electrodes have been divided into three groups based on the products. Pb, Hg and Tl give oxalate ($C_2O_4^{2-}$) as the main product. With a small amount of water in the electrolyte, oxalic acid is partly reduced to glycolic acid and glyoxylic acid. CO is predominantly produced on Cu, Ag, Au, Zn, In, Sn, Ni and Pt from the reduction of CO_2. On Fe, Cr, Mo, Pd and Cd electrodes, $C_2O_4^{2-}$ and CO are formed in comparable amount. The Faradaic efficiencies of products on all the metal electrodes were also evaluated. Haynes and Sawyer find CO and formate as the main product on Au and Hg electrodes in DMSO from the reduction of CO_2[27]. Oxalic acid is exclusively formed on Hg electrode in DMF reported by Tyssee et al.[28]. Oxalic acid is the main product at Pb electrode in nonaqueous electrolytes. It can be further reduced to higher carboxylic acids, glyoxylic acid, glycolic acid etc.[29]. The reaction schemes of the CO_2 electrochemical reduction in H_2O-DMF solutions have been discussed by Savéant et al.[30]. The $CO_2^{\bullet-}$ radical was assumed as an intermediate.

1.2. Nitrate electrochemical reduction

The nitrogen cycle is one of the most important nutrient cycles in terrestrial ecosystems. Everything that lives needs nitrogen. It is required for the building of proteins, DNA and enzymes. It is also essential for bacteria to produce ATP and gain energy for cell growth. 70% of the atmosphere consists of nitrogen gas. However, it is not directly available for use. Nitrate ions (NO_3^-) and ammonium ions (NH_4^+) are the only forms that can be utilized by plants. When present in excess, nitrogen compounds may pose risks both to environment and human health. Nitrate is commonly used as fertilizer in agriculture. The overuse of fertilizer leads to the excess of nitrate in the soil, which will be leached into groundwater. High level of nitrate in drinking water can cause methemoglobinemia or blue baby syndrome, which is a disease especially found in infants. The maximum contaminant level of nitrate in drinking water has therefore been set at 10 mg/L[31].

The electrocatalytic reduction of nitrate is currently attracting much attention as one possible way to remove nitrate from ground- and waste-water. However, different kinds of products can be produced from the nitrate electrochemical reduction. The equilibrium potentials of the formation of various products are listed in Table 2[32].

Table 2: The equilibrium potentials for the formation of various products from the electrochemical reduction of nitrate.

Reactions	E^0 /V vs NHE
$NO_3^- + 2H^+ + 2e^- \longrightarrow NO_2^- + H_2O$	0.835
$NO_3^- + 4H^+ + 3e^- \longrightarrow NO(g) + 2H_2O$	0.958
$2NO_3^- + 10H^+ + 8e^- \longrightarrow N_2O(g) + 5H_2O$	1.116
$2NO_3^- + 12H^+ + 10e^- \longrightarrow N_2(g) + 6H_2O$	1.246
$NO_3^- + 8H^+ + 6e^- \longrightarrow NH_3OH^+ + 2H_2O$	0.727
$NO_3^- + 10H^+ + 8e^- \longrightarrow NH_4^+ + 3H_2O$	0.875

Platinum is the most studied electrode material for the nitrate reduction. The nitrate reduction on platinum follows a direct mechanistic pathway at moderate nitrate

concentration and acidity, while an indirect pathway applies to high nitrate concentrations (>1 M) and high acidity (pH < 0)[33]. The electrochemical reduction of nitrate on polycrystalline platinum at low nitrate concentration and low pH has been studied intensively[34-37]. The cyclic voltammetry of the electrochemical reduction of nitrate on a polycrystalline platinum electrode in sulfuric and perchloric acid illustrates that the reaction is strongly hindered by the presence of specifically adsorbing anions, such as sulfate, as well as other anions[35,36]. Investigations on the steady-state nitrate reduction in sulfuric acid show that the formation of adsorbed hydrogen (upd H) on the platinum surface inhibits the nitrate reduction[37,38]. Nitric oxide (NO) is found to be the main surface-bonded intermediate by FTIR measurements and stripping experiments[39]. Nakata et al. have argued that a chelating bidentate nitrate chemisorbs on the Pt surface instead of nitric oxide[40]. Ammonia is the only product from the nitrate reduction on polycrystalline platinum electrode according to rotating ring-disk and online electrochemical mass spectrometry measurements[41-43].

The nitrate reduction on single-crystal platinum electrode offers more detailed mechanistic insights. Pt (110) is the most active platinum surface for the nitrate reduction in perchloric acid, while Pt (111) is more active than Pt (110) in sulfuric acid. Dima et al. have argued that the structure-sensitivity of the nitrate reduction on platinum single-crystal is due to the sensitivity of the adsorption of other species, such as hydrogen and anions[44]. NO is found to accumulate at step sites of Pt (554) and Pt (553) electrode[44]. Taguchi and Feliu presented a detailed study on the influence of step density on nitrate reduction on single-crystal platinum. They found that the electrocatalytic activity for nitrate reduction is non-linear with the step density[45]. Based on the Tafel slopes, the conversion of nitrate to nitrite is considered to be the most difficult step. NO is considered to be the important intermediate, which is produced after nitrite formation.

Vijh was the first one to compare the activity of different metals for the nitrate electrochemical reduction. He found that metals with high overpotential for the nitrate reduction also tend to have a high overpotential for the hydrogen evolution reaction[46]. Dima et al. investigated the activity of various transition-metal electrodes (Pt, Pd, Rh, Ru and Ir)

and coinage-metal electrodes (Cu, Ag and Au) toward the reduction of nitrate in acid solution[41]. The activity of transition-metal electrodes follows the order of Rh>Ru>Ir>Pt>Pd in sulfuric acid. The main products formed on a rhodium electrode are ammonia and nitrite. Among the coinage-metal electrodes, Cu is the most active one, followed by silver and gold. Pletcher and Poorabedi found that ammonia is the main product on copper electrode. NO is also found as a product on Cu electrodes[41]. "Poor metals" were also investigated for the reduction of nitrate in acid media, such as mercury[47], indium[48], cadmium[49] and tin[50,51]. The high overpotential for the nitrate reduction on these metal electrodes is in agreement with the assertion of Vijh. The mechanism of the nitrate and nitrite reduction on noble-metal electrodes has been summarized by Duca et al. as shown in Figure 2.[52]

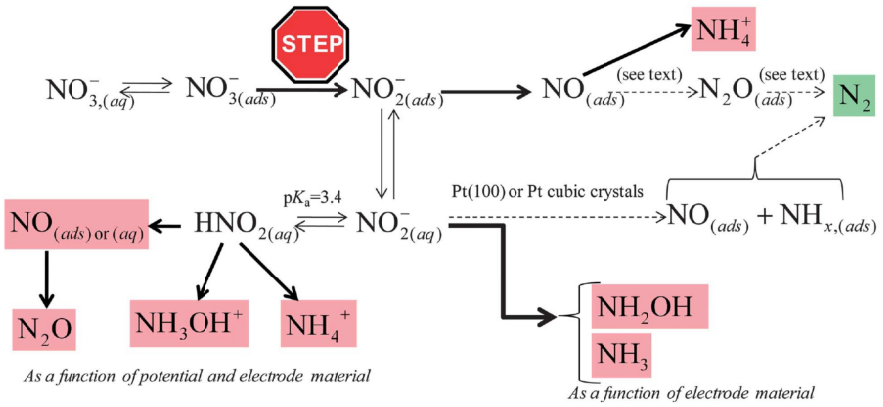

Figure 2. The major reaction pathways for nitrate and nitrite reduction on noble-metal electrodes. The ideal product, N_2, is highlighted in green, other products in red. The cartoon of the "STEP" sign highlights the rate-determining step. Thick lines emphasize those pathways that occur most often, where broken lines indicate reactions taking place under more specific conditions. Reprinted from Ref.52.

Besides metal electrodes, functionalized electrodes were also utilized for the electrochemical reduction of nitrate. Hydroxylamine (NH_2OH) and ammonia (NH_4) are the main products formed on the functionalized electrodes on different catalysts, such as metal cyclams and phthalocyanine modified electrodes [53-55]. In previous work, de Groot et al. have investigated the electrochemical reduction of NO by hemin (FePP) adsorbed at pyrolytic graphite[56]. The formation of NH_2OH as main product was confirmed using rotating ring-disc electrode (RRDE), while N_2O was a minor product observed by on-line

electrochemical mass spectroscopy (OLEMS). They suggested pH-dependent competing pathways for the NO reduction, one of which leads to the formation of NH_3OH^+ (in acid media), the other one of which leads to N_2O formation (in alkaline media). In later work, the electrocatalytic nitrite reduction was studied at a hemin immobilized pyrolytic graphite electrode by Duca et al.[57]. They concluded that NO is the substrate reduced by FePP in acidic media, which implies that the behavior of the nitrite reduction on FePP is closely related to that described for NO reduction by de Groot et al..

1.3. Experimental techniques

1.3.1On-line electrochemical mass spectrometry (OLEMS)

Measurements of the volatile products have been conducted by combining the on-line electrochemical mass spectrometry (European Spectrometry systems Ltd) with the cyclic voltammetry (CV). These measurements allow the qualitative detection of various gaseous products formed during the reaction. In the electrochemical cell, cyclic voltammograms are collected from 0 V to -1.5 V with a scan rate of 1 mVs^{-1} by an Ivium A06075 potentiostat. The gaseous products formed at the working electrode enter into high-vacuum (< 10^{-6} mbar) mass chamber through a porous Teflon tip (inner diameter, 0.5mm). Prior the experiment, the tip is cleaned by dipping into a 0.2 M $K_2Cr_2O_7$ in 2 M H_2SO_4 solution for 15 minutes and rinsing thoroughly with MilliQ water. A 2400V SEM voltage is applied for all studied mass fragments, except for m/z=2 (corresponding to H_2) which has a SEM voltage of 1500 V to decrease the intensity of the signal. More details on the experimental setup can be found in Ref.[58].

1.3.2 Gas Chromatography (GC)

Quantitative measurements of the volatile products have been conducted by combining gas chromatography with long-term electrolysis. In a completely sealed two-compartment Teflon flow cell (with a volume of 12 mL for each compartment), the electrolysis is conducted at a given potential for 1h at atmospheric pressure. The reference electrode used in the flow cell is a Ag/AgCl electrode and the counter electrode is an Au

foil. A flow rate of CO_2 is first applied at 5 mL min^{-1} for 30 minutes to saturate the electrolyte and then decreased to 2 mL min^{-1} when the electrolysis started. The electrolysis was also conducted at high CO_2 pressure (P=10 atm) in a stainless-steel autoclave for 2h. CO_2 is continuously purged through the autoclave before and during the electrolysis with a flow rate of 50 mL min^{-1}. The gaseous products are collected every 6 minutes. CO, CO_2, H_2 and hydrocarbons are simultaneously separated using two columns in serie (a ShinCarbon 2 m micropacked column and a Rtx-1 column). A thermal conductivity detector is used for H_2 and CO, while a flame ionization detector is used for hydrocarbons. More details on the setup can be found in Ref.[59].

1.3.3 On-line high performance liquid Chromatography (HPLC)

The liquid products have been detected using high performance liquid chromatography (Prominence HPLC, Shimadzu) combined with linear voltammetry or electrolysis. Like in the OLEMS system, a Teflon tip (inner diameter: 0.38 mm) is positioned ~10 μm from the middle of the working electrode. Samples with a volume of 60 μL are collected and stored in a 96-well microtiter plate (270 μL per well, Screening Device b.v.) using an automatic fraction collector (FRC-10A, Schimadzu). The flow rate of the sample collection is 60 μL min^{-1} by using a Schimadzu pump (LC-20AT). The microtiter plate is then placed into an auto-sampler (SIL-20A) holder to analyze samples. 30 μL of sample is injected into an Aminex HPX 87-H (Bio-Rad) column whose temperature is maintained at 85°C using a column oven (CTO-20A). The separated compounds are detected with a refractive index detector (RID-10A). Diluted sulfuric acid (5 mM) is used as the eluent with a flow rate of 0.6 mL min^{-1}. The linear voltammetry is conducted from 0 V to -1.5 V with a scan rate of 1 mV s^{-1}. More details on the setup can be found in Ref.[60].

1.3.4 On-line ion Chromatography (IC)

The ionic products are measured using on-line ion chromatography combined with linear voltammetry. The principle of on-line IC is similar as on-line HPLC. Samples are collected using a Teflon tip positioned in the center of the working electrode while the linear voltammetry is conducted from 0 V to -1.5 V at scan rate of 1 mVs^{-1}. A microtiter

plate with collected samples is placed onto an auto-sampler (SIL-20A) holder of an ion chromatography unit (Schimadzu, Prominence) with a conductivity detector (CCD-10Ap, Schimadzu). 20 μL of sample is injected and analyzed through two series of Shodex IC Y-521 columns, whose temperature is 30 ^{0}C. A 2.5 mM nitric acid solution is used as an eluent at a flow rate of 8 mL min^{-1}.

1.4. Outline of this thesis

The focus of this thesis is on studying the catalytic activity of immobilized metal-porphyrin complexes toward the electrochemical reduction of small inorganic molecules, specifically CO_2 and nitrate, and in particular on the mechanistic aspects of the reactions. In general, pH and the natural of the metal center of the complexes play an important role on the selectivity. Therefore, the selectivity of both electrochemical reduction reaction of CO_2 and nitrate has been studied by varying pH and the metal centers of the complexes. We start in Chapter 2 by investigating the electrochemical reduction of CO_2 catalyzed by cobalt protoporphyrin immobilized on a pyrolytic graphite electrode in aqueous solution. New insights into the mechanism of the CO_2 electrochemical reduction on molecular catalysts will be proposed based on thorough investigations of the electrochemical reduction of possible intermediates as well as the influence of pH on CO_2 reduction.

In Chapter 3, we identify key intermediates of the CO_2 electrochemical reduction on a cobalt porphyrin using density functional theory (DFT) calculation. The most favorable pathways of the reaction are identified. The results of the theoretical investigation will be compared to the mechanistic conclusions from Chapter 2, to obtain a more comprehensive mechanistic understanding of the CO_2 electrochemical reduction on cobalt porphyrin complex.

The similarity of the requirements of electron and proton of the reduction of CO_2 and nitrate makes it interesting to study the catalysis of the nitrate reduction using metal-porphyrin complexes immobilized on pyrolytic graphite electrodes. Chapter 4 builds on previous work on de Groot and Duca on NO and nitrite reduction, respectively, by investigating the catalytic activity of various metal-porphyrin complexes for the nitrate

reduction. The cobalt porphyrin is shown to have the highest activity and selectivity toward hydroxylamine production, making it the most interesting catalyst. Furthermore, pH is shown to play a crucial role in determining the selectivity toward either hydroxylamine or ammonia, suggesting the sequential mechanism in which hydroxylamine is an important precursor for ammonia formation.

REFERENCES

1. Pacala, S.; Socolow, R. Stabilization Wedges: Solving the Climate Problem for the Next 50 Years with Current Technologies. *Science* **2004,** *305* (5686), 968-972.

2. Song, C. Global challenges and strategies for control, conversion and utilization of CO_2 for sustainable development involving energy, catalysis, adsorption and chemical processing. *Catal. Today* **2006,** *115* (1–4), 2-32.

3. Bard, A. J. Encyclopedia of Electrochemistry of the Elements. *Dekker* **1976,** *7*.

4. Ryu, J.; Andersen, T. N.; Eyring, H. Electrode reduction kinetics of carbon dioxide in aqueous solution. *J. Phys. Chem.* **1972,** *76* (22), 3278-3286.

5. Azuma, M; Hashimoto, K.; Hiramoto, M.; Watanabe, M.; Sakata, T.. Electrochemical Reduction of Carbon Dioxide on Various Metal Electrodes in Low-Temperature Aqueous $KHCO_3$ media. *J. Electrochem. Soc.*. **1990,** *137,* 1772-1778.

6. Hori, Y. Electrochemical CO_2 redcution on metal electrodes *Modern Aspects of Electrochemistry*. **2008**, *42,* 42. 89-189.

7. Noda, H.; Ikeda, S.; Oda, Y.; Ito. K.. Potential Dependencies of the Products on Electrochemical Reduction of Carbon Dioxide at a Copper Electrode. *Chem. Lett.* **1989**, *18*, 289-292.

8. Noda H.; Ikesa S.; Oda Y.; Imai K.; Maeda M.; Ito K..Electrochemical Reduction of Carbon Dioxide at Various Metal Electrodes in Aqueous Potassium Hydrogen Carbonate Solution. *Bull. Chem. Soc. Jpn.* **1990,** *63,* 2459-2462.

9. Cook, R. L.; MacDuff, R. C.; Sammells, A. F. Electrochemical Reduction of Carbon Dioxide to Methane at High Current Densities. *J. Electrochem. Soc.* **1987,** *134* (7), 1873-1874.

10. Cook, R. L.; MacDuff, R. C.; Sammells, A. F. Efficient High Rate Carbon Dioxide Reduction to Methane and Ethylene at in situ Electrodeposited Copper Electrode. *J. Electrochem. Soc.* **1987,** *134* (9), 2375-2376.

11. Azuma, M.; Hashimoto, K.; Hiramoto, M.; Watanabe, M.; Sakata, T. Carbon dioxide reduction at low temperature on various metal electrodes. *J. Electroanal. Chem. Interfacial electrochem.* **1989,** *260* (2), 441-445.

12. Kuhl, K. P.; Cave, E. R.; Abram, D. N.; Jaramillo, T. F. New insights into the electrochemical reduction of carbon dioxide on metallic copper surfaces. *Energ. Environ. Sci.* **2012,** *5* (5), 7050-7059.

13. Hori, Y.; Murata, A.; Takahashi, R.; Suzuki, S. Electroreduction of carbon monoxide to methane and at a copper electrode in aqueous solutions at ambient temperature and pressure. *J. Am. Chem. Soc.* **1987,** *109* (16), 5022-5023.

14. Peterson, A. A.; Abild-Pedersen, F.; Studt, F.; Rossmeisl, J.; Norskov, J. K. How copper catalyzes the electroreduction of carbon dioxide into hydrocarbon fuels. *Energ. Environ. Sci.* **2010,** *3* (9), 1311-1315.

15. Schouten, K. J. P.; Kwon, Y.; van der Ham, C. J. M.; Qin, Z.; Koper, M. T. M. A new mechanism for the selectivity to C1 and C2 species in the electrochemical reduction of carbon dioxide on copper electrodes. *Chem. Sci.* **2011,** *2* (10), 1902-1909.

16. Gattrell, M.; Gupta, N.; Co, A. A review of the aqueous electrochemical reduction of CO_2 to hydrocarbons at copper. *J. Electroanal. Chem.* **2006,** *594* (1), 1-19.

17. Cook, R. L.; MacDuff, R. C.; Sammells, A. F. Evidence for Formaldehyde, Formic Acid, and Acetaldehyde as Possible Intermediates during Electrochemical Carbon Dioxide Reduction at Copper. *J. Electrochem. Soc.* **1989,** *136* (7), 1982-1984.

18. Kortlever, R.; Shen, J.; Schouten K. J. P.; Calle-Vallejo, F.; Koper M. T. M.. Catalysts and reaction pathways for the electrochemical reduction of carbon dioxide. *J. Phys. Chem. Lett.* **2015**, *6*, 4073-4082.

19. Atoguchi, T.; Aramata, A.; Kazusaka, A.; Enyo, M. Electrocatalytic activity of Co^{II} TPP-pyridine complex modified carbon electrode for CO_2 reduction. *J. Electroanal. Chem. Interfacial electrochem.* **1991,** *318* (1–2), 309-320.

20. Magdesieva, T. V.; Yamamoto, T.; Tryk, D. A.; Fujishima, A. Electrochemical Reduction of CO_2 with Transition Metal Phthalocyanine and Porphyrin Complexes Supported on Activated Carbon Fibers. *J. Electrochem. Soc.* **2002,** *149* (6), D89-D95.

21. Zhao, H.-Z.; Chang, Y.-Y.; Liu, C. Electrodes modified with iron porphyrin and carbon nanotubes: application to CO_2 reduction and mechanism of synergistic electrocatalysis. *J. Solid State Electrochem.* **2013,** *17* (6), 1657-1664.

22. Meshitsuka, S.; Ichikawa, M.; Tamaru, K. Electrocatalysis by metal phthalocyanines in the reduction of carbon dioxide. *Chem. Commun.* **1974,** (5), 158-159.

23. Lieber, C. M.; Lewis, N. S. Catalytic reduction of carbon dioxide at carbon electrodes modified with cobalt phthalocyanine. *J. Am. Chem. Soc.* **1984,** *106* (17), 5033-5034.

24. Kapusta, S.; Hackerman, N. Carbon Dioxide Reduction at a Metal Phthalocyanine Catalyzed Carbon Electrode. *J. Electrochem. Soc.* **1984,** *131* (7), 1511-1514.

25. Ramos Sende, J. A.; Arana, C. R.; Hernandez, L.; Potts, K. T.; Keshevarz-K, M.; Abruna, H. D. Electrocatalysis of CO_2 Reduction in Aqueous Media at Electrodes Modified with Electropolymerized Films of Vinylterpyridine Complexes of Transition Metals. *Inorg. Chem.* **1995,** *34* (12), 3339-3348.

26. Ikeda S.; Takagi T.; and Ito K.. Selective formation of formic acid, oxalic aicd and carbon monoxide by electrochemical reduction of carbon dioxide. *Bull. Chem. Soc. Jpn.* **1987,** *60*, 2517-2522.

27. Weatherburn, M. W. Phenol-hypochlorite reaction for determination of ammonia. *Anal. Chem.* **1967,** *39* (8), 971-974.

28. Tyssee, D. A.; Wagenknecht, J. H.; Baizer, M. M.; Chruma, J. L. Some cathodic organic syntheses involving carbon dioxide. *Tetrahedron Lett.* **1972,** *13* (47), 4809-4812.

29. Eggins, B. R.; Ennis, C.; McConnell, R.; Spence, M. Improved yields of oxalate, glyoxylate and glycolate from the electrochemical reduction of carbon dioxide in methanol, *J. Appl. Electrochem.* **1997,** 27, 706-712.

30. Amatore, C.; Savéant, J. M.. Mechanism and kinetic characteristics of the electrochemical reduction of carbon dioxide in meida of low proton availability. *J. Am. Chem. Soc.* **1981**, *103*(17), 5021-5023..

31. Nolan, B. T.; Ruddy, B. C.; Hitt, K. J.; Helsel, D. R. Risk of Nitrate in Groundwaters of the United States A National Perspective. *Environ. Sci. Technol.* **1997,** *31* (8), 2229-2236.

32. Rosca, V.; Duca, M.; de Groot, M. T.; Koper, M. T. M. Nitrogen Cycle Electrocatalysis. *Chem. Rev.* **2009,** *109* (6), 2209-2244.

33. de Groot, M. T.; Koper, M. T. M. The influence of nitrate concentration and acidity on the electrocatalytic reduction of nitrate on platinum. *J. Electroanal. Chem.* **2004,** *562* (1), 81-94.

34. Nishimura, K.; Machida, K.; Enyo, M. On-line mass spectroscopy applied to electroreduction of nitrite and nitrate ions at porous Pt electrode in sulfuric acid solutions. *Electrochim. Acta* **1991,** *36* (5), 877-880.

35. Horányi, G.; Rizmayer, E. M. Role of adsorption phenomena in the electrocatalytic reduction of nitric acid at a platinized platinum electrode. *J. Electroanal. Chem. Interfacial electrochem.* **1982,** *140* (2), 347-366.

36. Horányi, G.; Rizmayer, E. M. Indirect radiotracer study of the adsorption of NO_3^- ions at a platinized platinum electrode in acidic medium. *J. Electroanal. Chem. Interfacial electrochem.* **1985,** *188* (1–2), 273-279.

37. Petrii, O. A.; Safonova, T. Y. Electroreduction of nitrate and nitrite anions on platinum metals: A model process for elucidating the nature of the passivation by hydrogen adsorption. *J. Electroanal. Chem.* **1992,** *331* (1–2), 897-912.

38. Safonova, T. Y.; Petrii, O. A. Chemisorption of nitrate anions on platinum acid solutions. *Russ.. J. Electrochem.* **1995,** *31*, 1269-1273.

39. da Cunha, M. C. P. M.; Weber, M.; Nart, F. C. On the adsorption and reduction of NO_3^- ions at Au and Pt electrodes studied by in situ FTIR spectroscopy. *J. Electroanal. Chem.* **1996,** *414* (2), 163-170.

40. Nakata, K.; Okubo, A.; Shimazu, K.; Yamakata, A.; Ye, S.; Osawa, M. Surface-Enhanced Infrared Absorption Spectroscopic Studies of Adsorbed Nitrate, Nitric Oxide, and Related Compounds 1: Reduction of Adsorbed NO on a Platinum Electrode. *Langmuir* **2008,** *24* (8), 4352-4357.

41. Dima, G. E.; de Vooys, A. C. A.; Koper, M. T. M. Electrocatalytic reduction of nitrate at low concentration on coinage and transition-metal electrodes in acid solutions. *J. Electroanal. Chem.* **2003,** *554–555*, 15-23.

42. Gootzen, J. F. E.; Peeters, P. G. J. M.; Dukers, J. M. B.; Lefferts, L.; Visscher, W.; van Veen, J. A. R. The electrocatalytic reduction of NO_3^- on Pt, Pd and Pt + Pd electrodes activated with Ge. *J. Electroanal. Chem.* **1997,** *434* (1–2), 171-183.

43. Dima, G. E.; Rosca, V.; Koper, M. T. M. Role of germanium in promoting the electrocatalytic reduction of nitrate on platinum: An FTIR and DEMS study. *J. Electroanal. Chem.* **2007,** *599* (2), 167-176.

44. Dima, G. E.; Beltramo, G. L.; Koper, M. T. M. Nitrate reduction on single-crystal platinum electrodes. *Electrochim. Acta* **2005,** *50* (21), 4318-4326.

45. Taguchi, S.; Feliu, J. M. Electrochemical reduction of nitrate on Pt(S)[n(1 1 1) × (1 1 1)] electrodes in perchloric acid solution. *Electrochim. Acta* **2007,** *52* (19), 6023-6033.

46. Vijh, A. K. Electrocatalysis of the electroreduction of nitric acid by metals. *J. Catal.* **1974,** *32* (2), 230-236.

47. Boese, S. W.; Archer, V. S. Electrochemical reduction of nitrate in the presence of ytterbium(III). *J. Electroanal. Chem. Interfacial electrochem.* **1982,** *138* (2), 273-294.

48. Hampson, N. A.; Piercy, R. Note of oscillation of potential observed during the reduction of the nitrate ion at solid indium. *J. Electroanal. Chem. Interfacial electrochem.* **1973,** *45* (2), 326-329.

49. Davenport, R. J.; Johnson, D. C. Voltammetric determination of nitrate and nitrite ions using a rotating cadmium disk electrode. *Anal. Chem.* **1973,** *45* (11), 1979-1980.

50. Katsounaros, I.; Ipsakis, D.; Polatides, C.; Kyriacou, G. Efficient electrochemical reduction of nitrate to nitrogen on tin cathode at very high cathodic potentials. *Electrochim. Acta* **2006,** *52* (3), 1329-1338.

51. Katsounaros, I.; Kyriacou, G. Influence of the concentration and the nature of the supporting electrolyte on the electrochemical reduction of nitrate on tin cathode. *Electrochim. Acta* **2007,** *52* (23), 6412-6420.

52. Duca, M.; Koper, M. T. M. Powering denitrification: the perspectives of electrocatalytic nitrate reduction. *Energ. Environ. Sci.* **2012,** *5* (12), 9726-9742.

53. Taniguchi, L.; Nakashima, N.; Yasukouchi, K. Reduction of nitrate to give hydroxylamine at a mercury electrode using cobalt(III)-and nickel(II)-cyclams as catalysts. *Chem. Commun.* **1986,** (24), 1814-1815.

54. Ma, L.; Zhang, B.-Y.; Li, H.-L.; Chambers, J. Q. Kinetics of nitrate reduction by cobalt-cyclam incorporated Nafion® redox polymer. *J. Electroanal. Chem.* **1993,** *362* (1–2), 201-205.

55. Li, H. L.; Chambers, J. Q.; Hobbs, D. T. Electroreduction of nitrate ions in concentrated sodium hydroxide solutions at lead, zinc, nickel and phthalocyanine-modified electrodes. *J. Appl. Electrochem.* **1988,** *18* (3), 454-458.

56. de Groot, M. T.; Merkx, M.; Wonders, A. H.; Koper, M. T. M. Electrochemical Reduction of NO by Hemin Adsorbed at Pyrolitic Graphite. *J. Am. Chem. Soc.* **2005,** *127* (20), 7579-7586.

57. Duca, M.; Khamseh, S.; Lai, S. C. S.; Koper, M. T. M. The Influence of Solution-Phase HNO_2 Decomposition on the Electrocatalytic Nitrite Reduction at a Hemin–Pyrolitic Graphite Electrode. *Langmuir* **2010,** *26* (14), 12418-12424.

58. Wonders, A. H.; Housmans, T. H. M.; Rosca, V.; Koper, M. T. M. On-line mass spectrometry system for measurements at single-crystal electrodes in hanging meniscus configuration. *J. Appl. Electrochem.* **2006,** *36* (11), 1215-1221.

59. Kas, R.; Kortlever, R.; Milbrat, A.; Koper, M. T. M.; Mul, G.; Baltrusaitis, J. Electrochemical CO_2 reduction on Cu_2O-derived copper nanoparticles: controlling the catalytic selectivity of hydrocarbons. *Phys. Chem. Chem. Phys.* **2014,** *16* (24), 12194-12201.

60. Kwon, Y.; Koper, M. T. M. Combining Voltammetry with HPLC: Application to Electro-Oxidation of Glycerol. *Anal. Chem.* **2010,** *82* (13), 5420-5424.

Chapter 2

Electrocatalytic reduction of carbon dioxide to carbon monoxide and methane at an immobilized cobalt protoporphyrin in aqueous solution

ABSTRACT

In this Chapter we report that a cobalt protoporphyrin immobilized on a pyrolytic graphite electrode is able to reduce carbon dioxide in acidic solution at relatively low overpotential (-0.5 V), with an efficiency and selectivity that is comparable to the best porphyrin-based electrocatalyst in the literature. Whilst carbon monoxide is the main reduction product, we also observe methane (and smaller amounts of formic acid and methanol) as by-product. We find that an unbuffered solution of pH=3 is most advantageous for selective carbon dioxide reduction. Our results are explained consistently by a mechanism in which carbon dioxide is activated by the cobalt-protoporphyrin through the stabilization of a anion intermediate, which acts as Brønsted base. The basic character of this intermediate explains how the carbon dioxide reduction circumvents a mechanism in which concerted proton-electron transfer takes place, in contrast to the hydrogen evolution mechanism. Our results and their mechanistic interpretations suggest strategies for designing improved catalysts.

This chapter has been published in: Jing Shen, Ruud Kortlever, Recep Kas, Yuvraj Y. Birdja, Oscar Diaz-Morales, Youngkook Kwon, Isis Ledezma-Yanez, Klaas Jan P. Schouten, Guido Mul and Marc T.M. Koper. *Nature Communications* **2015**, 6, Article number: 8177

2.1. Introduction

The efficient electrochemical reduction of carbon dioxide to a fuel with a high-energy density would be a major step forward in the introduction of a CO_2-neutral energy cycle, as it would allow for the direct low-temperature conversion of photo-generated electrical current to stored chemical energy, in a fashion very similar to the way nature stores solar energy. Plants fix CO_2 from the atmosphere by photosynthesis, in an enzymatic complex called Rubisco, which selectively binds CO_2 and inserts it into existing carbon chains by reductive carboxylation. The high-energy electrons necessary for this process are photo-generated by Photosystem II.

Synthetic catalysts for the electrocatalytic reduction of CO_2, which could facilitate such an artificial CO_2 neutral redox cycle, have been studied for many decades[1-4]. A main challenge in electrochemical CO_2 reduction is to develop catalysts that are capable of reducing CO_2 beyond the two-electron products carbon monoxide (CO), formic acid (HCOOH), and oxalate ($C_2O_4^{2-}$). Unfortunately, the formation of reduction products requiring 4 or more electrons is invariably associated with considerable overpotentials due to the multiple intermediates involved in the reaction mechanisms[5] (although more reduced products often have higher stability and correspondingly more positive equilibrium potentials). Metallic copper is unique in producing significant amounts of high-energy multi-electron transfer products such as methane, ethylene and ethanol[3,6,7]. Molecular catalysts capable of reducing CO_2 to a product different from one of the abovementioned two-electron products, are much less common and typically involve a strong interaction with the working electrode[8]. A second important challenge in CO_2 electrocatalysis concerns the suppression of the concomitant evolution of hydrogen, which is a dominant side reaction for CO_2 reduction from aqueous electrolytes. Strategies for suppressing hydrogen evolution typically involve working with high(er) CO_2 to proton ratios, such as high CO_2 pressures or solvents with a higher CO_2 solubility.

Recent fundamental and theoretical work has reconsidered porphyrin-based molecular catalysts for electrochemical CO_2 reduction. Tripkovic et al. have performed extensive

density functional theory calculations of metal-functionalized porphyrin-like graphene surfaces and predicted the potential formation of methane and methanol from CO_2[9]. Costentin et al. considered ligand modifications of iron-based porphyrins and found that local proton sources built into the porphyrin ring give rise to high activity and good Faradaic efficiency for the reduction of CO_2 to CO in a mixed DMF-water solvent[10]. In fact, it has been known since the early 1980s that cobalt-based macrocyclic complexes, either in solution or adsorbed onto carbon electrodes, act as effective electrocatalysts for CO_2 reduction, producing CO, formic acid, methanol and methane, though at relatively high overpotential and with varying selectivity[11-15].

In this Chapter, we report on the electrochemical reduction of CO_2 to CO and methane, as well as smaller amounts of formic acid and methanol, on a simple cobalt-protoporphyrin molecular catalyst immobilized onto a pyrolytic graphite electrode in a purely aqueous electrolyte solution. Previous similar work employing immobilized cobalt-porphyrins or cobalt-phthalocyanines has shown the capability of Co-based catalysts to achieve a high Faradaic efficiency towards CO, which is highly sensitive to pH and potential[16-18]. Our work confirms that immobilized cobalt-based porphyrins are good CO_2 reduction electrocatalysts capable of producing multi-electron products such as methane and methanol. More significantly, our work underscores the important role of pH in steering the catalytic activity and selectivity toward CO and CH_4, especially in the very narrow pH=1-3 range in the absence of coordinating anions. This high sensitivity to pH is explained by a mechanism highlighting the important role of the initial electron transfer in activating CO_2 electrochemically. For the first time we demonstrate how such a mechanism for CO_2 reduction manifests experimentally and how this property can be exploited to suppress concomitant hydrogen evolution. Furthermore, we show that the overpotential and corresponding turnover frequency for CO_2 reduction of our catalyst compare favorably to the best molecular porphyrin-based catalyst in the literature[10]. Therefore, we believe that these insights have significant implications for the design of new and improved molecular catalyst electrodes and for the formulation of optimized process conditions for efficient electrochemical CO_2 reduction to CO as well as to products reduced to a more significant degree.

2.2. Experimental

2.2.1. Electrochemistry and chemicals

The experiments were performed on home-made pyrolytic graphite electrodes (Carbone-Lorraine; diameter, 5mm). Before each experiment, the electrodes were polished using P500 and P1000 SiC sandpaper consecutively, and ultrasonicated in ultrapure water (MilliQ gradient A10 system, 18.2 MΩ cm) for 1 min and dried in a flow originating from compressed air. The electrodes were subsequently immersed in the cobalt protoporphyrin (CoPP, Frontier Scientific) solution (0.5 mM in borate buffer) for 5 min to immobilize the protoporphyrin on the surface and rinsed with ultrapure water prior to the experiments. A one-compartment electrochemical cell was used, with a platinum flag as counter electrode and a reversible hydrogen electrode (RHE) as a reference, to which all potentials in this work are referred. The reference electrode was separated from the working electrode compartment through a Luggin capillary. An Ivium potentiostat/galvanostat (IviumStat) was used for the electrochemical measurements. Solutions were prepared from $HClO_4$ (Merck, 70%), $NaClO_4$ (Sigma-Aldrich, $\geqslant$ 98.0%), NaOH (Sigma-Aldrich, 99.998%), Borate (Sigma-Aldrich) and ultrapure water. Argon (Hoekloos, purity grade 6.0) was purged though the solutions for 30 min before the experiment to remove dissolved oxygen. The reported current densities refer to the geometric surface area.

2.2.2. Online electrochemical mass spectrometry

The volatile products of the CO_2 electrochemical reduction were detected using on-line electrochemical mass spectroscopy (OLEMS) with an Evolution mass spectrometer system (European Spectrometry systems Ltd)[19]. A porous Teflon tip (inner diameter, 0.5mm) with a pore size of 10-14 μm was positioned close (~10 μm) to the center of the electrode. Prior the experiments, the tip was dipped into a 0.2 M $K_2Cr_2O_7$ in 2 M H_2SO_4 solution for 15 min and rinsed with ultrapure water thoroughly. The gas products were collected through a PEEK capillary into the mass spectrometer. A 2400V SEM voltage was applied for all the fragments except for hydrogen (m/z=2) which is 1500 V. The OLEMS measurement was

conducted while cyclic voltammetry was scanning from 0 V to -1.5 V and back at a scan rate of 1 mV s^{-1}.

2.2.3. Gas Chromatography

The quantitative measurements of the gas products were carried out using Gas Chromatography (GC) [20,21]. At atmospheric pressure, CO_2 was continuously purged through a two-compartment flow cell with a volume of 12 mL for each compartment at a rate of 5 mL/min for 30 min to saturate the electrolyte. The flow rate declined to 2 mL/min while a constant potential was applied for 1h. The reference electrode used here is a Ag/AgCl electrode. The experiments at high CO_2 pressure (P=10 atm) were conducted in a stainless-steel autoclave using a Pt mesh as a counter electrode, and a home-made Ag/AgCl in 3 M KCl as a reference electrode. All potentials were scaled to RHE after the experiments for both atmospheric and high pressure, with E (vs Ag/AgCl) = E(vs RHE) – 0.197 V – pH*0.059. CO_2 was continuously purged through the autoclave before and during the electrolysis with a flow rate of 50 mL min^{-1}. The reactor effluent was sampled via GC once every 6 min. CO, CO_2, H_2 and hydrocarbons were simultaneously separated using two series columns in series (a ShinCarbon 2 m micropacked column and a Rtx-1 column). The quantitative analysis of the gas products was performed using a thermal conductivity detector (H_2 and CO) and flame ionization detector (hydrocarbons).

2.2.4. Online High Performance Liquid Chromatography

High-performance liquid chromatography (HPLC, Prominence HPLC, Shimadzu) was used to detect liquid products produced during electrochemical reduction of CO_2 using a method described in previous work[22]. Samples were collected using a Teflon tip (inner diameter: 0.38 mm) positioned ~10 μm from the center of the electrode surface (diameter: 1 cm). The sample volume collected was 60 μL stored in a 96-well microtiter plate (270 μL per well, Screening Device b.v.) using an automatic fraction collector (FRC-10A, Shimadzu). The flow rate of the sample collection was adjusted to 60 μL per min with a Shimadzu pump (LC-20AT). A linear sweep voltammogram was recorded while the sample was collecting at a scan rate of 1 mV s^{-1} from 0 V to -1.5 V vs RHE. The microtiter plate with collected

samples was then placed in an auto-sampler (SIL-20A) holder and 30 μL of sample was injected into an Aminex HPX 87-H (Bio-Rad) column. The eluent was diluted sulfuric acid (5 mM) with a flow rate of 0.6 mL per min. The temperature of column was maintained at 85^{o}C using a column oven (CTO-20A) and the separated compounds were detected with a refractive index detector (RID-10A).

2.3. Results

2.3.1. Voltammetry and online electrochemical mass spectrometry

The cobalt protoporphyrin coated pyrolytic graphite ("CoPP-PG") electrode was prepared following a procedure described earlier[23] and detailed in the Methods section. In situ electrochemical scanning tunneling microscopy and atomic force microscopy images of iron and zinc protoporphyrins on basal plane graphite electrodes by Tao et al. suggest that these molecules form monolayer films on the electrode with the molecules lying flat[24]. The blank cyclic voltammograms of the PG electrode, the CoPP-PG electrode in 0.1 M $HClO_4$, and the voltammetry of the dissolved CoPP in the same electrolyte, are compared in Appendix A Figure 1. The voltammetry in Appendix A Figure 1 shows the reversible redox peak of the Co^{III}/Co^{II} transition at 0.8-0.85 V vs. RHE, from which the coverage of the Co-PP on the PG electrode can be determined to be ca. $4x10^{-10}$ mol cm^{-2}, in good agreement with previous experiments of protoporphyrins on pyrolytic graphite[23,25]. No further redox transition of the CoPP is observed at more negative potential, with the onset of hydrogen evolution being at ca. -0.5 V vs. RHE. However, we note that we have previously observed a Co^{II}/Co^{I} transition at ca. -0.6 V vs. NHE for CoPP immobilized in a DDAB (didodecyl dimethylammonium bromide) film on PG[23]. The observation of this peak in the DDAB films may be related to the higher hydrophobicity of DDAB. The Co^{II}/Co^{I} redox transition has previously been associated with the onset of electrocatalytic hydrogen evolution on Co porphyrins[26].

Figure 1 shows the voltammetry at 1 mV s^{-1} of the CoPP-PG electrode in unbuffered 0.1 M perchlorate solution of pH=1, 2 and 3, saturated with CO_2, together with the mass

signals corresponding to H_2 (m/z=2), CH_4 (m/z=15, corresponding to the CH_3 fragment) and CO (m/z=28) as measured simultaneously using online electrochemical mass spectrometry (OLEMS)[27]. The OLEMS experiment samples the gases formed at the electrode surface by a tip covered with a hydrophobic membrane placed at a distance of ca. 10 μm from the surface. This technique can follow gas production online during cyclic voltammetry. Calibration of our experiment is cumbersome as the signals depend on parameters which are not easy to control (tip distance, tip porosity). Quantitative measurements were therefore performed using long-term electrolysis combined with gas chromatography (to be discussed later). Depending on the quality of the gas-sensing tip used in the OLEMS experiment shown in Fig.1, m/z=31 was also measured, corresponding to the formation of methanol (see Appendix A Figure 2). Using HPLC, we could also detect formic acid as one of the products (see Appendix A Figure 3), though both formic acid and methanol appear to be minority products under these conditions. This confirms, for the first time in a single study, that all four products, CO, HCOOH, CH_3OH, and CH_4 can be formed from CO_2 reduction on a Co-based porphyrin. Fig. 1(a, d, g) measured at pH=1, shows that the reduction current is accompanied by the simultaneous formation of H_2 and CH_4. The m/z=28 signal in Figure 1 was not corrected for the CO_2 fragmentation, and therefore the CO signal combines CO production from CO_2 electroreduction with CO formation from CO_2 fragmentation in the MS. This explains why the CO signal decreases for more negative potentials at which the CO_2 reduction rate is higher, as a result of the lower local CO_2 concentration near the electrode surface. However, at pH=2 and 3, an increase in the CO signal with more negative potential is observed, simultaneously with the CH_4 production, suggesting that CO is an intermediate in the reaction (as also suggested by the fact that CO may be reduced to CH_4 on CoPP-PG; see Figure 4 below). Most significantly, at pH=3, CO and CH_4 production is observed at less negative potentials than H_2 evolution, showing that the CO_2 reduction has a different pH dependence from the hydrogen evolution reaction. We chose to restrict ourselves to pH$\leqslant$3 in perchlorate solution in order to avoid the interference of buffering anions such as bicarbonate or phosphate (see below) with the CO_2 reduction process.

We have performed a number of experiments to convince ourselves that the Co-PP is indeed the active catalytic center turning over dissolved CO_2. On the unmodified PG electrode and on a PG electrode modified with Co-free protoporphyrin, H_2 evolution was observed, but no CO_2 reduction (Appendix A Figures 5 and 6). A PG electrode onto which a small amount of Co was electrodeposited was also tested for CO_2 reduction, but showed no activity (Appendix A Figure 7). Finally, the reduction of isotopically labeled $^{13}CO_2$ in deuterated water yielded m/z=19 (corresponding to $^{13}CD_3$) as reduction product (Appendix A Figure 8), which irrefutably proves the reduction of dissolved CO_2 into methane. These combined results show that the immobilized Co-protoporphyrin is responsible for the production of carbon monoxide and methane from CO_2 electroreduction.

As mentioned, the most important conclusion from Figure 1 is the remarkable role of the pH. Initially, we performed the CO_2 reduction experiments at pH=2 and 3 in buffered phosphate solution, also yielding methane as a product but with a pH dependence that was not straightforward to understand. Therefore, we decided to remove the buffering phosphate anions, as they are suspected to interfere with the reactivity by coordinating to the catalytic center[28] or interacting with the catalytic intermediates. In non-adsorbing perchlorate solution, the role of the proton concentration can be better understood by comparing the voltammetry of the CoPP-PG in the absence of CO_2 at pH=1, 2, and 3, as shown in Figure 2. At pH=1, there is only a single catalytic reduction wave in the potential window studied, corresponding to the reduction of H^+ to H_2. The voltammetry at pH=2 and 3 shows two waves, one at less negative potential that is proportional to the H^+ concentration and corresponds to H^+ reduction, and one starting at -1.1 V that corresponds to H_2O reduction. This is also reflected in the H_2 formation profiles observed in the mass signals in Figure 1. We must also take into account here that because of the relatively low proton concentration at pH=3, the direct proton reduction quickly runs into diffusion limitations, and further H_2 evolution can only take place at more negative potentials by direct water reduction, which

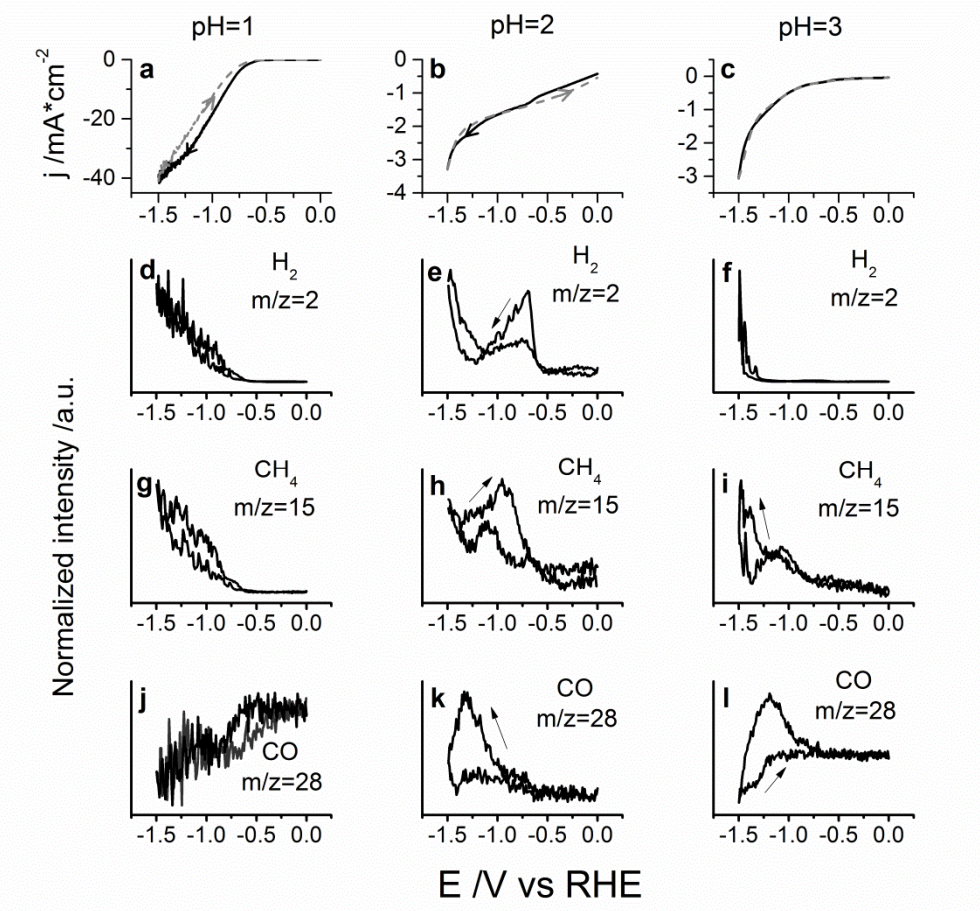

Figure 1 | Voltammetry and volatile product identification by online electrochemical mass spectrometry (OLEMS). This figure shows the electrochemical reduction of CO_2 on cobalt protoporphyrin immobilized on a pyrolytic graphite electrode and the various volatile products detected by OLEMS. (a) Cyclic voltammetry (CV) in 0.1 M $HClO_4$, (b) CV in 10 mM $HClO_4$ + 90 mM $NaClO_4$, (c) CV in 1 mM $HClO_4$ + 99mM $NaClO_4$, (d) m/z=2 (H_2) signal in 0.1 M $HClO_4$, (e) m/z=2 (H_2) signal in 10 mM $HClO_4$ + 90 mM $NaClO_4$, (f) m/z=2 (H_2) signal in 1 mM $HClO_4$ + 99mM $NaClO_4$, (g) m/z=15 (CH_4) signal in 0.1 M $HClO_4$, (h) m/z=15 (CH_4) signal in 10 mM $HClO_4$ + 90 mM $NaClO_4$, (i) m/z=15 (CH_4) signal in 1 mM $HClO_4$ + 99mM $NaClO_4$, (j) m/z=28 (CO) signal in 0.1 M $HClO_4$, (k) m/z=28 (CO) signal in 10 mM $HClO_4$ + 90 Mm $NaClO_4$, (l) m/z=28 (CO) signal in 1 mM $HClO_4$ + 99mM $NaClO_4$. Blank plots, forward scans; Gray plots, back scans in (a), (b) and (c). Scan rate was 1 mV s^{-1} in all cases. Appendix A Figure 4 shows the same data with the unnormalized MS signals as well as the signals obtained in the first and second CV scan.

does not suffer from such diffusion limitations. By comparing the results in Figure 1 and 2, we conclude that H_2 evolution dominates over CO_2 reduction in the presence of a high concentration of protons in solution, whereas the opposite is the case for pH=3. The activation of CO_2 is apparently less sensitive to the presence of protons, implying that water molecules are just as powerful in hydrogenating the activated CO_2. This remarkable pH dependence is somewhat similar to observations made by Noda et al. during CO_2 reduction on a gold electrode[28]. The important new finding here is that this small pH shift is the key to favoring CO_2 reduction over H_2 evolution, also on our molecular catalyst, especially in the absence of buffering anions. This is also evidenced by the Faradaic efficiency measurements summarized in Figure 3, to be discussed next. A mechanistic explanation for this pH sensitivity will be given at the end of this section.

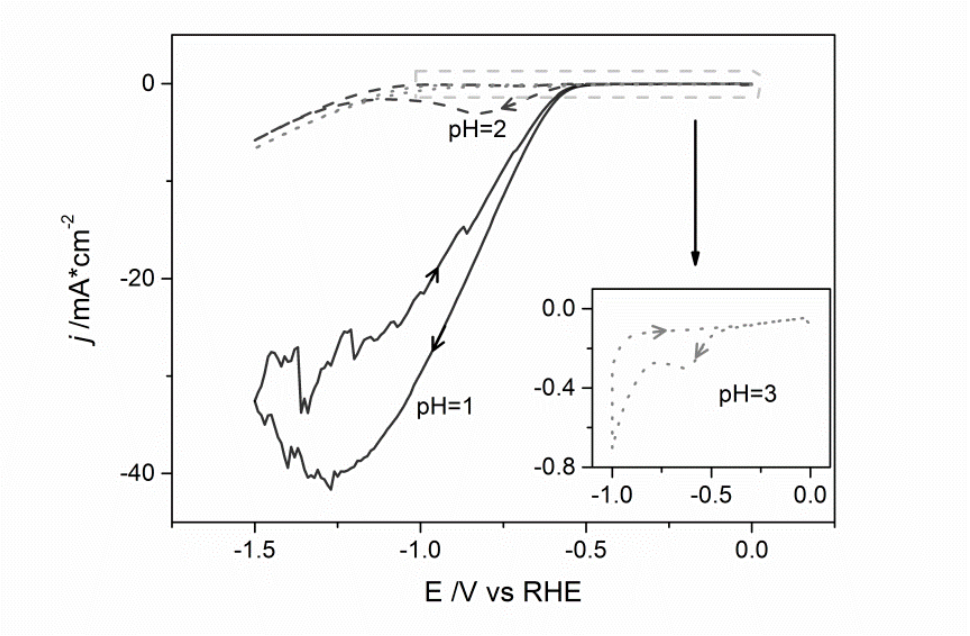

Figure 2. pH dependence of hydrogen evolution reaction on the CoPP-PG electrode. Hydrogen evolution reaction at pH=1 (black curve), pH=2 (dark gray dash curve) and pH=3 (gray dot curve) on Cobalt protoporphyrin modified PG electrode in the absence of CO_2. Inserted: highlight of the voltammetry at pH=3. Scan rate was is 100 mV s^{-1} in all cases. All electrolyte solutions were 0.1 M perchlorate, with different ratios of H^+ and Na^+.

2.3.2. Faradaic efficiency

The Faradaic efficiency (FE) for the simultaneous CO_2 and water reduction to hydrogen, carbon monoxide and methane was determined separately with long-term electrolysis experiments, using a gas chromatography setup coupled to an electrochemical cell, as detailed elsewhere[20,21]. Figure 3 shows results for CO and CH_4 at pH =1 and 3 for different potentials. The remaining current is used to form H_2. The quantitative data and error bars are summarized and further explained in Appendix A Table 1. Formic acid was also observed as a minority product at pH=1 using High Performance Liquid Chromatography, but was not observed at pH=3 (see Appendix A Figure 3). As mentioned above, methanol was observed as a product using OLEMS (Appendix A Figure 2), but it remained below the detection limit during the GC measurements. At pH=1, the Faradaic efficiency to CO and methane is low, on the order of a percent, and the dominant product is H_2, and therefore for pH=1 we show results at only a single potential in Figure 3. Note however that at pH=1, more methane is produced than CO. At pH=3, a dramatic change in selectivity is observed, with now CO being a majority product, especially at less cathodic potentials, for which the Faradaic efficiency to CO is around 40%. This high selectivity is maintained for at least one hour during the long-term electrolysis experiment at fixed potential (see Appendix A Figure 9), testifying to the good stability of the catalyst. The stability and integrity of the CoPP-PG electrode was also confirmed by pre- and post-electrolysis analysis using XPS, Raman and NMR (Appendix A Figures 10-12). Raman spectroscopy showed no significant change in the spectral features of the CoPP-PG surface; XPS showed no change in Co oxidation state after 1 hour of electrolysis; and NMR showed no decomposition products in solution that could be related to CoPP. Figure 3 also illustrates that less methane is produced at pH=3 as compared to pH=1. We ascribe this lower methane production to the slower reduction of CO to CH_4 at pH=3 compared to pH=1 (see next paragraph). The efficiency towards CO can be further boosted by performing the experiment at higher CO_2 pressure. Figure 3 illustrates this for a CO_2 pressure of 10 atm, which leads to a Faradaic efficiency of ~ 60% at pH=3 at a potential of -0.6 V. Note that at pH=1, both the efficiency towards CO and CH_4 increase to a few % when the reduction is carried out at increased CO_2 pressure. We emphasize that OLEMS

and GC experiments exhibited good consistency and reproducibility. The error bars shown in Figure 3 were based on single long-term electrolysis experiments sampled every six minutes.

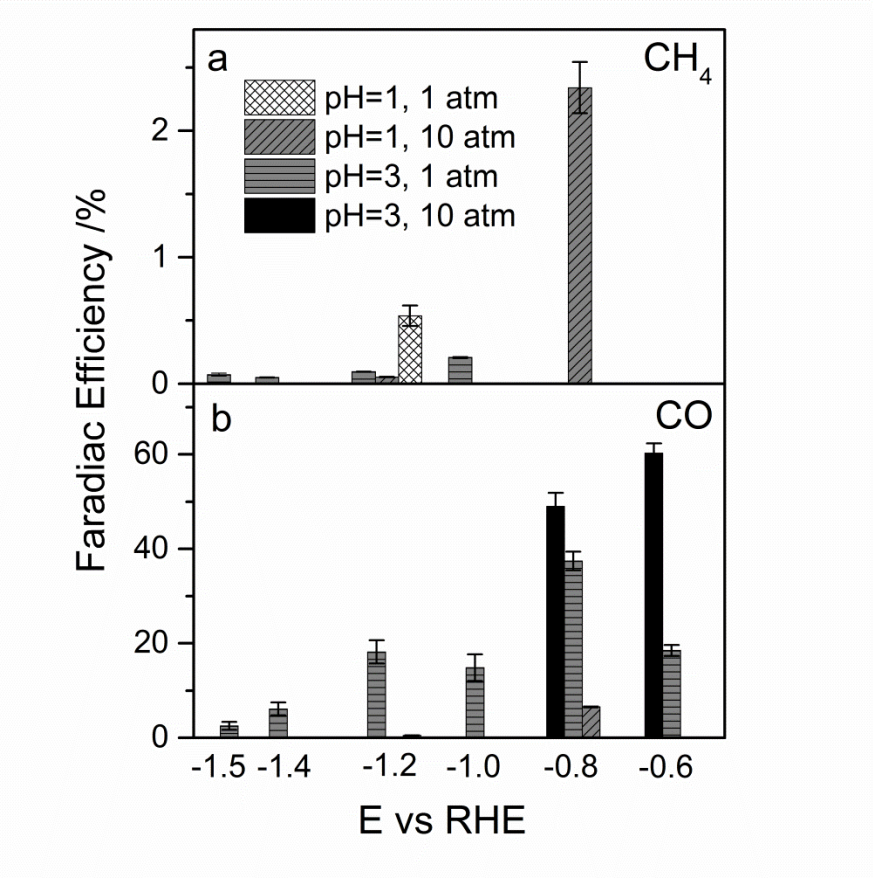

Figure 2 Faradaic efficiency of carbon dioxide reduction to carbon monoxide and methane. Faradaiac efficiencies to CO and CH_4 were determined for bars: pH=1, P_{CO2}=1 atm; bars: pH=1, P_{CO2}=10 atm; bars: pH=3, P_{CO2}=1 atm and bars pH=3, P_{CO2}=10 atm. Faradaic efficiency of (**a**) CH_4 and (**b**) CO in 0.1 M perchlorate solution saturated with CO_2. At each potential the electrolysis was conducted for 1 hour at P_{CO2}=1 atm, while it is 90 minutes at P_{CO2}=10 atm due to the longer time to reach the steady state. Error bars were determined from 3-8 data points based on samples taken every five minutes during the steady state of a single electrolysis run.

2.3.3. Reduction of CO, formic acid and formaldehyde

To determine the involvement of potential intermediates, we also studied the reduction of formic acid (HCOOH), carbon monoxide (CO) and formaldehyde (HCHO), by combined voltammetry-OLEMS. Formic acid was not reduced at either pH=1 or 3 (Appendix A Figure 13) and is therefore an end product, not an intermediate. Figure 4 shows the voltammetry and associated OLEMS mass signals on the CoPP-PG electrode for CO reduction at pH=1 and 3 and for HCHO reduction at pH=1. Remarkably, CO is clearly reduced to methane at pH=1, simultaneous with H_2 evolution, but the CO reduction activity is much lower compared to hydrogen evolution at pH=3, with an insignificant amount of CH_4 detected. This observation is consistent with the results in Figure 3 showing that methane production from CO_2 is lower at pH=3. HCHO is reduced to methane at pH=1 and 3 (Figure 4 only shows pH=1). Interestingly, formaldehyde is not reduced to significant amounts of methanol, whereas methanol is the product of formaldehyde reduction on copper electrodes[6]. Figure 4 suggests that carbon monoxide and formaldehyde, or their catalyst-bound derivatives, are intermediates in the reaction mechanism from CO_2 to CH_4, but formic acid is not. It also shows that the reduction of CO exhibits a different pH dependence compared to CO_2 reduction, explaining why the selectivity of CO_2 towards CO increases with higher pH, but the selectivity towards CH_4 decreases with higher pH.

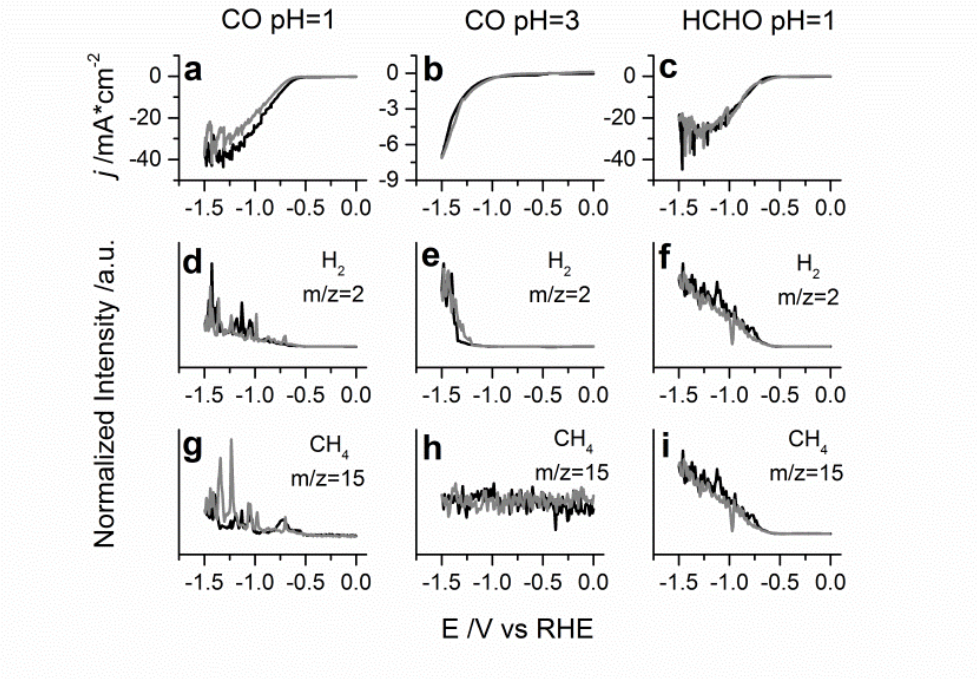

Figure 4 Identification of volatile products by OLEMS during electrochemical reduction of CO and HCHO. Cyclic voltammetry of CO reduction in **(a)** 100 mM $HClO_4$ and **(b)** 1mM $HClO_4$ + 99 mM $NaClO_4$ saturated with CO with associated mass fragments of volatile products detected with OLEMS. (**c**) Cyclic voltammetry of HCHO (5 mM) reduction in 100 mM $HClO_4$ with associated mass fragments measured with OLEMS. Black plots, forward scans; gray plots, backward scans. Scan rate: 1 mVs^{-1}. Appendix A Figure 14 shows the same data with the unnormalized MS signals as well as the signals obtained in the first and second CV scan.

2.4. Discussion

The results presented above give unique new insights into the mechanism of CO_2 electroreduction on immobilized Co-protoporphyrins, and the observed pH dependence reveals the important role of the initial electron transfer to CO_2 in the overall mechanism as explained below, and as illustrated in our suggested mechanistic scheme in Figure 5. At pH=1, the dominant reaction is hydrogen evolution:

$$2\ H^+ + 2\ e^- \longrightarrow H_2 \qquad (1)$$

At pH=3, the main origin of hydrogen evolution is direct water reduction:

$$2\ H_2O + 2\ e^- \longrightarrow H_2 + 2\ OH^- \qquad (2)$$

with reaction 1 generating a smaller amount of H_2 at less negative potential due to diffusion limitations (see Figure 2). This observation is very similar to recent experiments on platinum electrodes[29]. The observation that CO_2 reduction to CO becomes much more dominant at higher pH, must mean that CO_2 activation does not sensitively depend on the presence of protons, and hence must involve an intermediate that can easily react with water at any pH. Such an intermediate is most likely a negatively charged Brønsted base, and the most obvious candidate for this intermediate is a CO_2 anion[28,30,31] bound to the Co complex "M":

$$CO_2 + M + e^- \longrightarrow M\text{-}(CO_2^-) \qquad (3)$$

which subsequently reacts with water to a metal-bound carboxyhydroxyl intermediate:

$$M\text{-}(CO_2^-) + H_2O \longrightarrow M\text{-}COOH + OH^- \qquad (4)$$

The formation of the CO_2^- anion normally has a very negative redox potential,[3,8] but may be shifted to less negative potential by the stabilization provided by the coordination of CO_2^- to the catalyst. The carboxyhydroxyl intermediate then generates CO:

$$M\text{-}COOH + e^- \longrightarrow M\text{-}CO + OH^- \qquad (5)$$

with the CO subsequently dissociating from the complex. Due to the presence of the negatively charged intermediate in reaction 4, the pH dependence of this pathway is different from that of the mechanism for reactions 1 and 2, in which no such intermediate is assumed. For reactions 1 and 2, we assume:

$$H^+ + M + e^- \longrightarrow M\text{-}H \qquad (6)$$

$$H^+ + M\text{-}H + e^- \longrightarrow H_2 + M \qquad (7)$$

and,

$$H_2O + M + e^- \longrightarrow M\text{-}H + OH^- \quad (8)$$

$$H_2O + M\text{-}H + e^- \longrightarrow H_2 + M + OH^- \quad (9)$$

which involve concerted proton-coupled electron transfer at every step[32,33]. Reaction 4 is different from the reaction suggested by the DFT calculations of Leung et al., because we specify that the proton donor may be water, rather than H^+, due to the basic character of the CO_2 anion intermediate[23,31]. Note that in this mechanism the reaction rate for CO_2 reduction itself does not depend on pH, only its relative rate with respect to the hydrogen evolution. Another way of formulating our mechanism is by stating that in the potential window of interest, CO_2 reduction is approximately zero-th order in proton concentration, whilst hydrogen evolution is first-order in proton concentration.

The further reduction of CO must be slower than its generation, explaining the relatively low overall Faradaic efficiency of CO_2 reduction to methane. To explain the pH dependence of CO reduction and methane selectivity from CO_2, we must assume that CO is reduced to methane without the involvement of negatively charged intermediates. Our experiments also show that an intermediate or byproduct of CO reduction to methane is formaldehyde. Our suggested overall mechanism is summarized in Figure 5.

The above mechanism, which we believe explains our observations consistently, has important implications for future catalyst design. The onset potential for CO_2 reduction is determined by reaction 3, i.e. by the stabilization of the CO_2 anion coordinated to the complex. As noted above, the onset potential appears to be related to the Co^{II}/Co^{I} redox transition, based on cyclic voltammetry[23] and on the previous observation that the Co^{I} oxidation state is the active state for proton reduction[26]. Nielsen and Leung have also concluded, based on literature data and their own DFT calculations, that CO_2 binds to the Co^+ state of the porphyrin[23,31]. Therefore, we assume that Co^{I} oxidationstate of the CoPP is the catalytically active state. The closer the Co^{II}/Co^{I} redox potential lies to the overall equilibrium potential, the lower the overpotential for CO_2 reduction. Reaction 3 is therefore

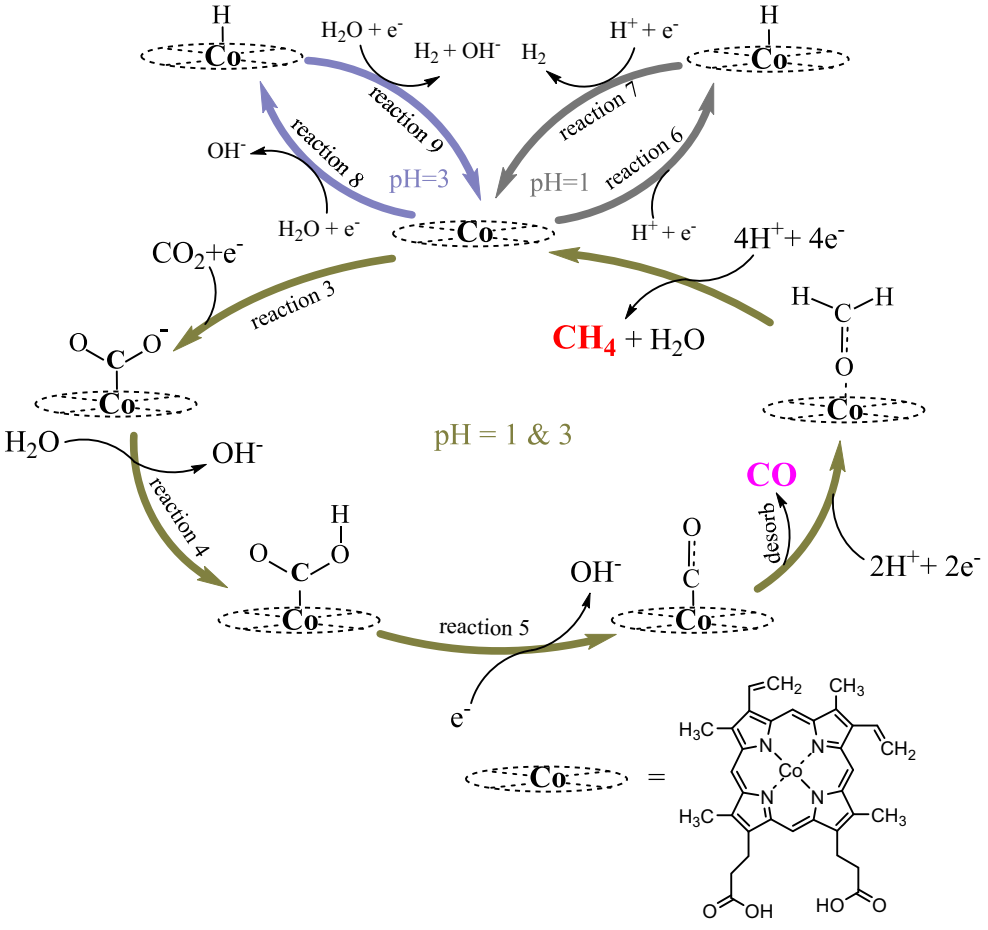

Figure 5 Proposed mechanism scheme for the electrochemical reduction of CO_2 on cobalt-protoporphyrin. H^+ and H_2O are the hydrogen source for the hydrogen evolution reaction at pH=1 and pH=3 respectively. $CO_2^{\bullet-}$ is the initial intermediate for the CO_2 reduction to CO. CO can be further reduced to methane with formaldehyde as an intermediate.

the potential-determining step[34,35]. The key point is that the formation of this intermediate is decoupled from proton transfer, as otherwise we cannot explain the observed pH dependence, an important feature not included in the recent DFT calculations of Tripkovic

et al.[9]. Therefore, future calculations must take into account the existence of such intermediates, and should aim at enhancing the stability of the intermediate in reaction 3. Moreover, in order to have a higher overall efficiency towards methane, the rate of the reduction of CO to methane must be enhanced. Presumably the rate of this reaction can be tuned by the binding of CO to the complex. This will also require further experiments and calculations aimed at screening various catalyst alternatives. We also believe that our mechanism provides a possible rationale for tuning the H_2/CO ratio from electrochemical CO_2 reduction, as was recently reported for Ru-based molecular catalyst in aqueous solution[36].

A final word on the overpotential and the Turnover Frequencies (TOF) of our catalyst compares to previous work on molecular catalysts for CO_2 electroreduction to CO. From our experiment, we calculate TOFs through the formula [FE for CO production] x [current density/2*F] / [number of Co-PP per cm^2]. In Figure 3, the average current densities measured over one hour at potentials of -0.6 and -0.8 V vs. RHE, corresponding to overpotentials of ca. 0.5 and 0.7 V, were 0.08 and 0.16 mA cm^{-2} (at atmospheric pressure), respectively. This corresponds to TOFs of ca. 0.2 s^{-1} and 0.8 s^{-1}. Costentin et al. have recently reported on the enhanced activity of a modified Fe tetraphenylporphyrin for CO_2 reduction to CO in a mixed DMF/water solvent[10]. In their experiment, the porphyrin was in solution. Their measured current densities and corresponding effective CO_2 turnover rates, are very similar to ours, namely 0.3 mA cm^{-2} (see Figure 5 in their paper) at a similar overpotential of ca. 0.5 V. Note that this comparison does not take into account that the solubility of CO_2 is considerably higher in DMF-water mixtures than in water[36] leading to correspondingly higher turnover rates in the DMF-water mixture. From a mathematical model for their reactive system including mass transport of the catalyst to the electrode surface, they report a catalytic TOF of ca. 3000 s^{-1}. This is a TOF of a homogeneous catalyst corrected for the slow mass transport in their system, and can therefore not be compared directly with the “effective” TOF of our heterogeneous catalyst. However, from the similar real current densities at a similar overpotential, we believe that we can safely state that our immobilized catalyst system has a similar efficiency.

2.5. Conclusion

Summarizing, we have shown that a cobalt-protoporphyrin immobilized on a pyrolytic graphite electrode can reduce CO_2 to CO and even to the 6- and 8-electron products methanol and methane, in a purely aqueous electrolyte phase, with a very moderate overpotential of ca. 0.5 V. The efficiency of our catalyst (i.e. effective rate at given overpotential) compares favorably to best porphyrin-based catalyst reported in the literature[10]. For optimal Faradaic efficiency, i.e. low concomitant H_2 production, the proton concentration needs to be suitably tuned to the CO_2 concentration. The pH dependent activity and selectivity are explained by a mechanism in which the initial step of CO_2 reduction leads to a catalyst-bound CO_2^- anion. This intermediate has a strong Brønsted-base character and can abstract a proton from water, thereby leading to an overall reactivity of the CO_2 reduction whose pH dependence is substantially different from the competing H_2 evolution. Lowering the potential for the formation of this catalyst-bound CO_2^- anion is therefore the key to making a better catalyst with a lower overpotential, and a suitable adjustment of pH will contribute significantly to a high Faradaic efficiency of such a catalyst. The further reduction of CO to methane and methanol is slow due to the weak adsorption of CO to the catalyst, and due to the fact that CO reduction prefers a more acidic environment. These new insights into the mechanism of CO_2 reduction on immobilized molecular catalysts in aqueous solution provide important design rules for future catalyst improvement.

2.6. Acknowledgments

J.S. acknowledges the award of a grant of the Chinese Scholarship Council (CSC). This work was financed in part by NanoNextNL, a micro and nanotechnology consortium of the Government of the Netherlands and 130 partners, by the BioSolar Cells open innovation consortium, supported by the Dutch Ministry of Economic Affairs, Agriculture and Innovation, and by The Netherlands Organization for Scientific Research (NWO).

REFERENCES

1 Costentin, C., Robert, M. & Saveant, J.-M. Catalysis of the electrochemical reduction of carbon dioxide. *Chem. Soc. Rev.* **42**, 2423-2436, (2013).

2 Qiao, J., Liu, Y., Hong, F. & Zhang, J. A review of catalysts for the electroreduction of carbon dioxide to produce low-carbon fuels. *Chem. Soc. Rev.* **43**, 631-675, (2014).

3 Hori, Y. Electrochemical CO_2 redcution on metal electrodes. *Modern Aspects of Electrochemistry*. **42**, 89-189 (2008).

4 Finn, C., Schnittger, S., Yellowlees, L. J. & Love, J. B. Molecular approaches to the electrochemical reduction of carbon dioxide. *Chem. Commun.* **48**, 1392-1399, (2012).

5 Koper, M. T. M. Thermodynamic theory of multi-electron transfer reactions: Implications for electrocatalysis. *J. Electroanal. Chem.* **660**, 254-260, (2011).

6 Schouten, K. J. P., Kwon, Y., van der Ham, C. J. M., Qin, Z. & Koper, M. T. M. A new mechanism for the selectivity to C1 and C2 species in the electrochemical reduction of carbon dioxide on copper electrodes. *Chem. Sci.* **2**, 1902-1909, (2011).

7 Li, C. W., Ciston, J. & Kanan, M. W. Electroreduction of carbon monoxide to liquid fuel on oxide-derived nanocrystalline copper. *Nature* **508**, 504-507, (2014).

8 Savéant, J.-M. Molecular Catalysis of Electrochemical Reactions. Mechanistic Aspects. *Chem. Rev.* **108**, 2348-2378, (2008).

9 Tripkovic, V. *et al*. Electrochemical CO_2 and CO Reduction on Metal-Functionalized Porphyrin-like Graphene. *J. Phys. Chem. C* **117**, 9187-9195, (2013).

10 Costentin, C., Drouet, S., Robert, M. & Savéant, J.-M. A Local Proton Source Enhances CO_2 Electroreduction to CO by a Molecular Fe Catalyst. *Science* **338**, 90-94, (2012).

11 Fisher, B. J. & Eisenberg, R. Electrocatalytic reduction of carbon dioxide by using macrocycles of nickel and cobalt. *J. Am. Chem. Soc.* **102**, 7361-7363, (1980).

12 Kapusta, S. & Hackerman, N. Carbon Dioxide Reduction at a Metal Phthalocyanine Catalyzed Carbon Electrode. *J. Electrochem. Soc.* **131**, 1511-1514, (1984).

13 Furuya, N. & Matsui, K. Electroreduction of carbon dioxide on gas-diffusion electrodes modified by metal phthalocyanines. *J. Electroanal. Chem. Interfacial electrochem.* **271**, 181-191, (1989).

14 Sonoyama, N., Kirii, M. & Sakata, T. Electrochemical reduction of CO_2 at metal-porphyrin supported gas diffusion electrodes under high pressure CO_2. *Electrochem. Commun.* **1**, 213-216, (1999).

15 Magdesieva, T. V., Yamamoto, T., Tryk, D. A. & Fujishima, A. Electrochemical Reduction of CO_2 with Transition Metal Phthalocyanine and Porphyrin Complexes Supported on Activated Carbon Fibers. *J.Electrochem. Soc.* **149**, D89-D95, (2002).

16 Atoguchi, T., Aramata, A., Kazusaka, A. & Enyo, M. Cobalt(II)-tetraphenylporphyrin-pyridine complex fixed on a glassy carbon electrode and its prominent catalytic activity for reduction of carbon dioxide. *Chem. Commun*., 156-157, (1991).

17 Yoshida, T. *et al*. Selective electrocatalysis for CO_2 reduction in the aqueous phase using cobalt phthalocyanine/poly-4-vinylpyridine modified electrodes. *J. Electroanal. Chem.* **385**, 209-225, (1995).

18 Tanaka, H. & Aramata, A. Aminopyridyl cation radical method for bridging between metal complex and glassy carbon: cobalt(II) tetraphenylporphyrin bonded on glassy carbon for enhancement of CO_2 electroreduction. *J. Electroanal. Chem.* **437**, 29-35, (1997).

19 Wonders, A. H., Housmans, T. H. M., Rosca, V. & Koper, M. T. M. On-line mass spectrometry system for measurements at single-crystal electrodes in hanging meniscus configuration. *J. Appl. Electrochem.* **36**, 1215-1221, (2006).

20 Kas, R. *et al*. Electrochemical CO_2 reduction on Cu_2O-derived copper nanoparticles: controlling the catalytic selectivity of hydrocarbons. *Phys. Chem. Chem. Phys.* **16**, 12194-12201, (2014).

21 Kas, R., Kortlever, R., Yılmaz, H., Koper, M. T. M. & Mul, G. Manipulating the Hydrocarbon Selectivity of Copper Nanoparticles in CO_2 Electroreduction by Process Conditions. *ChemElectroChem* **2**, 354-358, (2015).

22 Jödecke, M., Pérez-Salado Kamps, Á. & Maurer, G. An Experimental Investigation of the Solubility of CO_2 in (N,N-Dimethylmethanamide + Water). *J. Chem. Eng. Data* **57**, 1249-1266, (2012).

23 de Groot, M. T. & Koper, M. T. M. Redox transitions of chromium, manganese, iron, cobalt and nickel protoporphyrins in aqueous solution. *Phys. Chem. Chem. Phys.* **10**, 1023-1031, (2008).

24 Tao, N. J., Cardenas, G., Cunha, F. & Shi, Z. In Situ STM and AFM Study of Protoporphyrin and Iron(III) and Zinc(II) Protoporphyrins Adsorbed on Graphite in Aqueous Solutions. *Langmuir* **11**, 4445-4448, (1995).

25 de Groot, M. T., Merkx, M., Wonders, A. H. & Koper, M. T. M. Electrochemical Reduction of NO by Hemin Adsorbed at Pyrolitic Graphite. *J. Am. Chem. Soc.* **127**, 7579-7586, (2005).

26 Kellett, R. M. & Spiro, T. G. Cobalt porphyrin electrode films as hydrogen catalysts. *Inorg. Chem.* **24**, 2378-2382, (1985).

27 Diaz-Morales, O., Hersbach, T. J. P., Hetterscheid, D. G. H., Reek, J. N. H. & Koper, M. T. M. Electrochemical and Spectroelectrochemical Characterization of an Iridium-Based Molecular Catalyst for Water Splitting: Turnover Frequencies, Stability, and Electrolyte Effects. *J. Am. Chem. Soc.* **136**, 10432-10439, (2014).

28 Noda, H., Ikeda, S., Yamamoto, A., Einaga, H. & Ito, K. Kinetics of electrochemical redcution of carbon-dioxide on a gole electrode in phosphate buffer solutions. *Bull. Chem. Soc. Jpn.* **68**, 1889-1895, (1995).

29 Strmcnik, D. *et al*. Improving the hydrogen oxidation reaction rate by promotion of hydroxyl adsorption. *Nat. Chem.* **5**, 300-306, (2013).

30 Leung, K., Nielsen, I. M. B., Sai, N., Medforth, C. & Shelnutt, J. A. Cobalt–Porphyrin Catalyzed Electrochemical Reduction of Carbon Dioxide in Water. 2. Mechanism from First Principles. *J. Phys. Chem. A* **114**, 10174-10184, (2010).

31 Nielsen, I. M. B. & Leung, K. Cobalt–Porphyrin Catalyzed Electrochemical Reduction of Carbon Dioxide in Water. 1. A Density Functional Study of Intermediates. *J. Phys. Chem. A* **114**, 10166-10173, (2010).

32 Koper, M. T. M. Theory of the transition from sequential to concerted electrochemical proton-electron transfer. *Phys. Chem. Chem. Phys.* **15**, 1399-1407, (2013).

33 Koper, M. T. M. Theory of multiple proton-electron transfer reactions and its implications for electrocatalysis. *Chem. Sci.* **4**, 2710-2723, (2013).

34 Nørskov, J. K. *et al*. Origin of the Overpotential for Oxygen Reduction at a Fuel-Cell Cathode. *J. Phys. Chem. B* **108**, 17886-17892, (2004).

35 Koper, M. T. M. Analysis of electrocatalytic reaction schemes: distinction between rate-determining and potential-determining steps. *J. Solid State Electrochem.* **17**, 339-344, (2013).

36 Kang, P., Chen, Z., Nayak, A., Zhang, S. & Meyer, T. J. Single catalyst electrocatalytic reduction of CO_2 in water to H_2+CO syngas mixtures with water oxidation to O_2. *Energ. Environ. Sci.* **7**, 4007-4012, (2014).

Chapter 3

DFT Study on the Mechanism of the Electrochemical Reduction of CO_2 Catalyzed by Cobalt Porphyrin

ABSTRACT

The electrochemical reduction of CO_2 is a promising way to store renewable energy in fuels or other chemicals. However, the high overpotential and low efficiency of the reaction hinder the development of the area. More work is needed on the investigation of the mechanism in order to obtain new insights into developing effective catalysts. We report here a density functional theory (DFT) study of the electrochemical reduction of CO_2 on a cobalt porphyrin. The CO_2^- anion adduct is demonstrated to be the key intermediate formed only when the cobalt center of the complex is in the Co^I oxidation state. We find that formic acid can be produced as minor product through $[Co(P)\text{-}(OCHO)]^-$ as intermediate, while CO is the main product through a decoupled electron-proton transfer. CH_4 is produced as minor product from subsequent CO reduction by concerted proton-coupled electron transfer assumed at each electrochemical step. Our theoretical interpretations are consistent with the experimental results presented in Chapter 2, and give deeper insights into the mechanism of the CO_2 electrochemical reduction on cobalt porphyrin complexes.

This chapter has been submitted as: Jing Shen, Manuel J. Kolb, Adrien J. Göttle and Marc T.M. Koper. *J. Phys. Chem.C*.

3.1. Introduction

In nature, carbohydrates are produced from CO_2 from the atmosphere by utilizing sun light through photosynthesis. The fossil energy crisis and current excess emissions of CO_2 urgently call for a new utilization of CO_2. Mimicking natural photosynthesis, the electrochemical reduction of CO_2 is a promising method to store renewable energy such as sunlight and wind into small organic molecules. Different kinds of products can be produced, such as carbon monoxide (CO), formic acid (HCOOH), formaldehyde (HCHO), methanol (CH_3OH), methane (CH_4) and even ethylene (C_2H_4) in aqueous solution[1-4], or oxalate ($C_2O_4^{2-}$) mainly in aprotic solvents. However, there are still challenges in the electrochemical reduction of CO_2. One important challenge is that the reaction requires considerable overpotentials, especially those reactions yielding products that need the transfer of more than 2 electron[5]. The other challenge is that the hydrogen evolution reaction is a competing reaction with CO_2 reduction, which often leads to hydrogen as dominant product (as hydrogen is a 2-electron product).

Different kinds of catalysts have been utilized for the the electrochemical eduction of CO_2 in order to reduce the reaction overpotential. Hori et al. have made a comprehensive investigation on different metal catalysts which give different products depending on the nature of the metal and the experimental conditions[6]. Copper, for which a reasonable understanding of the mechanism has been obtained, is an exceptional catalyst which gives CH_4, C_2H_4 and ethanol (CH_3CH_2OH) as main products[7-9]. Metal complexes, especially with phthalocyanine, porphyrin and cyclam ligands[10-12], have also been used as catalysts for the electrochemical reduction of CO_2 and mainly lead to 2-electron transfer products, such as CO, HCOOH and $C_2O_4^{2-}$ (in aprotic solvents). The speculation on the first intermediate is that it is either a $CO_2^{\bullet-}$ anion radical which gains a proton or a CO_2 that inserts into metal hydride to form –OCHO[9]. Tripkovic et al.[13] have performed first-principles density functional theory calculations on the possible product spectrum of the electrochemical reduction of CO_2 and CO on metal-functionalized porphyrin-like graphene surfaces. HCOOH was found by them as an end product wherea CO is a precursor for more reduced products like methanol and methane. They claim that M-COOH is the key intermediate for

further reaction, which is competing with M-H. Nielsen and Leung et al.[14,15] have investigated in detail the formation of CO on a Co-based porphyrin. Their mechanism involves the $[Co(P)-(CO_2)]^{2-}$ intermediate which is subsequently protonated to give $[Co(P)-(COOH)]^-$. The latter species readily decomposes to give CO. In Chapter 2 we studied the pH dependence of the electrochemical reduction of CO_2 on a cobalt protoporphyrin immobilized on a pyrolytic graphite electrode[16]. From our results, we proposed a mechanism in which a CO_2^- anion adduct forms first. The CO_2^- anion adduct will subsequently be protonated by a water molecule to give the $[Co(P)-(COOH)]^0$ intermediate. The $[Co(P)-(CO)]^0$ intermediate which is formed next will either form CO as a product or be further reduced to CH_4 through a series of concerted proton-electron transfer reactions.

In this Chapter, we report on a theoretical study using DFT calculations of the electrochemical reduction of CO_2 on cobalt porphyrin complex (the simplest porphyrin ligand) in aqueous solution. Our calculations emphasize the anionic character of the CO_2 when bound to the reduced $[Co^IP]^-$ complex. This is due to the charge transfer from the metal center to the substrate upon binding. The formation of CO takes place through the $[Co(P)-(COOH)]^0$ intermediate. The [Co(P)-(OCHO)] intermediate, which gives formic acid as minor product, competes with the formation of the [Co(P)-(COOH)] intermediate. The formation of CH_4 and CH_3OH is studied assuming concerted proton-electron transfer steps.

3.2. Computational Method

DFT calculations have been performed with the Amsterdam Density Functional program (ADF 2014.06)[17]. The revised version of Perdew-Burke-Ernzerhof exchange-correlation functional RPBE[18] was used together with Grimme's dispersion correction D3[19]. For all atoms, a Slater type basis set of triple-ζ quality including a polarization function has been used (TZP)[20]. Geometries have been fully optimized with the conductor-like screening model (COSMO)[21-23] to account for solvation effects (water). We have considered both the low spin and high spin electronic configurations for each geometry. In all cases, the energy of the low spin configuration is the lowest except for the $[Co(P)-(OCHO)]^-$ intermediate. The $[Co(P)-(CH_2)]^-$ intermediate is only stable at high spin state (shown in Appendix B

Table 1). Frequency calculations have been performed to check that the optimized geometries are actual minima on the potential energy surface and also to obtain Gibbs free energies. Since the analytical frequencies are not available in ADF when using D3 dispersion corrections, we used the finite temperature and entropic contributions computed from geometries optimized at the RPBE/TZP/COSMO calculation level and added these contributions to the energy computed with RPBE-D3. The standard equilibrium potentials of electrochemical steps were computing using the computational hydrogen electrode (CHE) model[24]. This model allows treating electrochemical reactions as if they were chemical by making use of the definition of the standard hydrogen electrode. However, the CHE model is restricted to steps in which an equal number of protons and electrons are transferred (concerted proton-electron transfer). The values of the corresponding potentials for concerted proton-electron transferred reactions are calculated as:

$$E^0 = -\Delta G/e$$

Where ΔG is the free energy change of the reaction, e is the elementary charge, and E^0 is the standard equilibrium potential.

3.3. Results and Discussion

3.3.1. Activation of CO_2 to CO and HCOOH

In our recent work[16], we found that the onset potential of both the CO_2 reduction and hydrogen evolution reaction (-0.5 V) is very close to the redox potential of the $Co^{II}P/Co^{I}P$ couple (-0.6 V)[25]. This strongly indicates that the catalytic reaction is triggered by the initial reduction of the catalyst. We also concluded that CO_2 is activated by its association with the reduced catalyst $[Co^{I}P]^-$. Based on literature and their own DFT calculations, Nielsen and Leung et al. have also concluded that CO_2 binds to the Co^{I} oxidation state of the porphyrin[14-15]. In the adduct $[Co(P)-(CO_2)]^-$ that is formed, we assumed that CO_2 is bound as a CO_2^- anion which explains the basicity of this species. Therefore, in the mechanism we proposed from the experiment, the first electro-proton pair addition goes through a

decoupled electron transfer-proton transfer (ET-PT) mechanism. The corresponding sequence of reactions proposed is therefore:

$$[CoP]^0 + e^- \longrightarrow [CoP]^- \quad (1)$$

$$[CoP]^- + CO_2 \longrightarrow [Co(P)\text{-}(CO_2)]^- \quad (2)$$

We have investigated the basic character of the $[Co(P)\text{-}(CO_2)]^0$ and $[Co(P)\text{-}(CO_2)]^-$ adduct as they are the key point to explain the pH dependence of the CO_2 reduction observed experimentally. To do so, we have performed a Mulliken charge analysis of $[CoP]^0$ and $[CoP]^-$ intermediates to know where the additional charge is localized after reduction of the catalyst (eq. 1), and of the $[CoP\text{-}CO_2]^-$ adduct to address how the charge is redistributed upon the binding of CO_2 to the reduced catalyst (eq. 2). Both $[CoP]^0$ and $[CoP]^-$ complexes have a planar structure. The Co-N distance in $[CoP]^-$ is 1.976 Å which is slightly shorter than in $[CoP]^0$, which is 1.994 Å. The Mulliken charge on cobalt center is +0.87 for $[CoP]^0$ and +0.47 for $[CoP]^-$, respectively, while the charges on nitrogen atoms are -0.52 for both molecules. Therefore, in the negatively charged porphyrin, a significant amount of the extra negative charge is located on cobalt atom. We have tried to optimize CO_2 adduct with both the neutral and negatively charged complex. Any attempt to optimize CO_2 adduct with the neutral complex failed, which indicates that the neutral CO_2 adduct is not stable (no minimum on the potential energy surface). By contrast, we managed to optimize the negatively charged CO_2 adduct, $[Co(P)\text{-}(CO_2)]^-$. It is important to note that the negatively charged CO_2 adduct is not stable without solvation. This can be explained by the fact that a significant charge transfer from the cobalt atom to the CO_2 adduct occurs upon the binding process, and the presence of a polar solvent is crucial to stabilize this charge transfer process. However, the binding process is almost thermoneutral (see Table 1). The structure of $[Co(P)\text{-}(CO_2)]^-$ complex is shown in Figure 1(a) and some relevant parameters have been collected in Table 1. In the $[Co(P)\text{-}(CO_2)]^-$ molecule, the distances of Co-N bonds are 1.991 Å which are elongated compared to the bare $[CoP]^-$ molecule. This may indirectly indicate that the electronic state of cobalt center has been changed upon CO_2 binding, back to the length of the Co-N bonds corresponding to the neutral $[CoP]^0$ complex

with Co^{II} oxidation state. The bond angle of O-C-O of adsorbed CO_2 is 134° . Compared to the bond angle of O-C-O of the CO_2 gas-phase molecule (180°), adsorbed CO_2 is bent. The calculated bond angle of O-C-O for CO_2^- in the gas phase is 133.2°. The Mulliken charge analysis for $[Co(P)-(CO_2)]^-$ and gas-phase CO_2 molecule shows that the charge on the cobalt atom in $[Co(P)-(CO_2)]^-$ molecule is +0.62, and the total charge on CO_2 molecule is -0.61 with +0.56 on the C atom and -0.59 on the two O atoms. Compared to the charge centered on cobalt atom of $[CoP]^-$ (+0.47) and on the carbon and oxygen atoms of gas CO_2 molecule, +0.87 and -0.44, respectively, we conclude that there is partial charge transfer from cobalt atom to CO_2 in $[Co(P)-(CO_2)]^-$ complex. In order to understand the origin of this charge transfer, we have analyzed the interaction between the cobalt and CO_2 using the molecular orbitals. Figure 1b shows the space representation of the HOMO-2 orbital which is responsible for most of the interaction between the cobalt and CO_2 in the $[Co(P)-(CO_2)]^-$ molecule. In Appendix B Figure 2, we also show the space representations of the first four highest occupied molecular orbitals (HOMO to HOMO-3). From Appendix B Figure 2 we can see that HOMO and HOMO-1 orbitals show no interaction between cobalt atom and CO_2 adduct, while HOMO-2 and HOMO-3 orbitals contribute to the interaction with different orientation. Therefore, we mainly focus on the HOMO-2 orbital to obtain an insight into the charge transfer. From Figure 1b we see that this orbital consists of the mixing of a hybrid metallic orbital (d_z^2 (ca. 20%) and d_x^2-$_y^2$ (ca. 40%)) with the antibonding π* orbital (ca. 40%) of CO_2. Therefore, the orbital interaction between the Co *d* state and the CO_2 π* orbital leads to a net charge delocalization from the cobalt to the CO_2. A similar conclusion was reached by Meshitsuka et al.[26] who suggested that the occupied d_z^2 orbital of the metal atom of a phthalocyaline complex plays an important role in the activation of CO_2.

To unravel the details of the mechanism of the CO_2 reduction to CO, we have first computed the equilibrium potential of the reaction step where the binding of the substrate and both the proton and electron addition are concerted (shown in Table 2).

$$[CoP]^0 + CO_2 + H^+ + e^- \longrightarrow [CoP\text{-}COOH]^0 \qquad (3)$$

Table 1: Binding of CO_2 to $[CoP]^-$ including solvation.

ΔG/ eV	q_{CO2} *	q_{Co} *	∠OCO /° *	r_{Co-N} /Å *
0.09	-0.61 (0)	0.62 (0.47)	134 (180)	1.991 (1.976)

* The numbers in the brackets correspond to the value of the CO_2 gas molecule and $[CoP]^-$ in their non-bonded state.

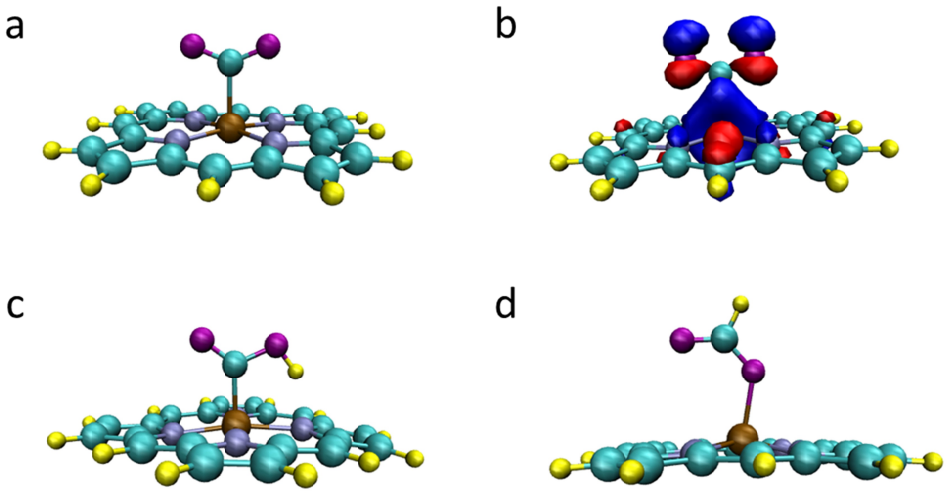

Figure 1 Optimized geometries of intermediates: (a) CO_2^- anion adduct on $[CoP]^-$, i.e. $[Co(P)\text{-}(CO_2)]^-$; (b) spatial representation of HOMO orbital of $[Co(P)\text{-}(CO_2)]^-$; (c) negatively-charged $[Co(P)\text{-}(COOH)]^-$ intermediate; (d) negatively charged $[Co(P)\text{-}(OCHO)]^-$ intermediate.

The computed equilibrium potential of this reaction (-0.43 V, shown in Table 2) is similar to the onset potential found experimentally (-0.5V). Therefore, we will refer to this potential as E_{onset}. This indicates that the concerted pathway can proceed, based on its thermodynamics, for E_{onset} and more negative potentials. As mentioned, any attempts to try to optimize the neutral $[Co(P)\text{-}(CO_2)]^0$ adduct invariably resulted in the dissociation of CO_2 from the complex. In contrast, we managed to optimize the anionic $[Co(P)\text{-}(CO_2)]^-$ adduct.

Furthermore, we have checked how the energy of the neutral and anionic complexes [Co(P)-(CO_2)] varies as the CO_2 approaches the metallic center at large Co-$C_{(CO2)}$ distances (shown in Appendix B Figure 1). To do so, we have created constrained structures corresponding to the optimized structure of the [Co(P)-(CO_2)]$^-$ adduct for which the Co-$C_{(CO2)}$ distance is elongated by 1 Å and decreased step by step the Co-$C_{(CO2)}$ distance to its initial value while all other parameters were fully relaxed at each step (relaxed scan). The corresponding energy profiles are reported in Appendix B (Figure 1). For the anionic complex, the energy continues to decrease as the CO_2 approaches the cobalt. The binding of CO_2 to the reduced catalyst (eq. 2) is therefore a barrierless process. In contrast, the energy increases for the neutral complex following the same reaction coordinate ($\Delta E \sim 0.7$ eV when Co-C distance is elongated by 0.5 Å from its optimized value in [Co(P)-(CO_2)]$^-$). This suggests that for the neutral complex the activation energy for the concerted pathway is large as the transition state of this step necessarily requires the approach between CO_2 and the catalyst. As a result, although the concerted pathway is possible based on its thermodynamics when $E_{applied} \leqslant -0.43$ V, it is kinetically slow or even hindered at room temperature due to a large thermal activation barrier. In contrast, as the association of CO_2 with the reduced catalyst has no thermal activation barrier (though we emphasize that this "barrier" is not a free energy barrier since no entropy corrections were included), the formation of the [Co(P)-(CO_2)]$^-$ adduct can readily proceed whenever the applied potential is suitable. The conclusion from our calculations is in agreement with what we proposed from the experimental results with the formation of the [Co(P)-(CO_2)]$^-$ intermediate.

Table 2: Computed equilibrium potentials for indicated reactions.

	Reaction Equation	E^0 /V_{RHE} With solvation
Reaction (3)	$[CoP]^0 + CO_2 + H^+ + e^- \longrightarrow [Co(P)\text{-}(COOH)]^0$	-0.43
Reaction (5)	$[Co(P)\text{-}(CO_2)]^- + H^+ + e^- \longrightarrow [Co(P)\text{-}(COOH)]^-$	-1.01
Reaction (6)	$[Co(P)\text{-}(COOH)]^0 + H^+ + e^- \longrightarrow [Co(P)\text{-}(CO)]^0 + H_2O$	0.16
Reaction (7)	$[Co(P)]^0 + CO_2 + H^+ + e^- \longrightarrow [Co(P)\text{-}(OCHO)]^0$	-0.92
Reaction (8)	$[Co(P)\text{-}(CO_2)]^- + H^+ + e^- \longrightarrow [Co(P)\text{-}(OCHO)]^-$	-0.21
Reaction (10)	$[Co(P)\text{-}(OCHO)]^- + H^+ + e^- \longrightarrow [CoP]^- + HCOOH$	-0.07
Reaction (11)	$[Co(P)\text{-}(OCHO)]^- + H^+ + e^- \longrightarrow [Co(P)\text{-}(OCH_2O)]^-$	-1.79
Reaction (12)	$[CoP]^0 + H^+ + e^- \longrightarrow [Co(P)\text{-}(H)]^0$	-0.23
Reaction (13)	$[CoP]^- + H^+ + e^- \longrightarrow [Co(P)\text{-}(H)]^-$	-0.10

After the formation of [Co(P)-(CO2)]-, the next step can be either the protonation or the hydrogenation of this reaction intermediate:

$$[Co(P)\text{-}(CO_2)]^- + H^+ \longrightarrow [Co(P)\text{-}(COOH)]^0 \quad (4)$$

$$[Co(P)\text{-}(CO_2)]^- + H^+ + e^- \longrightarrow [Co(P)\text{-}(COOH)]^- \quad (5)$$

The structure of the $[Co(P)\text{-}(COOH)]^-$ intermediate is displayed in Figure 1c. $[Co(P)\text{-}(COOH)]^0$ has a similar structure as the negatively charged complex. The latter has a shorter $Co\text{-}C_{(COOH)}$ bond length than the former which indicates a stronger interaction between the cobalt atom and the $C_{(COOH)}$ in $[Co(P)\text{-}(COOH)]^-$. Reaction step (5) has a relatively negative equilibrium potential (-1.01 V, see in Table 2), much more negative than the onset potential (-0.5 V). Therefore, the formation of the $[Co(P)\text{-}(COOH)]^-$ intermediate is unlikely if the applied potential is close to the onset potential. Therefore, after formation of $[Co(P)\text{-}(CO_2)]^-$, reaction (4) is likely to occur to form the neutral $[Co(P)\text{-}(COOH)]^0$

intermediate. The sequence of reactions predicted by our calculations (1), (2) and (4) matches the decoupled ET-PT mechanism we proposed from the experimental results[16].

After the formation of the $[Co(P)\text{-}(COOH)]^0$ intermediate, it can be subsequently undergo the following concerted electron-proton transfer step:

$$[Co(P)\text{-}(COOH)]^0 + H^+ + e^- \longrightarrow [Co(P)\text{-}(CO)]^0 + H_2O \quad (6)$$

The equilibrium potential of this reaction step is 0.16 V which indicates that it should spontaneously occur at applied potentials $E \leqslant E_{onset}$. The $[Co(P)\text{-}(CO)]^0$ intermediate can either desorb CO (the binding energy of CO is -0.26 eV) or the bound CO can be further reduced to CH_4 (see below).

Apart from the formation of the ''carboxyhydroxyl" $[Co(P)\text{-}(COOH)]^0$ and $[Co(P)\text{-}(COOH)]^-$ intermediates, "formate-type" intermediates $[Co(P)\text{-}(OCHO)]^0$ and $[Co(P)\text{-}(OCHO)]^-$ (the structure of $[Co(P)\text{-}(OCHO)]^-$ is shown in Figure 1d) can be produced through alternative competing reaction pathways. We assume this "formate-type" intermediate can be produced through the following reaction steps:

$$[CoP]^0 + CO_2 + H^+ + e^- \longrightarrow [Co(P)\text{-}(OCHO)]^0 \quad (7)$$

$$[CoP\text{-}CO_2]^- + H^+ + e^- \longrightarrow [Co(P)\text{-}(OCHO)]^- \quad (8)$$

Like reaction (3), reaction step (7) is associated with the concerted substrate binding and electron-proton transfer. Its equilibrium potential is significantly negative (-0.92 V). In contrast, the equilibrium potential of reaction (8) is much less negative (-0.21 V). It is noteworthy that any attempts to optimize, from a premade structure, a [Co(P)-(OCHO)] adduct where the CO_2 is bonded by one oxygen to the Co center, failed and invariably resulted in the dissociation of the CO_2 for both neutral and anionic charge state. Like for the formation of $[Co(P)\text{-}(COOH)]^0$ through the fully concerted pathway (reaction (3)), reaction (8) is probably kinetically hindered by a large thermal activation barrier due to the switching of the binding mode of the CO_2 from C-bonded to O-bonded to form [Co(P)-

$(OCHO)]^-$. After the formation of $[Co(P)-(OCHO)]^-$, the next possible steps can be either the protonation (reaction (9)) or the concerted electron-proton transfer (reaction (10)) to form formic acid as final product:

$$[Co(P)-(OCHO)]^- + H^+ \longrightarrow [CoP]_0 + HCOOH \quad (9)$$

$$[Co(P)-(OCHO)]^- + H^+ + e^- \longrightarrow [CoP]^- + HCOOH \quad (10)$$

Or, if no desorption occurs, the concerted electron-proton transfer can form the intermediate $[Co(P)-(OCH_2O)]^-$:

$$[Co(P)-(OCHO)]^- + H^+ + e^- \longrightarrow [Co(P)-(OCH_2O)]^- \quad (11)$$

The equilibrium potential of reaction (11) is -1.79 V which is much more negative than the experimental onset potential. This indicates that this reaction is unlikely to occur in the potential range we investigated (0 V~-1.5 V). This is consistent with the results obtained for the electrochemical reduction of formic acid by combining on-line electrochemical mass spectroscopy (OLEMS) and cyclic voltammetry (CV) which show that this species cannot be further reduced and is thus an end product.

CO_2 could also insert into metal hydride to form the [Co(P)-(OCHO)] intermediate. The formation of the neutral and negatively charged metal hydride is through the following reactions:

$$[CoP]^0 + H^+ + e^- \longrightarrow [Co(P)-(H)]^0 \quad (12)$$

$$[CoP]^- + H^+ + e^- \longrightarrow [Co(P)-(H)]^- \quad (13)$$

As shown in Table 2, the equilibrium potentials for reaction (12) and (13) are -0.23 V and -0.10 V, respectively. This indicates that metal hydride is thermodynamically easy to form at E_{onset}. After the formation of metal hydride, H_2 could be produced spontaneously through a concerted proton-electron transfer process with the equilibrium potential of 0.23 V and 0.10 V for the neutral and negatively charged metal hydride, respectively.

Simultaneously, CO_2 could insert into metal hydride as a competing reaction through a chemical step; the free energies (ΔG) for the formation of the $[Co(P)-(OCHO)]^0$ and $[Co(P)-(OCHO)]^-$ intermediate from the final states ort reaction (12) and (13) are 0.69 eV and 0.20 eV, respectively.

Finally, as far as the competition between the formation of CO and formic acid is concerned, when the applied potential is close to the onset potential the selectivity between the two products is governed by the relative efficiencies of the reaction pathways that leads to their formation: the sequence of reactions (1), (2), (8) and (9) or (10) for formic acid formation and sequence of reactions (1), (2), (4) and (6) for CO formation. Since reaction (8) is presumably kinetically slow due to the switching of the CO_2 binding mode, the formation of formic acid is less competitive than the formation of CO. This is consistent with our experimental work in which we found that formic acid is produced as a minor product.

3.3.2. Reduction of CO to CH_4

In the previous section, we studied the formation of [Co(P)-(COOH)] which will form the [Co(P)-(CO)] as the next intermediate. This weakly bonded CO can either be released from complex to form the main product CO or be further reduced to produce CH_4 as minor final product. We speculate that the formation of CH_4 involves concerted proton-coupled electron transfer at each step. Therefore, pathways for CH_4 formation have been calculated using the CHE model. Figure 2 shows the most favorable pathway at two different potentials. The intermediate [Co(P)-(CO)] is first hydrogenated by proton-electron transfer to form [Co(P)-(CHO)], which will be further hydrogenated to form $[Co(P)-(OCH_2)]$. Experimentally, we confirmed that formaldehyde is probably an intermediate for CH_4 formation as the electrochemical reduction of formaldehyde and CO_2 under same conditions both give methane[16]. $[Co(P)-(OCH_2)]$ is subsequently hydrogenated to form the $[Co(P)-(OCH_3)]$ intermediate. Thermodynamically $[Co(P)-(OCH_3)]$ prefers to form methanol as product as compared to [Co(P)-(O)] and CH_4 as Tripkovic et al. have shown previously[13]. In our experiments, no significant amount of methanol was detected. In order

to make sure if methanol could be an intermediate for CH_4 formation from the CO_2 electrochemical reduction, the electrochemical reduction of methanol was studied under the same conditions as CO_2 reduction in Chapter 2[16] by combining CV (Cyclic Voltammetry) with OLEMS. The result is shown in Figure 3, showing that hydrogen is the main product but with CH_4 as minor by-product, which must be the result of methanol reduction. Therefore, we conclude that at sufficiently negative potential methanol may be reduced to CH_4. According to our DFT calculations, application of a potential of -0.51 V (vs RHE) makes the whole pathway from CO_2 to methane downhill, as shown by the brown line in Figure 2. This applied potential of -0.51 V is the onset potential for the potential-determining step in the mechanism, which agrees quite well with the onset potential we observe in experiment. At this potential, [Co(P)-(O)] is unstable and methanol will be reduced to methane.

Competing pathways have also been calculated, as shown in Figure 2, in addition to the most favorable pathway. The formation of [Co(P)-(COH)] is a competing reaction with [Co(P)-(CHO)] formation. The free energy change calculated for [Co(P)-(COH)] formation is 2.34 eV (with a corresponding potential of -2.34 V), which indicates that [Co(P)-(COH)] formation is thermodynamically unfavorable. [Co(P)-(CH_2O)] is a competing intermediate with [Co(P)-OCH_2]. The free energy difference for the reaction from [Co(P)-(CHO)] to [Co(P)-(CH_2O)] is -0.45 eV indicating a thermodynamically favorable reaction. The subsequent protonation of [Co(P)-(CH_2O)] will sequentially form the [Co(P)-(CH_2OH)] and [Co(P)-(CH_2)] intermediates. The free energy changes for these two reactions are 0.77 eV and 0.81 eV, respectively. The high free energy changes for both intermediates indicate that the further reduction of [Co(P)-(CH_2O)] is not thermodynamically favorable. Therefore we consider [Co(P)-(CH_2O)] an unlikely intermediate in a pathway toward methane formation, though ultimately the calculation of the free energy barrier will be necessary to determine which intermediate leads to [Co(P)-(OCH_3)] and finally to methane. Both [Co(P)-(OCH_2)] and [Co(P)-(CH_2O)] may dissociate from the complex to form formaldehyde. The free energy changes for those two processes are -0.93 eV and -0.03 eV, respectively. Note that, in the CHE method, application of a potential U pulls down the free energy change of each electrochemical step by eU eV, but has no effect on the energetics of a chemical reaction.

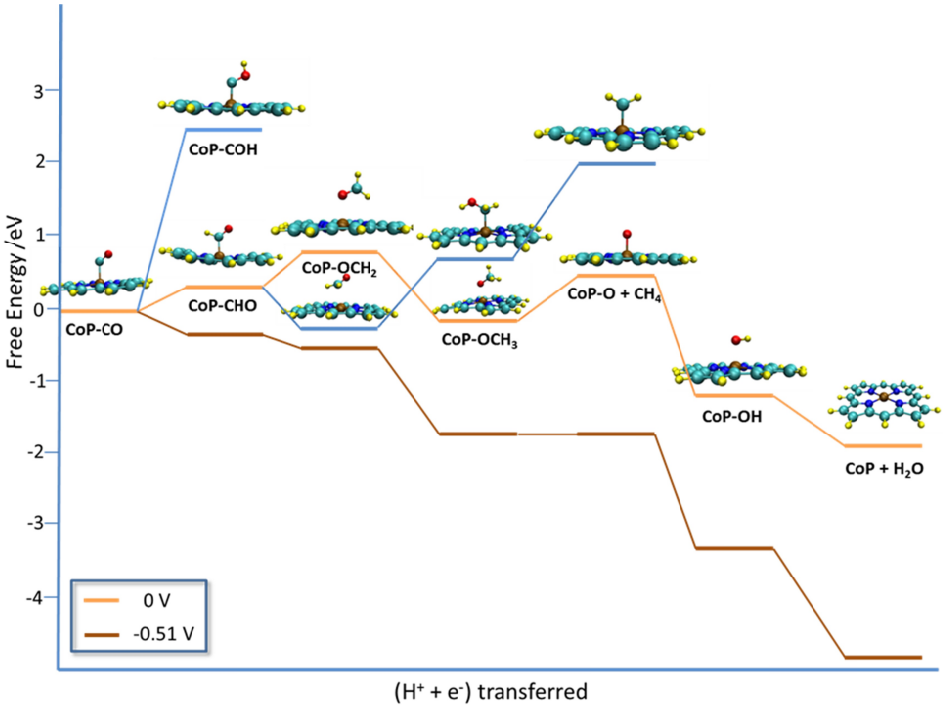

Figure 2 The possible pathways for CH_4 formation from [Co(P)-(CO)]. The Figure shows the most favorable pathway with applied potential U = 0 V (orange line), and the most favorable pathway with applied potential U = -0.51 V (brown lines), which makes each step downhill. Competing pathways are showing in blue lines.

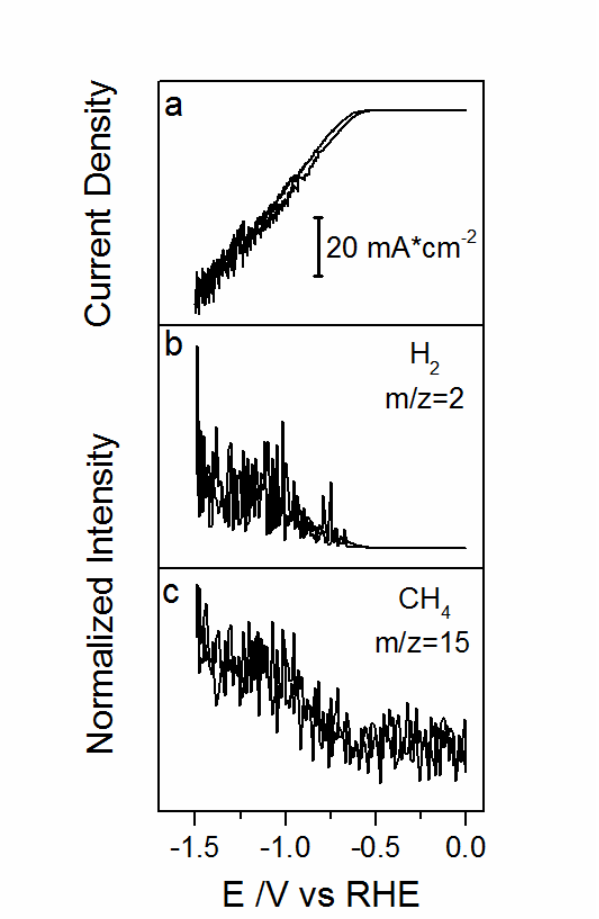

Figure 3 OLEMS measurements of the electrochemical reduction of methanol in 0.1 M $HClO_4$ solution with cyclic voltammetry, the concentration of methanol is 0.05 mol/L. (a) Cyclic Voltammetry, scan rate: 1 mV s^{-1}; (b) H_2 formation measured using OLMES, m/z=2; (c) CH_4 formation measured using OLEMS, m/z=15, the signal is not corrected from methanol. The OLEMS signal has been normalized by dividing the signal with the highest ion current. All experimental conditions as in ref[16].

3.4. Conclusions

In Chapter 2, we concluded that during electrocatalytic CO_2 reduction a CO_2^- anion bound to a Co-porphyrin is produced and acts as a Brønsted-base abstracting a proton from a nearby water molecule to form the [Co(P)-(COOH)] intermediate. Our DFT calculations presented here show that the Co^I oxidation state is the catalytically active state for [Co(P)-(CO_2)]$^-$ formation, in agreement with previous work by Nielsen and Leung[14-15], and consistent with our conclusions from the experiments. In the [Co(P)-(CO_2)]$^-$ complex, there is effective electron transfer from the Co atom to the CO_2 through the interaction between the hybrid $d_{x^2-y^2}$ and d_{z^2} orbital of the Co and the π^* antibonding orbital of the CO_2 such that the CO_2 resembles a CO_2^- anion and Co regains some of its Co^{II} character. Proper solvation correction appears to be very important for obtaining reliable energetics, underscoring the charge transfer character of the complex.

The formation of the [Co(P)-(COOH)]^n (n=0 or -1) intermediate through the concerted electron-proton transfer step is not favorable. The equilibrium potential of the formation of [Co(P)-(COOH)]^0 is slightly less negative than the experimental onset potential. However, CO_2 does not adsorb on the [CoP]^0 intermediate. The formation of [Co(P)-(COOH)]$^-$ has a large negative equilibrium potential, which makes it is thermodynamically unfavorable. Therefore, the formation of the [Co(P)-(COOH)]^n (n=0 or -1) goes through a decoupled electron-proton transfer process, with [Co(P)-(CO_2)]$^-$ as an intermediate. The [Co(P)-(COOH)]^0 intermediate reacts with a further electron and proton to produce [Co(P)-(CO)], which subsequently leads to either the formation of CO or to the transfer of more electrons and protons to produce the 8-electron transfer product CH_4.

The formation of the [Co(P)-(OCHO)] intermediate undergoing a concerted electron-proton transfer step is a competing reaction with the formation of the [Co(P)-(COOH)] intermediate. The formation of [Co(P)-(OCHO)]^0 is thermodynamically difficult as the equilibrium potential of the reaction is significantly negative (-0.92V). In contrast, the equilibrium potential of the formation of the [Co(P)-(OCHO)]$^-$ intermediate is less negative than experimental onset potential. However, it is probably kinetically slow as the

binding atom of CO_2 changed from C-bounded to O-bounded. The formic acid can be produced from the hydrogenation or protonation of the [Co(P)-(OCHO)] intermediate. Therefore, the formic acid is a minor product compare to the CO. The further reduction of [Co(P)-(OCHO)] is difficult because of the negative equilibrium potential for the formation of $[Co(P)-(OCH2O)]^-$, -1.79 V. From our experiments, we indeed found only a minor amount of formic acid formation and that the formic acid was not further reduced.

The formation of CH_4 from CO reduction was studied using the CHE model. Formaldehyde and methanol are the competing intermediates and products with methane. Formaldehyde has already been confirmed as the intermediate for the CH_4 formation in our prior experiments. The formation of methanol is more favorable than the formation of CH_4 from our calculations at low potential, due to the weak bonding of atomic oxygen to the [CoP]. However, at more negative potential, methane is the thermodynamically preferred. The electrochemical reduction of methanol conducted by combining CV and OLEMS indeed shows the formation of CH_4 from methanol.

In conclusion, DFT calculations suggest a relatively consistent mechanism for the electrochemical reduction of CO_2 with good agreement between theory and experiment. These new insights offer opportunities to design new catalysts for the CO_2 electrochemical reduction.

3.5. Acknowledgements

J.S. acknowledges the award of a grant of the Chinese Scholarship Council (CSC). This work was supported by the TOP grant from the Netherlands Organization for Scientific Research (NWO). This work is part of the programme 'CO_2 neutral fuels' of the Foundation for Fundamental Research on Matter (FOM), which is financially supported by NWO, co-financed by Shell Global Solutions International B.V..

REFERENCES

1. Hori, Y.; Kikuchi, K.; Suzuki, S., Production of CO and CH_4 in Electrochemical Reduction of CO_2 at Metal Electrodes in Aqeous Hydrogencarbonate Solution. *Chem. Lett.* **1985**, *14*, 1695-1698.

2. Hori, Y.; Murata, A.; Takahashi, R., Formation of Hydrocarbons in the Electrochemical Reduction of Carbon Dioxide at a Copper Electrode in Aqueous Solution. *J. Chem. Soc. Faraday Trans.* **1989**, *85*, 2309-2326.

3. Fisher, B. J.; Eisenberg, R., Electrocatalytic Reduction of Carbon Dioxide by Using Macrocycles of Nickel and Cobalt. *J. Am. Chem. Soc.* **1980**, *102*, 7361-7363.

4. Kortlever, R.; Balemans, C.; Kwon, Y.; Koper, M. T. M., Electrochemical CO2 Reduction to Formic Acid on a Pd-Based Formic Acid Oxidation Catalyst. *Catal. Today* **2015**, *244*, 58-62.

5. Koper, M. T. M., Thermodynamic Theory of Multi-Electron Transfer Reactions: Implications for Electrocatalysis. *J. Electroanal. Chem.* **2011**, *660*, 254-260.

6. Hori, Y. Electrochemical CO_2 Redcution on Metal Electrodes, *Modern Aspects of Electrochemistry*. **2008**.

7. Peterson, A. A.; Abild-Pedersen, F.; Studt, F.; Rossmeisl, J.; Norskov, J. K., How Copper Catalyzes the Electroreduction of Carbon Dioxide into Hydrocarbon Fuels. *Energ. Environ. Sci.* **2010**, *3*, 1311-1315.

8. Schouten, K. J. P.; Kwon, Y.; van der Ham, C. J. M.; Qin, Z.; Koper, M. T. M., A New Mechanism for the Selectivity to C1 and C2 Species in the Electrochemical Reduction of Carbon Dioxide on Copper Electrodes. *Chem. Sci.* **2011**, *2*, 1902-1909.

9. Kortlever R.; Shen J.; Schouten K. J. P.; Calle-Vallejo F.; Koper M. T. M., Catalysts and Reaction Pathways for the Electrochemical Reduction of Carbon Dioxide. *J. Phys. Chem. Lett.* **2015**, 6, 4073-4082.

10. Beley, M.; Collin, J. P.; Ruppert, R.; Sauvage, J. P., Electrocatalytic Reduction of Carbon Dioxide by Nickel $Cyclam^{2+}$ in Water: Study of the Factors Affecting the Efficiency and the Selectivity of the Process. *J. Am. Chem. Soc.* **1986**, *108*, 7461-7467.

11. Yoshida, T.; Kamato, K.; Tsukamoto, M.; Iida, T.; Schlettwein, D.; Wöhrle, D.; Kaneko, M., Selective Electroacatalysis for CO_2 Reduction in the Aqueous Phase Using Cobalt Phthalocyanine/Poly-4-Vinylpyridine Modified Electrodes. *J. Electroanal. Chem.* **1995**, *385*, 209-225.

12. Sonoyama, N.; Kirii, M.; Sakata, T., Electrochemical Reduction of CO_2 at Metal-Porphyrin Supported Gas Diffusion Electrodes under High Pressure CO_2. *Electrochem. Commun.* **1999**, *1*, 213-216.

13. Tripkovic, V.; Vanin, M.; Karamad, M.; Björketun, M. E.; Jacobsen, K. W.; Thygesen, K. S.; Rossmeisl, J., Electrochemical CO_2 and CO Reduction on Metal-Functionalized Porphyrin-Like Graphene. *J. Phys. Chem. C* **2013**, *117*, 9187-9195.

14. Leung, K.; Nielsen, I. M. B.; Sai, N.; Medforth, C.; Shelnutt, J. A., Cobalt–Porphyrin Catalyzed Electrochemical Reduction of Carbon Dioxide in Water. 2. Mechanism from First Principles. *J. Phys. Chem. A,* **2010**, *114*, 10174-10184.

15. Nielsen, I. M. B.; Leung, K., Cobalt–Porphyrin Catalyzed Electrochemical Reduction of Carbon Dioxide in Water. 1. A Density Functional Study of Intermediates. *J. Phys. Chem. A,* **2010**, *114*, 10166-10173.

16. Shen J.; Kortlever R.; Kas R.; Birdja Y. Y.; Diaz-Morales O.; Kwon Y.; Ledezma-Yanez I.; Schouten K. J. P.; Mul G.; Koper M. T.M., Electrocatalytic Reduction of Carbon Dioxide to Carbon Monoxide and Methane at an Immobilized Cobalt Protoporphyrin in Aqueous Solution. *Nat. Commun.* **2015**, 6, article number:8177.

17. te Velde, G.; Bickelhaupt, F. M.; Baerends, E. J.; Fonseca Guerra, C.; van Gisbergen, S. J. A.; Snijders, J. G.; Ziegler, T., Chemistry with Adf. *J. Comput. Chem.* **2001**, *22*, 931-967.

18. Hammer, B.; Hansen, L. B.; Nørskov, J. K., Improved Adsorption Energetics within Density-Functional Theory Using Revised Perdew-Burke-Ernzerhof Functionals. *Phys.Review B* **1999**, *59*, 7413-7421.

19. Grimme, S.; Antony, J.; Ehrlich, S.; Krieg, H., A Consistent and Accurate Ab Initio Parametrization of Density Functional Dispersion Correction (Dft-D) for the 94 Elements H-Pu. *J. Chem. Phys.* **2010**, *132*, 154104.

20. Van Lenthe, E.; Baerends, E. J., Optimized Slater-Type Basis Sets for the Elements 1–118. *J. Comput. Chem.* **2003**, *24*, 1142-1156.

21. Klamt, A.; Schuurmann, G., Cosmo: A New Approach to Dielectric Screening in Solvents with Explicit Expressions for the Screening Energy and Its Gradient. *J. Chem. Soc. Perkin Trans. 2* **1993**, 799-805.

22. Klamt, A., Conductor-Like Screening Model for Real Solvents: A New Approach to the Quantitative Calculation of Solvation Phenomena. *J. Phys. Chem.* **1995**, *99*, 2224-2235.

23. Klamt, A.; Jonas, V., Treatment of the Outlying Charge in Continuum Solvation Models. *J. Chem. Phys.* **1996**, *105*, 9972-9981.

24. Nørskov, J. K.; Rossmeisl, J.; Logadottir, A.; Lindqvist, L.; Kitchin, J. R.; Bligaard, T.; Jónsson, H., Origin of the Overpotential for Oxygen Reduction at a Fuel-Cell Cathode. *J. Phys. Chem. B* **2004**, *108*, 17886-17892.

25. de Groot, M. T.; Koper, M. T. M., Redox Transitions of Chromium, Manganese, Iron, Cobalt and Nickel Protoporphyrins in Aqueous Solution. *Phys. Chem. Chem. Phys.* **2008**, *10*, 1023-1031.

26. Meshitsuka, S.; Ichikawa, M.; Tamaru, K., Electrocatalysis by Metal Phthalocyanines in the Reduction of Carbon Dioxide. *Chem. Commun.* **1974**, 158-159.

Chapter 4

Electrocatalytic Nitrate Reduction by a Cobalt Protoporphyrin Immobilized on a Pyrolytic Graphite Electrode

ABSTRACT

A series of simple molecular catalysts, i.e. Cobalt (III), Iron (II), Nickel (II), Copper (II) and Rhodium (II) protoporphyrins (metal-PP), directly adsorbed on pyrolytic graphite, has been utilized for catalyzing the electrochemical reduction of nitrate. These catalysts are studied by combining cyclic voltammetry with online electrochemical mass spectrometry (OLEMS), to monitor volatile products, and online ion chromatography (IC), to detect ionic products in the aqueous electrolyte solution. Among all investigated porphyrins, the Co-based protoporphyrin shows highest selectivity towards hydroxylamine (NH_2OH), which made it the catalyst of primary interest in the paper. The reactivity and selectivity of the immobilized Co-protoporphyrin depends significantly on pH, more acidic conditions leading to higher reactivity and higher selectivity towards hydroxylamine over ammonia. Potential controlled electrolysis results show that the potential also greatly influences the selectivity: at pH 1, hydroxylamine is the main product around -0.5 V with approximately 100% selectivity, while hydroxylamine and ammonia are both formed at more negative potential, -0.75 V. The mechanism of the reaction is discussed, invoking of the possibility of two pathways for hydroxylamine/ammonia formation: a sequential pathway, in which hydroxylamine is produced as an intermediate, with ammonia subsequently formed through reduction of NH_2OH/NH_3OH^+; and a parallel pathway, in which the formation of hydroxylamine and ammonia derives from a common intermediate.

The contents of this chapter has been published in: Jing Shen, Yuvraj Y. Birdja and Marc T.M. Koper. Langmuir, **2015**, 31 (30), pp 8495–8501.

4.1. Introduction

The extensive use of ammonium nitrate as a fertilizer makes nitrate a major source of contamination in ground and drinking water. An excess of nitrate in drinking water can cause shortness of breath and blue baby syndrome[1-3]. The electrochemical reduction of nitrate would be a possible way to remove nitrate, provided it would convert nitrate in water to dinitrogen, which is harmless to the environment[4]. Nitrate reduction may also produce valuable chemicals like hydroxylamine, which is an important raw material for the chemical industry[5,6]. However a large number of stable products can be generated from electrochemical nitrate reduction: NO_2, NO_2^-, HNO_2, NO, N_2O, N_2, NH_2OH and NH_3, which makes selectivity a critical issue[7-10].

Metalloporphyrins and various other metal complexes have been employed as catalyst for the electrochemical reduction of nitrate, nitrite and nitric oxide. Iron porphyrin nitrosyls, FeP(NO), where P = TPP (tetraphenylporphyrin), TPC (tetraphenylchlorin), or OEP (octaethylporphyrin), were reduced in nonaqueous solvents to give hydroxylamine and ammonia as products[11]. In aqueous solution, the reduction of nitrite to ammonia has been shown to be catalyzed by FeTSPP (dianion of tetrakis(4-sulfonatophenyl) porphyrin)[12], and a water-soluble cobalt porphrin, Co(2-TMPyP) (tetrakis (N-methyl-2-pyridyl) porphine) was utilized for the electrochemical reduction of nitric oxide to hydroxylamine and ammonia[13]. Taniguchi et al. explored the ability of metal cyclams, Cobalt (III) and Nickel (II) cyclam (cyclam = 1,4,8,11-tetra-azacyclotetradecane), to electrocatalyze nitrate reduction on mercury electrode, giving hydroxylamine as main product. They also speculated that the effective catalyst was probably an adsorbed Co^I or Ni^I cyclam species[14, 15]. Later, these cyclams were immobilized on the surface of a gold electrode by incorporating them into a Nafion film, by direct adsorption or by linking to pyrrole and subsequent eletropolymerization, to catalyze nitrate reduction in alkaline solution[16-19]. A metal phthalocyanine modified on a glassy carbon electrode has also been shown to have activity for the nitrate reduction in alkaline media to give ammonia as the main product[20, 21]. Furthermore, a Mo-Fe cluster modified electrode[22], heteropolyanions containing tungsten, molybdenum, Copper (II) or Nickel(II),[23] and multicopper-containing

hetero-polyoxotungstates[24] have all been found to be active for the electrochemical reduction of nitrate.

Iron-protoporphyrin modified pyrolytic graphite electrodes have previously been shown to be very selective catalysts for the reduction of nitric oxide and nitrite in acidic media[25, 26]. Building on these previous results from our group, in this work, a simple metal-containing complex, cobalt protoporphyrin (CoPP), directly adsorbed on pyrolytic graphite (PG) electrode, was utilized as an electrocatalyst for the reduction of nitrate in acidic solution. CoPP was chosen among a series of metal-PPs because it has the highest reactivity and selectivity toward hydroxylamine. The electrochemical nitrate reduction was investigated by combining online electrochemical mass spectrometry (OLEMS) and ion chromatography (IC) with cyclic voltammetry. We find that pH and potential play a significant role in both reactivity and selectivity. A possible mechanism will also be discussed.

4.2. Experimental Details

4.2.1. Chemicals

Cobalt (III) protoporphyrin IX chloride (Frontier Science), Iron (II) protoporphyrin IX chloride (Fluka, 98%), Nickel (II) protoporphyrin IX chloride (Frontier Science), Copper (II) protoporphyrin IX chloride (Frontier Science), Rhodium (II) protoporphyrin IX chloride (Frontier Science) were used as received without further purification. All other chemicals were p.a. grade. Electrolyte solutions of pH 1, 2 and 3 were made of 0.1 M $HClO_4$ (Merck, 70%), 90 mM $NaClO_4$ (Sigma-Aldrich, $\geqslant$ 98.0%) with 10 mM $HClO_4$ and 99 mM $NaClO_4$ with 1 mM $HClO_4$, respectively. 0.1 M $NaNO_3$ (Merck, 99.99%) /$LiNO_3$ (Brunschwig chemie, 99.999%) was added for the nitrate reduction experiments and 4 mM $NaNO_2$ (Sigma-Aldrich, 99.999%) for the nitrite reduction experiments. Water was purified through a Milli-Q Plus Ultra-pure water systerm (Millipore Co.). Resistivity of the purified water was greater than 18.2 MΩ·cm. Pyrolytic graphite (Carbone-Lorraine) was fabricated into a home-made disc electrode with a diameter of 5 mm.

4.2.2. Electrochemistry

All glassware was boiled in a mixture of concentrated sulfuric acid and nitric acid, and subsequently boiled in Milli-Q water 5 times before all experiments. Electrolyte solutions were purged with Ar (purity grade 6.0, Hoekloos) for 15 minutes before measurement to remove dissolved oxygen. Either an Autolab PGSTAT20 (bi)potentiostat or an Ivium potentiosat was used for the cyclic voltammetry experiments. Electrochemical experiments were conducted in a home-made one-compartment three-electrode cell: the working electrode was a metal protoporphyrin immobilized pyrolytic graphite electrode; the counter electrode was a platinum wire; the reference electrode was a reversible hydrogen electrode (RHE), all potentials in this paper are referred to this electrode. The electrochemical reduction of nitrate/nitrite experiments were also conducted on blank pyrolytic graphite electrode, which showed no activity indicating that Platinum counter electrode did not interfere with the reaction.

The metalloprotoporphyrin solutions and the metalloprotoporphyrin immobilized PG electrode were prepared as in our previous work[27]. 1.6 mg of the particular metalloprotoporphyrin was dissolved in 5 ml of a 0.01 M borate solution (pH=10) to make a 0.5 mM metalloprotoporphyrin solution. The PG electrode was abraded using P500 and P1000 SiC sandpaper and ultrasonicated in MilliQ water for 1 min, after which it was dried using compressed air. The saturation of porphyrin on the electrode surface was done by dipping the electrode into certain metalloprotoporphyrin solution for 5 min. Before transferring to the electrochemical cell, the electrode was rinsed with MilliQ water.

Cyclic voltammetry (CV) was utilized to ascertain successful immobilization of metal-protoporphyrins (data not shown here). As in our prior work[27], a redox peak representing the Co^{III}/Co^{II} or Fe^{III}/Fe^{II} couple was observed around 0.82 V and 0.08 V, respectively. The Rh^{II}/Rh^{I} redox couple showed a peak around 0.2 V, while Ni^{II} and Cu^{II} protoporphyrins showed no peak in the potential range we studied. After the electrochemical reduction of nitrate, the presence of the Co^{III}/Co^{II} redox couple was checked again using cyclic voltammetry to investigate the stability of the catalyst. The

redox peak of the cobalt couple was still observed at pH 3, despite a lower current density, but no peak could be resolved at pH 1 due to a substantially higher background current. However, pre- and post-electrolysis inspection by means of ex situ XPS of the CoPP modified PG electrode before and after a 1 hour electrolysis experiment at -0.8 V showed no change in the cobalt oxidation state[28]. This suggests that at pH=1 the surface termination of the pyrolytic graphite changes significantly during the polarization to very negative potential, but that the Cobalt porphyrin is stable on this time scale.

4.2.3. On-line electrochemical mass spectroscopy (OLEMS)

The online electrochemical mass spectrometry (OLEMS) setup, which was used to detect the volatile products during cyclic voltammetry, consisted of an Evolution mass spectrometry system (European Spectrometry Systems Ltd)[29]. A PEEK tip with inner diameter of 0.51 mm, which contained a porous Teflon plug, was placed close (~10 μm) to the electrode surface. All the gas products were collected through a PEEK capillary (connected to the tip) leading to the mass spectrometer chamber, in which the pressure was kept below 10^{-6} mbar. A 2400 V SEM voltage was used except for hydrogen (m/z=2), for which the voltage was 1500 V. The tip was cleaned prior experiments by dipping into a solution of 0.2 M $K_2Cr_2O_7$ in 2 M H_2SO_4 for 15 minute and rinsing with MilliQ water thoroughly. The products were detected while the cyclic voltammogram was taken in the potential range from 0 V to -1.5 V by an Ivium A06075 potentiostat with the scan rate of 1 mVs^{-1}.

4.2.4. On-line ion chromatograpy (IC)

The online ion chromatography (IC) experiments were conducted as in our previous work[30]. The samples were collected every minute using an automatic fraction collector (FRC-10A, Schimadzu) by positioning a Teflon tip close to the middle of working electrode while a linear voltammogram was taken by an Autolab potentiostat (Pgstat20) in a range from 0 V to -1.5 V at a scan rate of 1 mVs^{-1}. The waiting time at the initial potential (0 V) has no influence on the products formed. A microtiter plate with collected samples was placed onto the autosampler (SIL-20A) holder of an ion chromatography unit

(Schimadzu, Prominence) with a conductivity detector (CCD-10Ap, Schimadzu). Samples with a volume of 20 μL were injected into and analyzed through two series of Shodex IC Y-521 columns, of which the temperature was set to 30 ºC, to monitor NH_4^+ and NH_3OH^+ cations. A 2.5 mM nitric acid solution (Merck, Suprapur, 65%) was used as eluent at a flow rate of 8 $mLmin^{-1}$. $LiNO_3$ and $NaNO_2$ were used as substrates for nitrate and nitrite reduction respectively. The concentration of $LiNO_3$ was 0.1 M. As $LiNO_2$ was unstable and a high concentration of sodium cation will overlap with the signal of NH_4^+ and NH_3OH^+, the concentration of $NaNO_2$ was 4 mM.

4.3. Results and Discussion

The catalytic activity of the PG electrode modified with five different metal-center protoporphyrins for the electrochemical reduction of nitrate has been investigated using online ion chromatography in 0.1 M $LiNO_3$ solution at pH 1. Figure 1(a) and 1(b) show the ammonium (NH_4^+) and hydroxylammonium (NH_3OH^+) formation respectively, with metal centers iron (Fe), cobalt (Co), nickel (Ni), copper (Cu) and rhodium (Rh). All metal protoporphyrins show similar trends in the formation of products except for iron which shows a significant increase in the formation of NH_4^+ and NH_3OH^+ from a potential more negative than -1.17 V. The concentration of NH_3OH^+ produced at all catalysts, except for iron protoporphyrin, is from 0.5 mM to 1 mM at the most negative potential, which is always higher than that of NH_4^+, which is below 0.5 mM. Figure 1(c) shows a plot of the NH_3OH^+ selectivity of all catalysts, which is defined as the ratio between the concentration of NH_3OH^+ and the sum of the concentration of NH_3OH^+ and NH_4^+. Cobalt protoporphyrin (CoPP) shows the highest selectivity towards NH_3OH^+ in the whole potential range. NH_3OH^+ is the only product from -0.44 V to -0.81 V, with the selectivity decreasing at more negative potentials but still NH_3OH^+ remains the dominant product. We note that the selectivity as shown in Fig.1c is sensitively dependent on the exact experimental conditions (i.e voltammetric sweep rate and sample collection frequency). Electrolysis experiments at fixed conditions yield NH_4^+ at lower potential (see below). Therefore, the value of Fig.1c is primarily qualitative, and leads to the conclusion that the superior selectivity of CoPP

toward NH_3OH^+ makes it the most interesting catalyst. Therefore we focused on this system in the rest of our studies.

The cyclic voltammograms (CVs) measured during the electrochemical reduction of nitrate at a CoPP modified PG electrode at pH 1 and pH 3 are reported in Figure 2 along with the CVs for hydrogen evolution reaction (HER) for comparison. At pH 1, the absolute peak current density for HER at -1.5 V is almost 2 times higher than that in the presence of nitrate, which means that nitrate, or intermediates formed during its electrochemical reduction, substantially suppresses the hydrogen evolution reaction. Therefore there must be a competition between protons and nitrate for the active site of the cobalt protoporphyrin. The electrochemical nitrate reduction leads to a reduction wave at potentials between ca. -0.5 and -1.5 V, in agreement with the formation of NH_3OH^+ and NH_4^+ in this potential window in Figure 1. Despite the suppression of the hydrogen evolution reaction, H_2 is still produced, as we will show further below using OLEMS. The reduction wave for nitrate reduction disappears almost completely when the pH is increased to 3. This agrees with our previous general observation that a high concentration of protons enhances the electrochemical reduction of nitrate[31]. Remarkably, the absolute current density for the HER at -1.5 V, which is about 10 mA/cm^2, is now lower than that of electrochemical reduction of nitrate, which is about 15 mA/cm^2. This suggests a pH-dependent competition between the reduction of nitrate, protons and water (which at pH=3 is probably the main contributor to the HER, in contrast to pH=1). Also, results to be presented below suggest that N_2O and N_2 are more important products of nitrate reduction at pH=3 than hydroxylamine and ammonia.

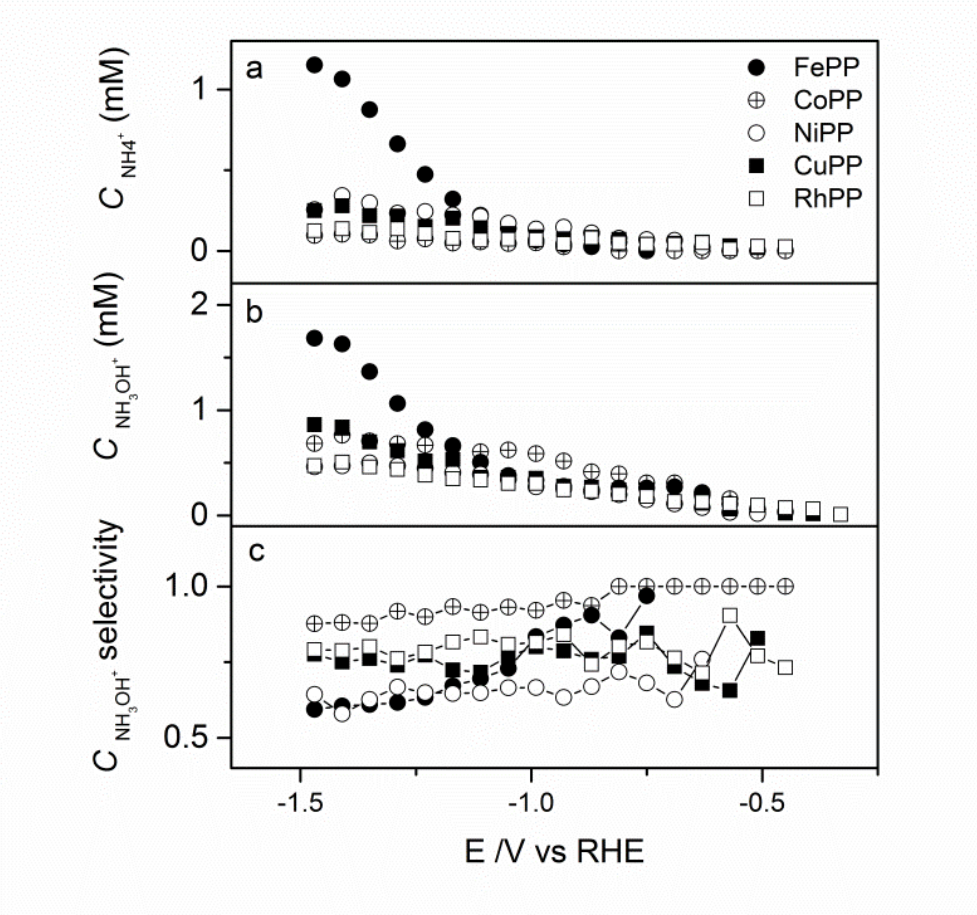

Figure 1. Nitrate reduction on different metal-center protoporphyrins at pH 1, concentration of products obtained while conducting linear sweep voltammetry (LSV) at a scan rate of 1 mVs^{-1} from 0 V to -1.5 V in combination with online ion chromatography (IC). (a) NH_4^+ concentration vs potential on Iron protoporphyrin (FePP), Cobalt protoporphyrin (CoPP), Nickel protoporphyrin (NiPP), Copper protoporphyrin (CuPP), and Rhodium protoporphyrin (RhPP); (b) NH_3OH^+ concentration vs potential on different metal-center protoporphyrins; (c) the ratio of the concentration of NH_3OH^+ to the sum of the concentration of NH_3OH^+ and NH_4^+.

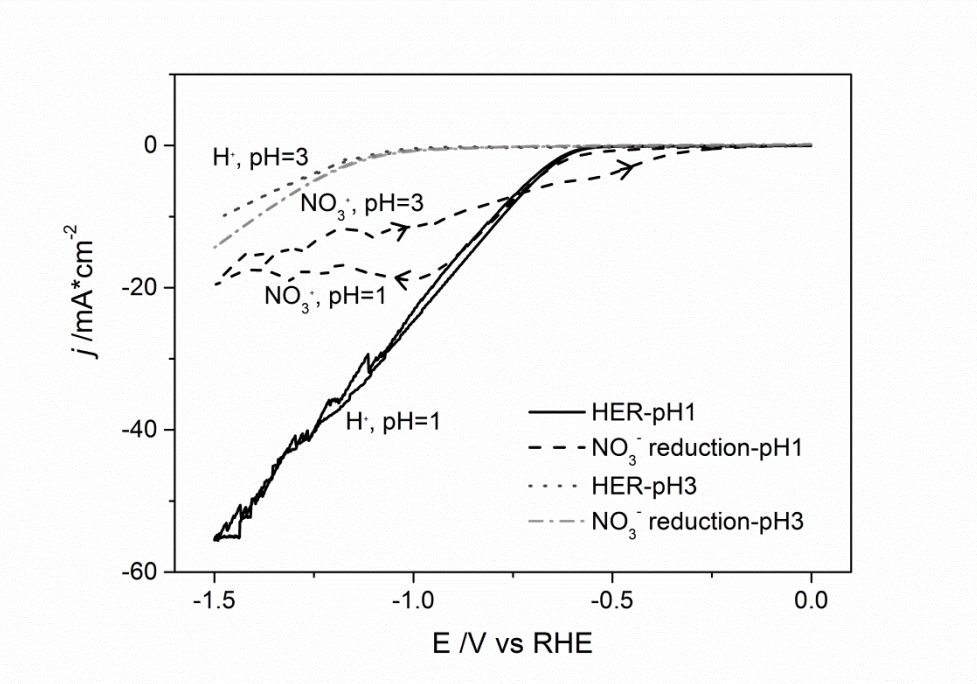

Figure 2. Influence of pH on the cyclic voltammetry profiles of nitrate reduction (0.1 M $NaNO_3$) and hydrogen evolution reaction (HER) on cobalt protoporphyrin immobilized PG electrode in 0.1 M perchlorate solution (pH =1 and 3), scan rate is 100 mV s^{-1}.

Figure 3 presents the plots of the concentration of NH_4^+ and NH_3OH^+ produced from electrochemical nitrate reduction by the immobilized CoPP as a function of potential at pH 1 and pH 2. Figure 3(a) shows that NH_4^+ is formed at an almost equal concentration at pH 1 and pH 2, with a slightly higher concentration for pH 2. The same experiment was conducted at pH 3, but no NH_4^+ was detected (result not shown here). Figure 3(b) shows that NH_3OH^+ is formed earlier than NH_4^+ regardless of pH, from around -0.5 V. At pH 1, NH_3OH^+ increases with potential until to -1.0 V where it reaches its maximum concentration and remains constant until the most negative potential, although with some fluctuation. However, the concentration of NH_3OH^+ is dramatically decreased with the pH increased to 2. The same experiment was also conducted at pH 3 and no NH_3OH^+ was detected. The significant conclusion of Figure 3 is that pH has a very substantial influence on the selective formation of NH_3OH^+. With a small pH increase from 1 to 2, the formation

of NH_3OH^+ is almost completely suppressed, whereas the production of NH_4^+ remains constant. At pH 3, neither NH_4^+ nor NH_3OH^+ is observed.

It is generally accepted that the difficult step in nitrate reduction is its conversion to nitrite[5]. It is therefore worthwhile to study the electrochemical reduction of nitrite under the same conditions as nitrate reduction. Figure 4 shows the formation of NH_3OH^+ and NH_4^+ from nitrite reduction on the CoPP immobilized PG electrode at different pH. It is important to keep in mind that the concentration of nitrite is only 4 mM which is 25 times smaller than the concentration of nitrate. The fact that the measured concentrations in Figure 4 are similar to Figure 3 shows that nitrite is indeed significantly more reactive than nitrate. Figure 4(a) shows the NH_4^+ formation at different pH. With a pH increase from 1 to 2, the concentration of NH_4^+ is slightly higher, which is similar to the case of nitrate reduction. There is still NH_4^+ produced at pH 3, only the amount is significantly less than that at pH 2. Figure 4(b) shows that the formation of NH_3OH^+ exhibits the same trend with pH as nitrate reduction, in the sense that the formation of NH_3OH^+ is dramatically suppressed with higher pH. The inserted plot in Figure 4(b) zooms in at the formation of NH_3OH^+ at pH 2 and 3, showing that NH_3OH^+ was barely produced at pH 3. Despite the small amount of NH_4^+ formed from nitrite reduction at pH 3, the electrochemical reduction of nitrate and nitrite exhibit the same selectivity and pH sensitivity, from which we can deduce that the electrochemical reduction of nitrate indeed goes through nitrite as intermediate.

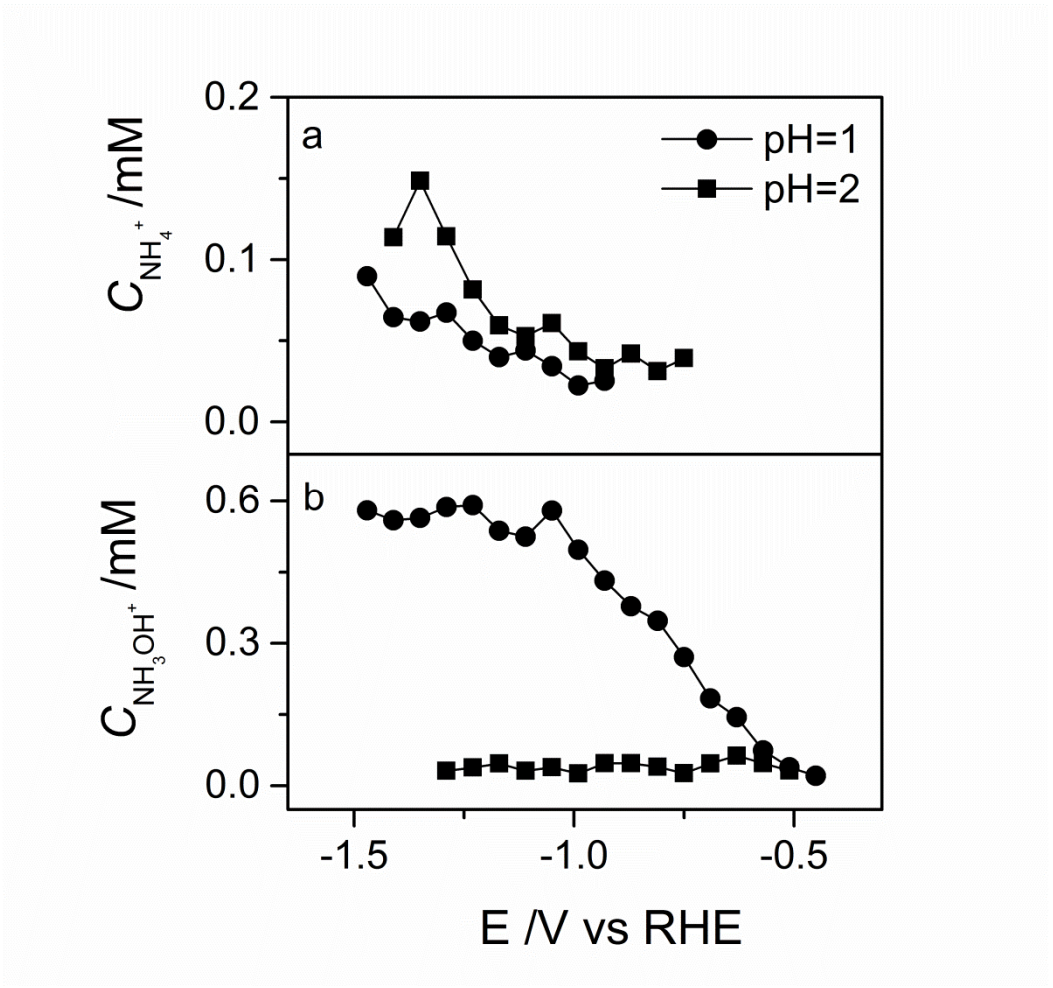

Figure 3. Nitrate electrochemical reduction on cobalt protoporphyrin immobilized PG electrode at pH=1 (0.1 M $HClO_4$) and pH=2 (10 mM $HClO_4$ + 90 mM $LiClO_4$). (a) the concentration of NH_4^+ as a function of potential; (b) the concentration of NH_3OH^+ as a function of potential, 0.1 M $LiNO_3$. Scan rate is 1 mV s^{-1}.

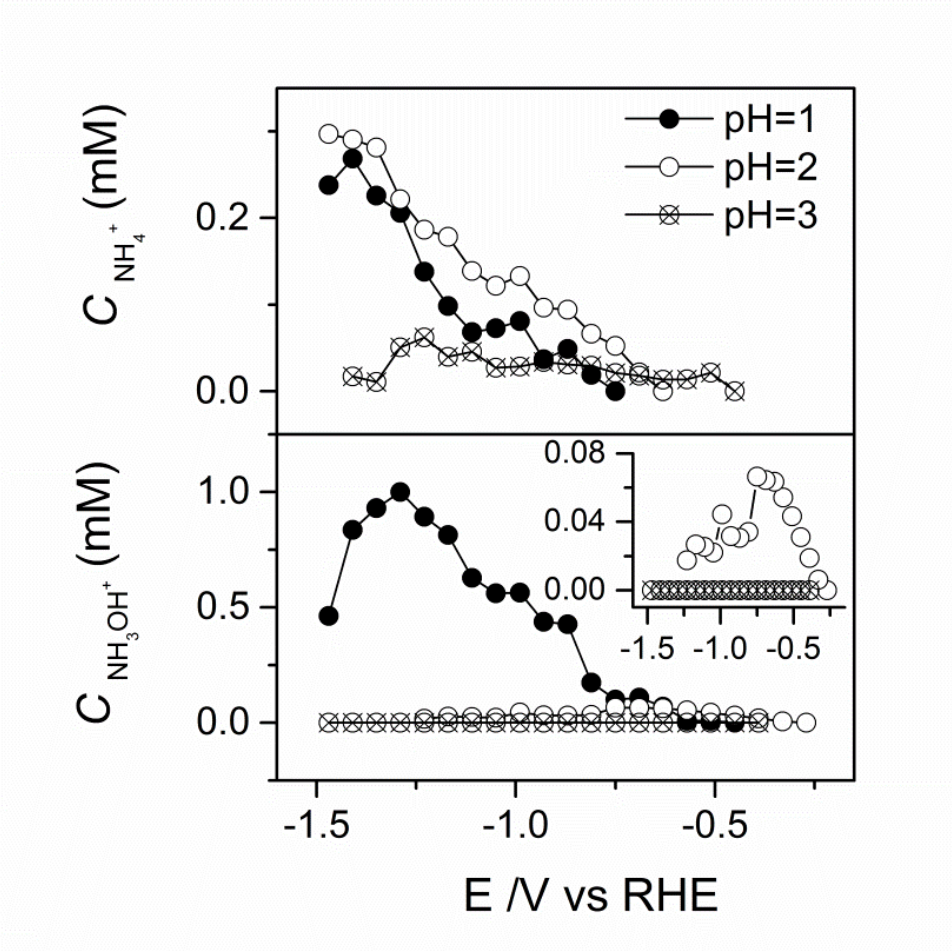

Figure 4. Nitrite electrochemical reduction on cobalt protoporphyrin immobilized PG electrode at pH=1 (0.1 M $HClO_4$), pH=2 (90 mM $NaClO_4$ + 10 mM $HClO_4$) and pH=3 (99 mM $NaClO_4$ + 1 mM $HClO_4$). (a) meausred NH_4^+ concentration vs potential; (b) measured NH_3OH^+ concentration vs potential, 4 mM $NaNO_2$. Scan rate is 1 mV s^{-1}.

NO is considered as the nitrite-derived substrate in acid media as there is a homogeneous-phase decomposition reaction of HNO_2 to NO for pH<5[26, 32]. It is therefore important to investigate the formation of NO at different pH on the immobilized cobalt protoporphyrin. Figure 5(d-f) shows the formation of NO at pH 1 to 3 detected by OLEMS during the electrochemical reduction of nitrate. It should be pointed out that the m/z=30 signal was not corrected for the N_2O fragmentation. Figure 5(d) shows the variation of NO

vs potential at pH 1, from which it is observed that NO forms at the beginning of the reaction (i.e. at positive potentials, when the electrochemical current is still very low) and is also formed when the voltammetry scans back in the positive direction. Figure 5(e) shows the same trend as Figure 5(d), but the intensity of the NO ionic current at pH 2 is 40 times lower than that at pH 1. We also find that a small amount of NO is produced at very negative potential, which we ascribe to the fragment of the N_2O detected as the by-product of the nitrate reduction, as will be discussed later. At pH 3, there is no NO detected at neither the beginning of the reaction nor the end of the back scan in Figure 5(f), which may indicate that NO is not produced from nitrate/nitrite at this pH. A small amount of NO was measured from -1.0 V to -1.5 V, which may come from the fragment of N_2O (see below). These results are in full agreement with our previous conclusion that the main source of NO is the pH-dependent decomposition reaction of HNO_2 in solution[27].

Other possible volatile products of electrochemical nitrate reduction were monitored using OLEMS at different pH, as is shown in Figure 5 (g-o). The N_2O formation exhibits a large difference between pH 1 and 2, 3 as shown in Figure 5(g) to Figure 5(i). At pH 1, N_2O is produced at the beginning of the electrochemical reduction of nitrate and the ion current decreases at around -0.4 V. As the potential goes to more negative potential, N_2O is observed again at -1.0 V. When cyclic voltammetry scans back toward positive direction, N_2O is formed again at -0.35 V. At pH 1, the formation of N_2O shows trends very similar to NO apart from the small amount of N_2O formation at very negative potential. However, N_2O is not formed neither at the beginning nor at the end of the back scan at pH 2 and 3, instead it is only observed at potentials below -1.0 V in a very small amount. Fragments m/z = 28 and m/z = 2, assigned to N_2 and H_2 respectively, are detected at pH 1 to 3 as shown Figure 5(j-o). The formation of N_2 and H_2 displays similar trends at different pH, as both are formed at relatively negative potential starting from -1.0 V. The exception is at pH 1 for which H_2 and N_2 evolution start earlier around -0.5 V. The ion current corresponding to H_2 shows a peak at ca. -1.0 V. Compared with results from the cyclic voltammograms at pH 1, the formation of H_2 is suppressed when the electrochemical reduction of nitrate reaches a plateau value.

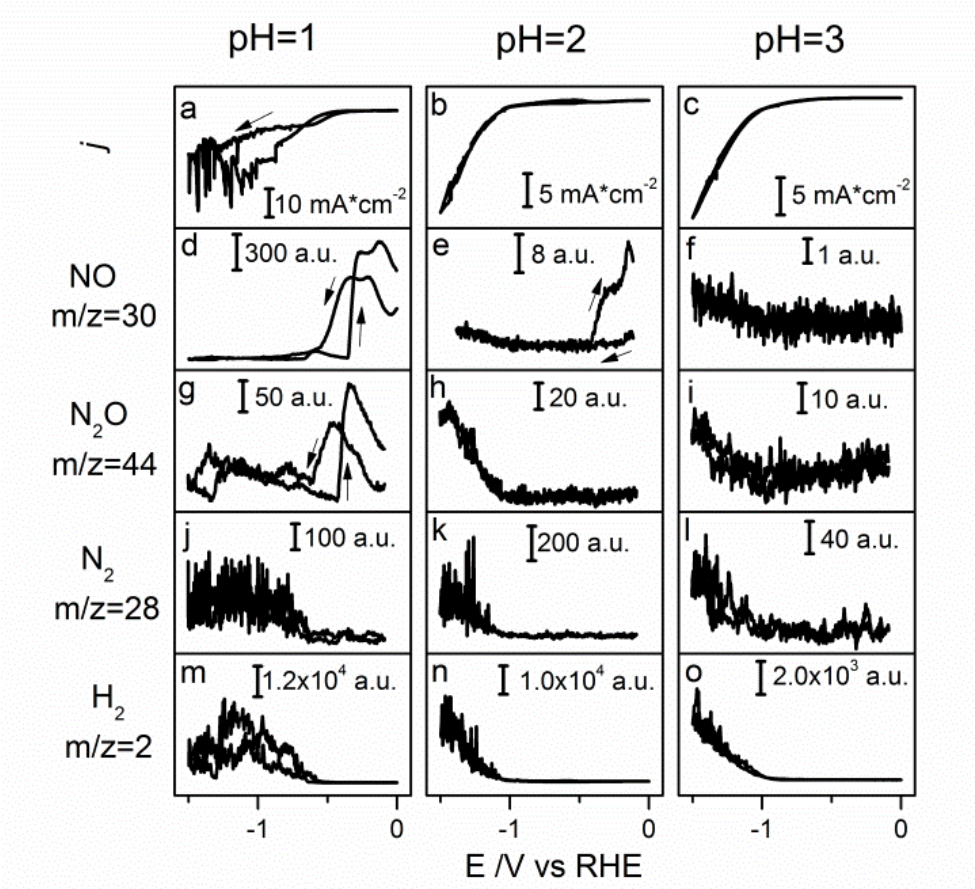

Figure 5. Volatile products detected by online electrochemical mass spectroscopy (OLEMS) during electrochemical nitrate reduction on cobalt protoporphyrin immobilized PG electrode in 0.1 M $NaNO_3$ at different pH. Rows show NO, N_2O, N_2 and H_2 formation respectively; First column: pH 1, 0.1 M $HClO_4$ solution; Second column: pH 2, 10 mM $HClO_4$ + 90 mM $NaClO_4$; and Third column: pH 3, 1 mM $HClO_4$ + 99 mM $NaClO_4$. Scan rate 1 mV s^{-1}.

Figure 6 shows the local concentrations of NH_3OH^+ and NH_4^+ formed from the electrochemical reduction of hydroxylamine verified vs potential at different pH. At pH 1, no NH_4^+ formed from hydroxylamine reduction. NH_4^+ is produced as the pH is increased to 2, and simultaneous with NH_4^+ formation, there is a decrease of hydroxylamine concentration. At pH 3, the concentration of NH_4^+ produced is higher than that at pH 2.

However, when the potential sweeps to potentials more negative than -1.25 V, the concentration of NH_4^+ begins to decline, while hydroxylamine concentration also diminishes. Comparing to Figure 2, this potential corresponds to the onset of H_2 evolution, which may perhaps lead to a local mixing and a lower local concentration of the NH_4^+ in the collected samples.

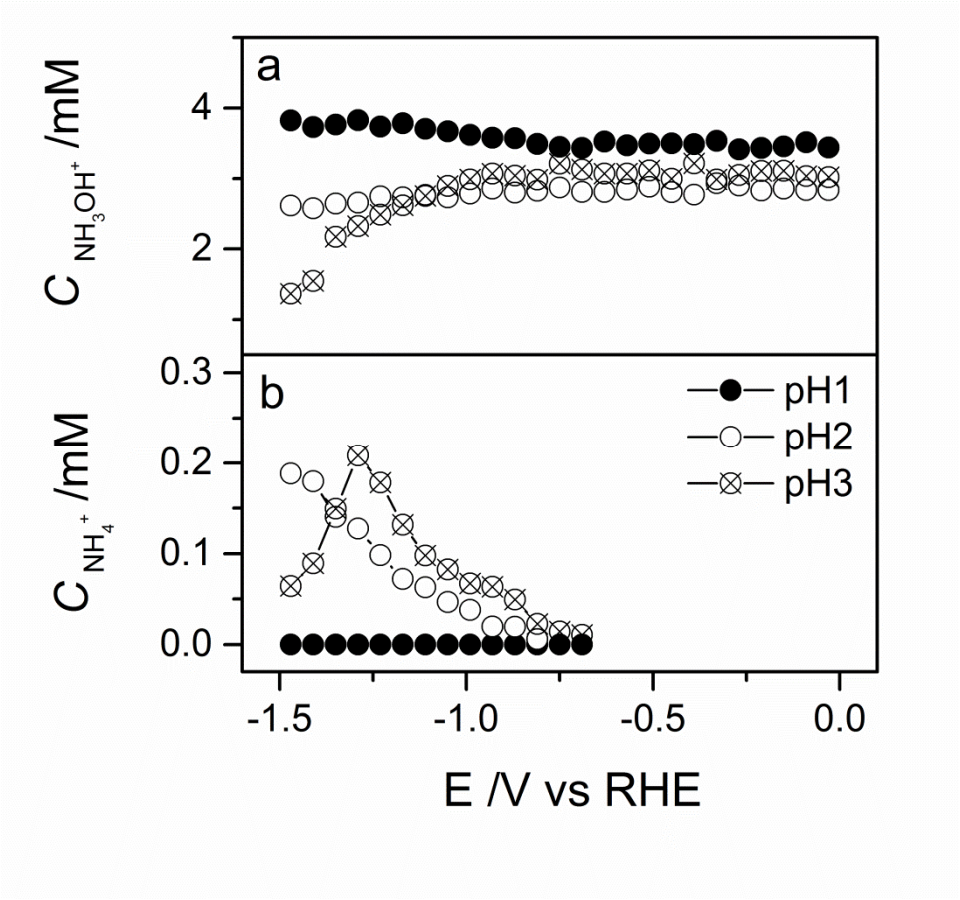

Figure 6. Electrochemical reduction of hydroxylamine on cobalt protoporphyrin immobilized PG electrode from pH 1 to 3. (a) the profiles of NH_3OH^+ concentration vs potential; (b) the profiles of NH_4^+ concentration vs potential. Scan rate is 1 mV s^{-1}. Solution concentration of hydroxylamine is 4 mM.

Finally, a potential controlled electrolysis was conducted for 2 hours to investigate the stability of cobalt protoporphyrin and the formation of NH_3OH^+ and NH_4^+. Figure 7 shows the plots of ion chromatography analysis of samples collected from long-term electrolysis of nitrate reduction in 0.1 M $LiNO_3$ at pH 1. Figure 7(a) shows that at a potential of -0.5 V, NH_3OH^+ is the only product, albeit in a relatively small amount. Up to 1 hour, NH_3OH^+ is stably produced despite some fluctuations from the sample collection. After 1 hour, the concentration gradually decreases, reaching 0.05 mM at the end of the electrolysis. Figure 7(b) displays the electrolysis results at -0.75 V. At this potential both NH_4^+ and NH_3OH^+ are produced and their amounts are dramatically increased compared to -0.5 V. The concentrations of NH_4^+ and NH_3OH^+ first increase to reach a maximum value at ca. 30 minutes after which they decrease to a steady state. Note that the concentration of NH_4^+ obtained in this experiment is considerably higher than in Figure 1, due to the different experimental conditions (i.e. longer electrolysis time at fixed potential).

Based on the results discussed above, we can formulate a tentative mechanism for the nitrate electroreduction catalyzed by cobalt protoporphyrin immobilized pyrolytic graphite electrode. In agreement with our previous work[31], nitrate electroreduction is highly pH dependent. The rate-determining step is the conversion of nitrate to nitrite, given by the following proton-coupled electron transfer reaction:

$$NO_3^- + 2H^+ + 2e^- \rightarrow NO_2^- + H_2O \quad (1)$$

Yang et al.[31] found that equation (1) is enhanced at low pH, suggesting that HNO_3 is the actual reducible species. The selectivity of the overall nitrate reduction then depends on the consecutive reduction of NO_2^-. However, in acidic solution (pH < 5) , Duca et al.[26] found that NO formed from a homogeneous decomposition reaction of HNO_2 is the main reactant on iron-based protoporphyrin, as opposed to the direct electrochemical reduction of NO_2^-:

$$NO_2^- + H^+ \leftrightarrow HNO_2 \quad (2)$$

$$2HNO_2 \leftrightarrow NO + NO_2 + H_2O \quad (3)$$

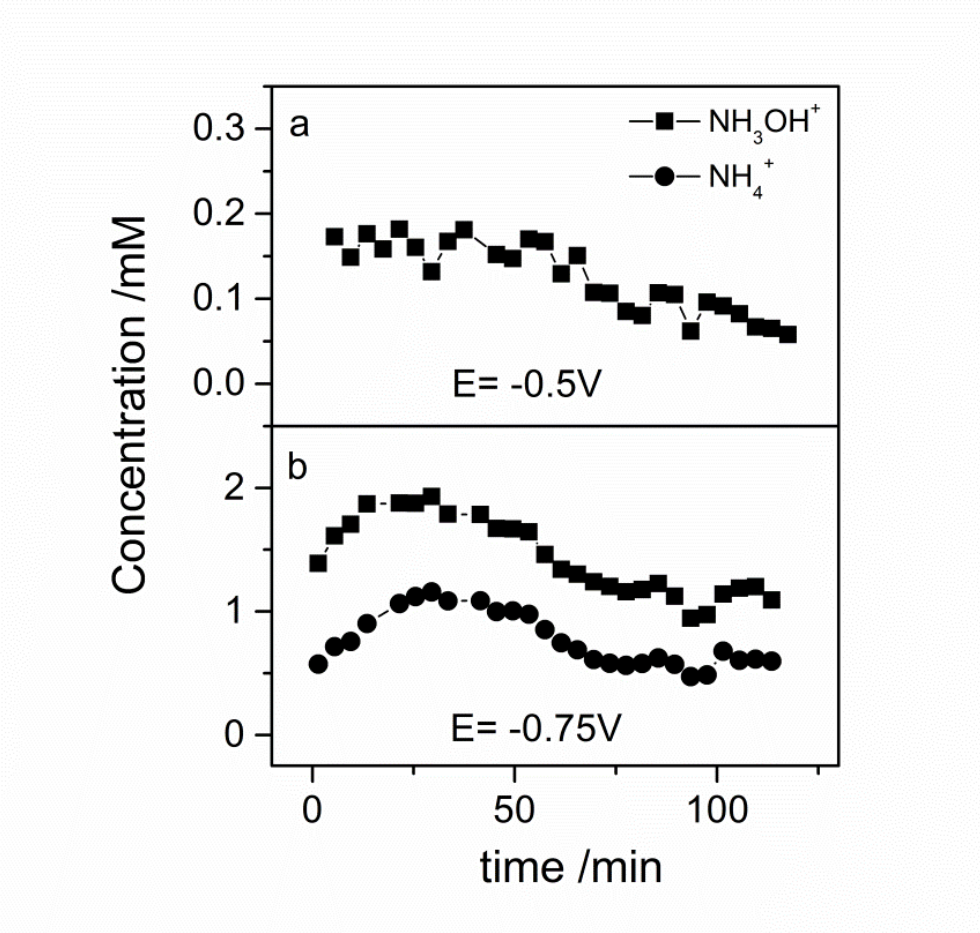

Figure 7. Concentrations of NH_3OH^+ and NH_4^+ as determined by online ion chromatography during a 2 hours potential controlled electrolysis of nitrate reduction (0.1M $LiNO_3$) at pH=1 (0.1M $HClO_4$). (a) E = -0.5 V; (b) E = -0.75 V.

The NO adduct formed through equation (4) was confirmed using spectroscopic studies by Cheung et al.[13] and Ma et al.[18]. The most stable NO adducts formed were $[Co^{II}(2\text{-}TMPyP)(NO)]^{4+}$ and $Fe^{II}(NO)PP$, which indicates that the M^{II} oxidation state is not the oxidation state catalyzing NO reduction. The NO adduct was reduced to M-HNO by a simultaneous one-proton, one-electron transfer as shown below in equation (5)[25,26], which is

the precursor to different gas and non-volatile products. The gaseous product N_2O is formed by the reaction of M-HNO adduct with the NO in the solution, a reaction whose mechanism on iron-based porphyrins has been studied in detail in our earlier work.[25,26] The overall reaction for the formation of N_2O is shown in equation (6) below. N_2O will consecutively react to N_2, but this reaction is very slow. We assume this reaction to be the source of N_2 formation in Figure 5. In Figure 5, there is a second pathway leading to the formation of N_2O at potentials below ca. -1 V (vs. RHE) which appears as distinct from the N_2O formation at higher potentials. The most likely source of N_2O at these very negative potentials is the homogeneous reaction between nitrite and hydroxylamine[5].

$$M + NO \rightarrow M\text{-}NO \quad (4)$$

$$M\text{-}NO + e^- + H^+ \rightarrow M\text{-}HNO \quad (5)$$

$$M\text{-}HNO + NO + H^+ + e^- \rightarrow M + N_2O + H_2O \quad (6)$$

The main non-volatile products are hydroxylamine and ammonia, which we speculate to be formed either through a sequential pathway or a parallel pathway. For the sequential pathway, the further reduction reaction of M-HNO leads to the formation of hydroxylamine through equation (7).

$$M\text{-}HNO + 2H^+ + 2e^- \rightarrow M + NH_2OH \quad (7)$$

Ammonia is then formed through the sequential reduction of hydroxylamine, as presented in Figure 6(b) for pH 2 and 3. We further speculate that the pH dependent selectivity in such a sequential reaction could depend on the protonation state of the hydroxylamine, i.e. NH_3OH^+ vs. NH_2OH, with the ratio of the concentrations between NH_3OH^+ and NH_2OH being strongly influenced by the pH as the corresponding pKa is 5.9. The results of hydroxylamine reduction confirm that NH_2OH is the actual precursor for the formation of ammonia, explaining why hydroxylamine reduction shows a higher activity at

pH 3. We suspect that there should be an optimal pH for the hydroxylamine reduction, which needs further investigation.

Figure 6 shows that hydroxylamine cannot be reduced to ammonia at pH 1, but the electrochemical reduction of nitrate does produce ammonia at pH 1 as presented in Figure 4. This suggests that the formation of hydroxylamine and ammonia may also follow a parallel pathway, with the HNO adduct being the precursor to both hydroxylamine and ammonia formation. In this case, the pH dependent electrochemical reactivity of M-HNO would determine the final product.

In our previous work, immobilized hemin (FePP) was used to catalyze the electrochemical reduction of NO and nitrite[25,26]. The main product at low pH was hydroxylamine with a small amount of N_2O. A possible explanation for the discrepancy with the results reported here is the different working potential window. In the former work, the most negative potential was -0.5 V, since both NO and nitrite are highly reactive at low pH, in contrast to the potential window of -0.5 to -1.5 V used here, due to the fact that nitrate is much less reactive. From the long-term electrolysis experiments reported here, hydroxylamine is the only product at the least negative potential -0.5 V, which is consistent with the previous study. Under more reductive conditions (i.e. more negative potentials), ammonia is also formed. Moreover, the formation of ammonia is time dependent, as can be concluded from the comparison of Figures 1 and 7. Longer electrolysis times at fixed potential (Figure 7) yield more ammonia than during linear sweep voltammetry (Figure1). We consider these observations further arguments in favor of the sequential pathway.

4.4. Conclusions

We have shown that adsorbed metal protoporphyrins can reduce nitrate to NH_2OH/NH_3OH^+ and NH_3/NH_4^+ in acid media at sufficiently negative potentials, from ca. -0.5 V (vs. RHE). At less negative potentials, NO and N_2O are formed, with a very small amount of N_2. Among all different metal centers, the cobalt protoporphyrin shows highest selectivity towards NH_2OH/NH_3OH^+. The mechanism of the reaction has been studied using voltammetry and online mass spectrometric and ion chromatographic methods.

Importantly, pH affects almost every step of the reaction, leading to a pH dependent product selectivity. Low pH (~1) enhances the rate-determining conversion of nitrate to nitrite and leads to a more selective formation of hydroxylamine. Slightly higher pH (2-3) lowers the overall reactivity and shifts selectivity to ammonia. The most likely explanation for this intricate pH dependence is a sequential pathway in which hydroxylamine is an intermediate in the formation of ammonia.

4.5. Acknowledgments

J.S. acknowledges the award of a grant of the Chinese Scholarship Council (CSC).

REFERENCES

1. Averill, B. A. Dissimilatory Nitrite and Nitric Oxide Reductases. *Chem. Rev.* **1996**, 96 (7), 2951-2964.

2. Spalding, R. F.; Exner, M. E. Occurrence of Nitrate in Groundwater—A Review. *J. Environ. Qual.* **1993**, 22 (3), 392-402.

3. Nolan, B. T.; Ruddy, B. C.; Hitt, K. J.; Helsel, D. R. Risk of Nitrate in Groundwaters of the United StatesA National Perspective. *Environ. Sci. Technol.* **1997**, 31 (8), 2229-2236.

4. Li, M.; Feng, C.; Zhang, Z.; Sugiura, N. Efficient electrochemical reduction of nitrate to nitrogen using Ti/IrO_2–Pt anode and different cathodes. *Electrochim. Acta* **2009**, 54 (20), 4600-4606.

5. Rosca, V.; Duca, M.; de Groot, M. T.; Koper, M. T. M. Nitrogen Cycle Electrocatalysis. *Chem. Rev.* **2009**, 109 (6), 2209-2244.

6. Hajipour, A. R.; Mohammadpoor-baltork, I.; Nikbaghat, K.; Imanzadeh, G. Solid-Phase Synthesis of Oximes. *Synth. Commun.* **1999**, 29 (10), 1697-1701.

7. da Cunha, M. C. P. M.; De Souza, J. P. I.; Nart, F. C. Reaction Pathways for Reduction of Nitrate Ions on Platinum, Rhodium, and Platinum−Rhodium Alloy Electrodes. *Langmuir* **2000**, 16 (2), 771-777.

8. Gauthard, F.; Epron, F.; Barbier, J. Palladium and platinum-based catalysts in the catalytic reduction of nitrate in water: effect of copper, silver, or gold addition. *J. Catal.* **2003**, 220 (1), 182-191.

9. Pronkin, S. N.; Simonov, P. A.; Zaikovskii, V. I.; Savinova, E. R. Model Pd-based bimetallic supported catalysts for nitrate electroreduction. *J. Mol. Catal. A: Chem.* **2007**, 265 (1–2), 141-147.

10. Santos, A. L.; Jay Deiner, L.; Varela, H. The effect of ultra-low proton concentration on the electrocatalytic reduction of nitrate over platinum. *Catal. Commun.* **2008**, 9 (2), 269-272.

11. Choi, I. K.; Liu, Y.; Feng, D.; Paeng, K. J.; Ryan, M. D. Electrochemical and spectroscopic studies of iron porphyrin nitrosyls and their reduction products. *Inorg. Chem.* **1991**, 30 (8), 1832-1839.

12. Barley, M. H.; Meyer, T. J. Electrocatalytic reduction of nitrite to ammonia based on a water-soluble iron porphyrin. *J. Am. Chem. Soc.* **1986**, 108 (19), 5876-5885.

13. Cheng, S.-H.; Su, Y. O. Electrocatalysis of Nitric Oxide Reduction by Water-Soluble Cobalt Porphyrin. Spectral and Electrochemical Studies. *Inorg. Chem.* **1994**, 33 (25), 5847-5854.

14. Taniguchi, L.; Nakashima, N.; Yasukouchi, K. Reduction of nitrate to give hydroxylamine at a mercury electrode using cobalt(III)-and nickel(II)-cyclams as catalysts. *Chem. Commun.* **1986**, (24), 1814-1815.

15. Taniguchi, I.; Nakashima, N.; Matsushita, K.; Yasukouchi, K. Electrocatalytic reduction of nitrate and nitrite to hydroxylamine and ammonia using metal cyclams. *J. Electroanal. Chem. Interfacial electrochem.* **1987**, 224 (1–2), 199-209.

16. Li, H.-L.; Chambers, J. Q.; Hobbs, D. T. Electrocatalytic reduction of nitrate and nitrite at nafionR-coated electrodes in concentrated sodium hydroxide solution. *J. Electroanal. Chem. Interfacial electrochem.* **1988**, 256 (2), 447-453.

17. Ma, L.; Zhang, B.-Y.; Li, H.-L.; Chambers, J. Q. Kinetics of nitrate reduction by cobalt-cyclam incorporated Nafion® redox polymer. *J. Electroanal. Chem.* **1993**, 362 (1–2), 201-205.

18. Ma, L.; Li, H. Electrocatalysis of adsorbed Co-cyclam at Au electrodes for nitrate reduction in concentrated alkaline solution. *Electroanalysis* **1995**, 7 (8), 756-758.

19. Simon, E.; Sablé, E.; Handel, H.; L'Her, M. Electrodes modified by conducting polymers bearing redox sites: Ni- and Co-cyclam complexes on polypyrrole. *Electrochim. Acta* **1999**, 45 (6), 855-863.

20. Li, H. L.; Chambers, J. Q.; Hobbs, D. T. Electroreduction of nitrate ions in concentrated sodium hydroxide solutions at lead, zinc, nickel and phthalocyanine-modified electrodes. *J. Appl. Electrochem.* **1988**, 18 (3), 454-458.

21. Chebotareva, N.; Nyokong, T. Metallophthalocyanine catalysed electroreduction of nitrate and nitrite ions in alkaline media. *J. Appl. Electrochem.* **1997**, 27 (8), 975-981.

22. Kuwabata, S.; Uezumu, S.; Tanaka, K.; Tanaka, T. Reduction of NO_3^- giving NH_3 using a $(Bu_4N)_3[Mo_2Fe_6S_8(SPh)_9]$-modified glassy carbon electrode. *Chem. Commun.* **1986**, (2), 135-136.

23. Keita, B.; Abdeljalil, E.; Nadjo, L.; Contant, R.; Belgiche, R. First examples of efficient participation of selected metal-ion-substituted heteropolyanions in electrocatalytic nitrate reduction. *Electrochem. Commun.* **2001**, 3 (2), 56-62.

24. Zhang, Z.; Qi, Y.; Qin, C.; Li, Y.; Wang, E.; Wang, X.; Su, Z.; Xu, L. Two Multi-Copper-Containing Heteropolyoxotungstates Constructed from the Lacunary Keggin Polyoxoanion and the High-Nuclear Spin Cluster. *Inorg. Chem.* **2007**, 46 (20), 8162-8169.

25. de Groot, M. T.; Merkx, M.; Wonders, A. H.; Koper, M. T. M. Electrochemical Reduction of NO by Hemin Adsorbed at Pyrolitic Graphite. *J. Am. Chem. Soc.* **2005**, 127 (20), 7579-7586.

26. Duca, M.; Khamseh, S.; Lai, S. C. S.; Koper, M. T. M. The Influence of Solution-Phase HNO_2 Decomposition on the Electrocatalytic Nitrite Reduction at a Hemin–Pyrolitic Graphite Electrode. *Langmuir* **2010**, 26 (14), 12418-12424.

27. de Groot, M. T.; Koper, M. T. M. Redox transitions of chromium, manganese, iron, cobalt and nickel protoporphyrins in aqueous solution. *Phys. Chem. Chem. Phys.* **2008**, 10 (7), 1023-1031.

28. Shen J.; Kortlever R.; Kas R.; Birdja Y. Y.; Diaz-Morales O.; Kwon Y.; Ledezma-Yanez I.; Schouten K. J. P.; Mul G.; Koper M.T. M. Electrocatalytic reduction of carbon dioxide to carbon monoxide and methane at an immobilized cobalt protoporphyrin. *Nature Commun.* **2015**, **6**, 8177.

29. Wonders, A. H.; Housmans, T. H. M.; Rosca, V.; Koper, M. T. M. On-line mass spectrometry system for measurements at single-crystal electrodes in hanging meniscus configuration. *J. Appl. Electrochem.* **2006**, 36 (11), 1215-1221.

30. Yang, J.; Kwon, Y.; Duca, M.; Koper, M. T. M. Combining Voltammetry and Ion Chromatography: Application to the Selective Reduction of Nitrate on Pt and PtSn Electrodes. *Anal. Chem.* **2013**, 85 (16), 7645-7649.

31. Yang, J.; Sebastian, P.; Duca, M.; Hoogenboom, T.; Koper, M. T. M. pH dependence of the electroreduction of nitrate on Rh and Pt polycrystalline electrodes. *Chem. Commun.* **2014**, 50 (17), 2148-2151.

32. Park, J. Y.; Lee, Y. N. Solubility and decomposition kinetics of nitrous acid in aqueous solution. *J. Phys. Chem.* **1988**, 92 (22), 6294-6302.

Appendix A: Supplementary Material for Chapter 2

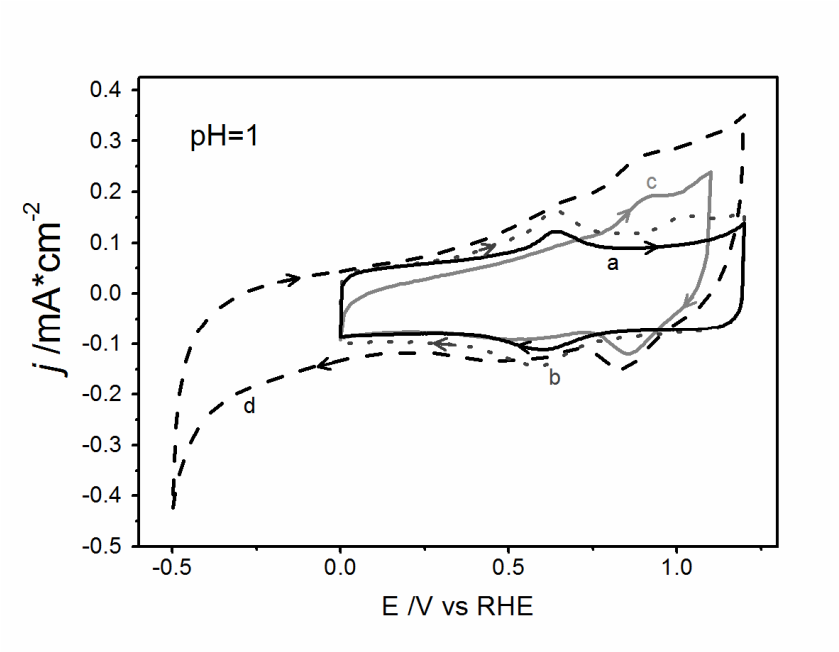

Figure 1. Characterization of immobilized cobalt protoporphyrin electrode. The cyclic voltammogram of: (a) pyrolytic graphite electrode; (b) pyrolytic graphite electrode with 100 μL 0.5 mM cobalt protoporphyrin solution in electrolyte; (c) cobalt protoporphyrin immobilized pyrolytic graphite electrode and (d) cobalt protoporphyrin immobilized pyrolytic graphite electrode scanned to more negative potential. All voltammograms obtained in 0.1 M $HClO_4$ solution; scan rate is 500 mVs^{-1}. From the peak corresponding to the Co^{III}/Co^{II} redox couple at 0.8-0.9 V (with due account of the capacitive background current), the coverage of cobalt protoporphyrin can be estimated as $4x10^{-10}$ mol cm^{-2}. The cleanliness of the solution was verified by blank voltammetry of a platinum electrode, which showed no impurities.

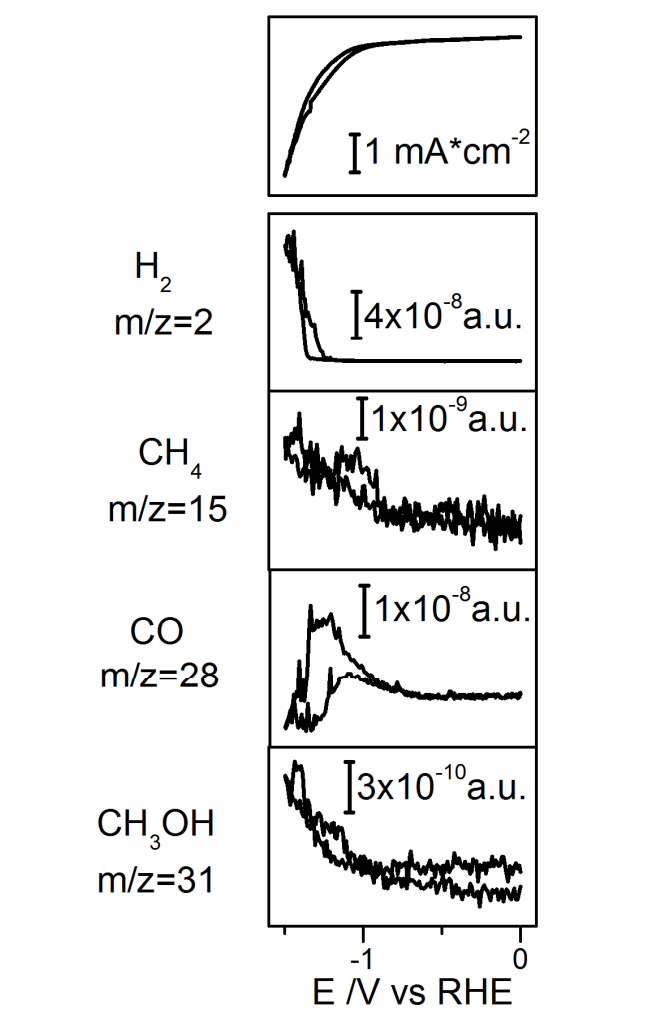

Figure 2. Cyclic voltammetry combined with OLEMS measurement of electrochemical reduction of CO_2 on a cobalt-tetramethoxyphenylporphyrin modified pyrolytic graphite electrode in 1 mM $HClO_4$ + 99 mM $NaClO_4$ (pH=3) solution, showing the cyclic voltammetry (upper panel) and the hydrogen, methane and methanol formation (lower panels). This experiment demonstrates that a small amount of alcohol (m/z=31) is produced from the CO_2 reduction catalyzed by the cobalt porphyrin. From the absence of higher alcohols C2 signals, we conclude that m/z=31 must correspond to methanol.

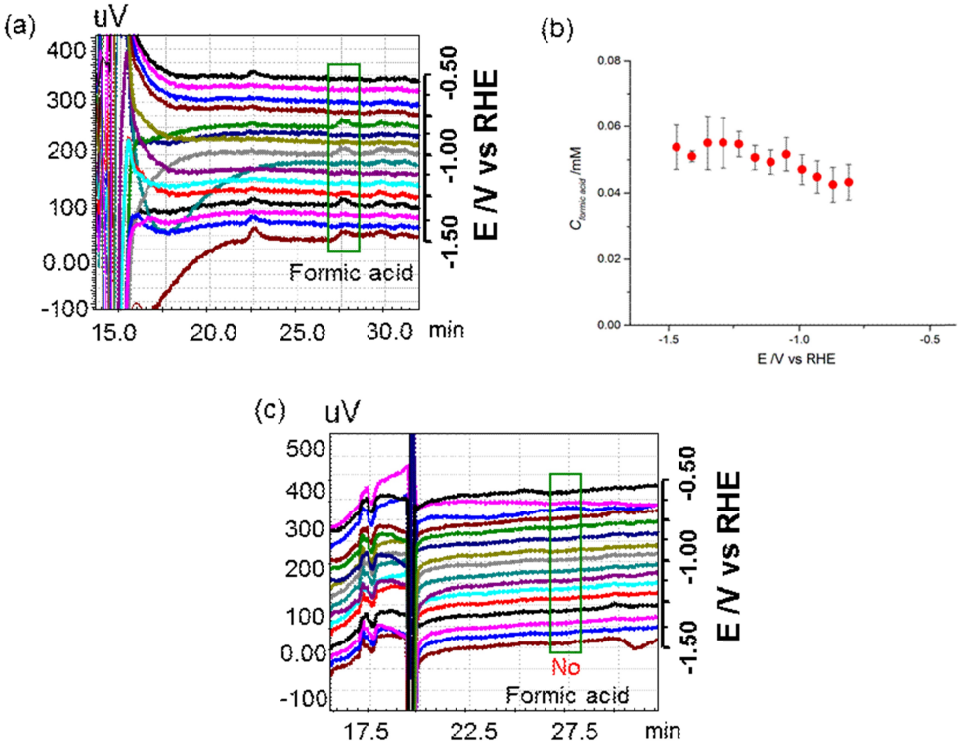

Figure 3. Liquid products detected using HPLC. (a) Chromatograms obtained during the electrochemical reduction of CO_2 on the CoPP-PG electrode in 0.1 M $HClO_4$ solution vs potential, which were collected every 60 mV. (b) The corresponding concentration of formic acid vs potential at pH=1; error bars determined from 3 separate experiments. (c) Chromatograms for electrochemical reduction of CO_2 on the CoPP-PG electrode in 1 mM $HClO_4$+ 99 mM $NaClO_4$ solution vs potential, which were collected every 60 mV, showing the absence of formation of formic acid at pH=3. The fluctuations of the detected HCOOH in Fig.(b) are due to the very small amount of formic acid formed from CO_2 electrochemical reduction in combination with the hydrogen formation and sample collection.

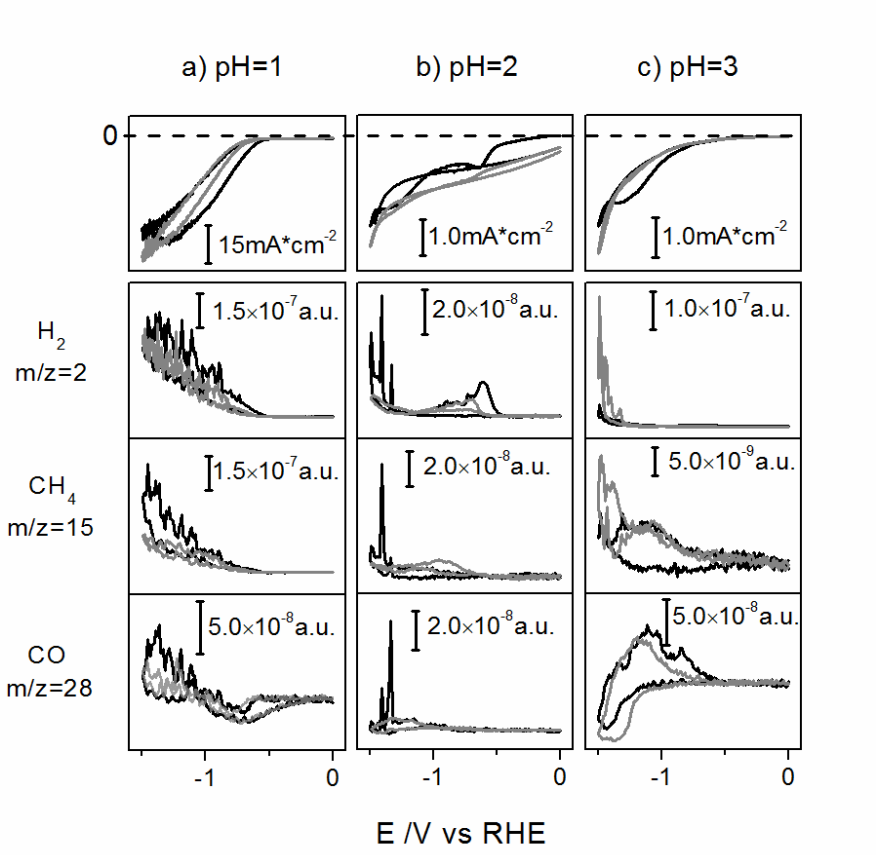

Figure 4. Voltammetry and the unnormalized signals of the volatile product identification by OLEMS during the electrochemical reduction of CO_2 on cobalt protoporphyrin immobilized pyrolytic graphite electrode. (a) 0.1 M $HClO_4$. (b) 10 mM $HClO_4$ + 90 mM $NaClO_4$ and (c) 1 mM $HClO_4$ + 99mM $NaClO_4$; showing first cycle (black curve) and second cycle (gray curve). Top panels: cyclic voltammetry. Lower panels: associated OLEMS mass signals for m/z=2 (H_2), 15 (CH_4) and 28 (CO). Scan rate in all cases 1 mV s^{-1}.

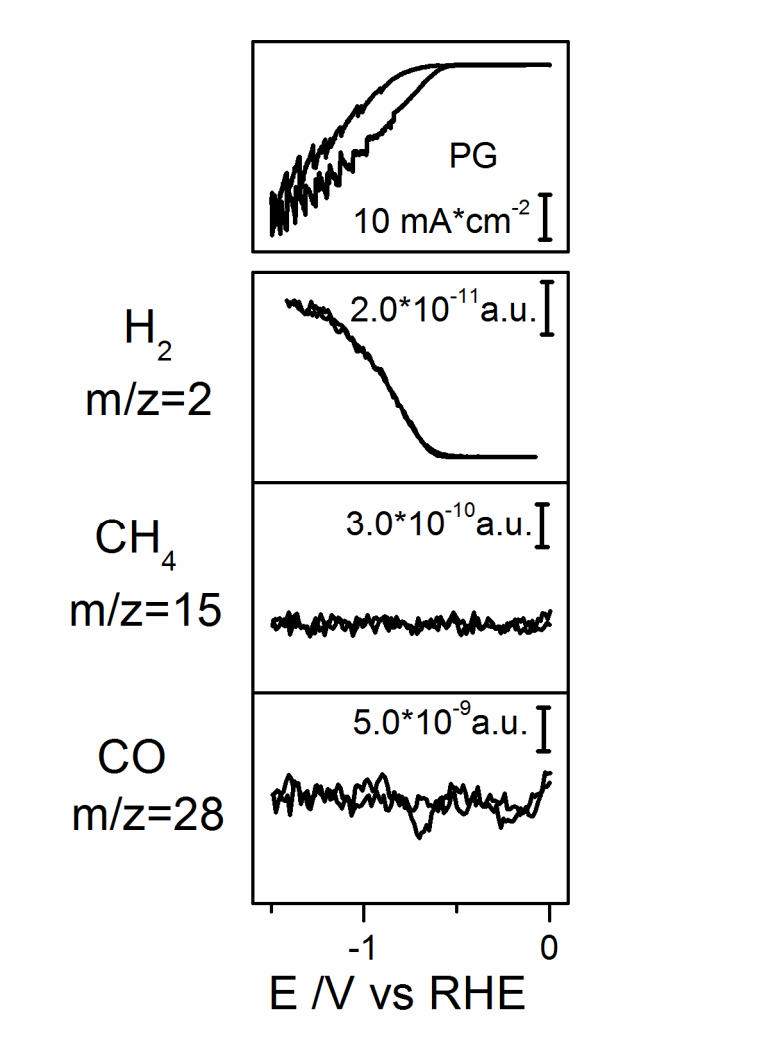

Figure 5. Combined CV-OLEMS measurement of electrochemical reduction of CO_2 on an unmodified pyrolytic graphite electrode in 0.1 M $HClO_4$ solution, showing the cyclic voltammetry (upper panel) and the hydrogen, methane, and carbon monoxide formation (lower panels). This experiment demonstrates that the catalytic activity towards CO_2 reduction is not from pyrolytic graphite.

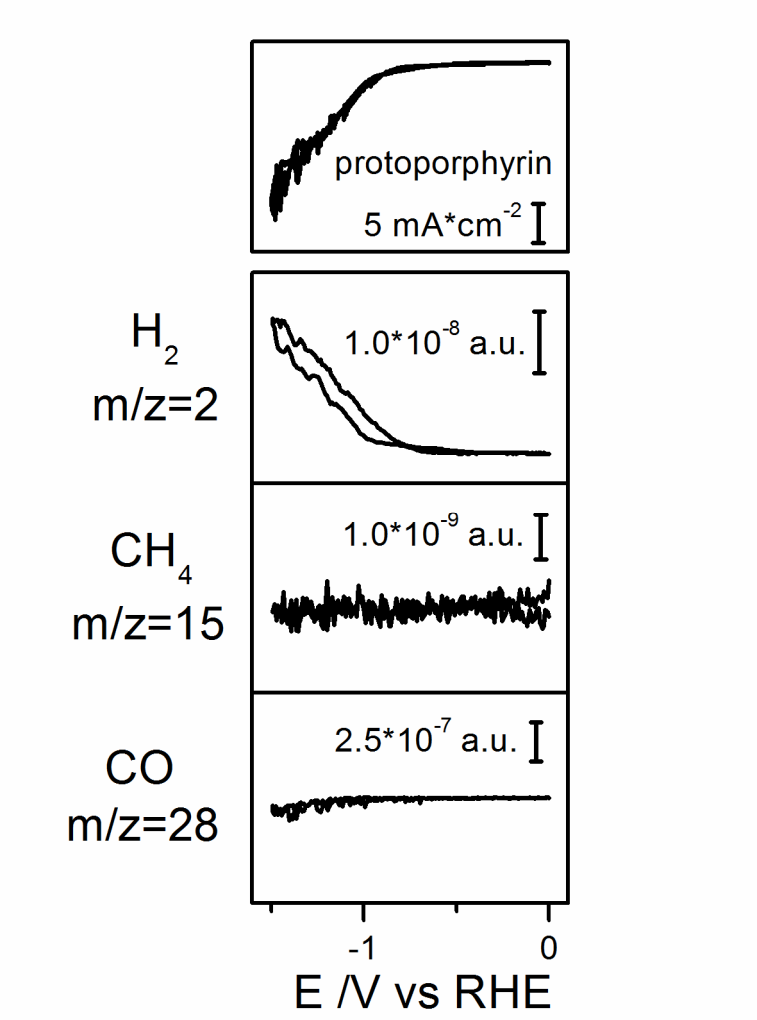

Figure 6. Combined CV-OLEMS measurement of electrochemical reduction of CO_2 on cobalt-free protoporphyrin modified pyrolytic graphite electrode in 0.1 M $HClO_4$ solution, showing the cyclic voltammetry (upper panel) and the hydrogen, methane and carbon monoxide formation (lower panels). This experiment demonstrates that the catalytic activity for CO_2 reduction comes from the interaction of the cobalt metal center and protoporphyrin ring.

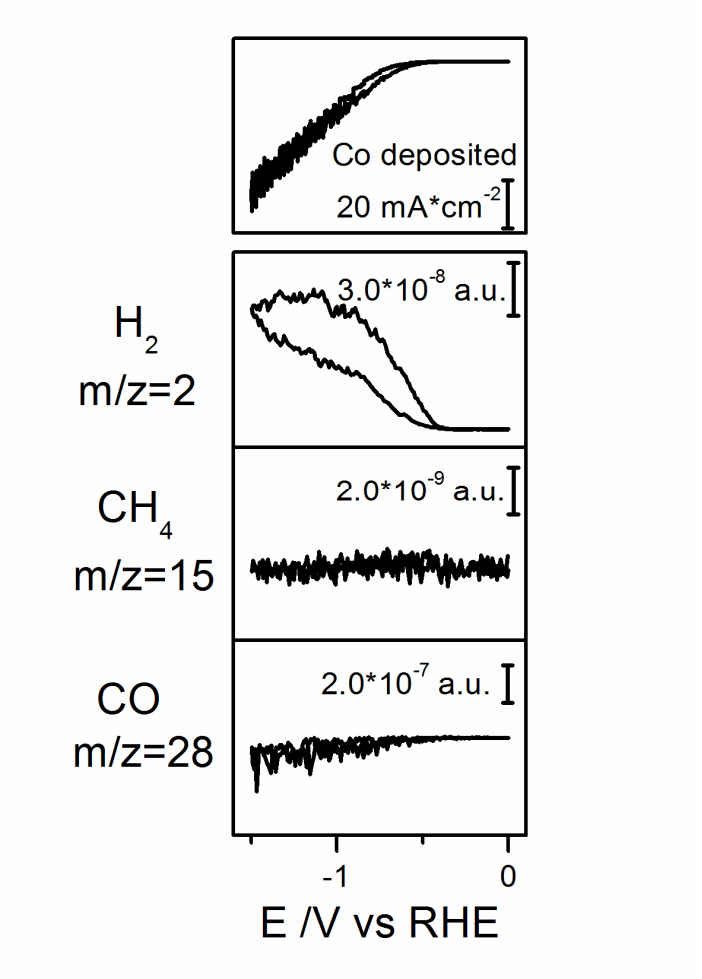

Figure 7. Combined CV-OLEMS measurement of electrochemical reduction of CO_2 on a cobalt electrodeposited pyrolytic graphite electrode in 0.1 M $HClO_4$ solution, showing the cyclic voltammetry (upper panel) and the hydrogen, methane and carbon monoxide formation (lower panels). This experiment demonstrates that the catalytic activity for CO_2 reduction is not from the cobalt released from cobalt protoporphyrin. The deposition of cobalt was conducted using the same procedure as described elsewhere[1]. The solution used for cobalt electrodeposition was 3.5 mM $CoCl_2$ in 1 M NH_4Cl solution (pH=4.5). Electrochemical experiments were conducted in a one-compartment three-electrode electrochemical cell with a pyrolytic graphite electrode (diameter:5mm) as working electrode, a graphite rod as a counting electrode and a KCl saturated Ag/AgCl electrode as a reference electrode, to which all potentials here were referred. Cyclic voltammetry was conducted from 0.4 V to -1.3 V to verify the electrochemistry of the working electrode in the electrodeposition bath, after which a current-time transient experiment was conducted by starting the potential at 400 mV for 60s, and jumping to first potential step at -1.3 V for 2s with an interval of 0.2s.

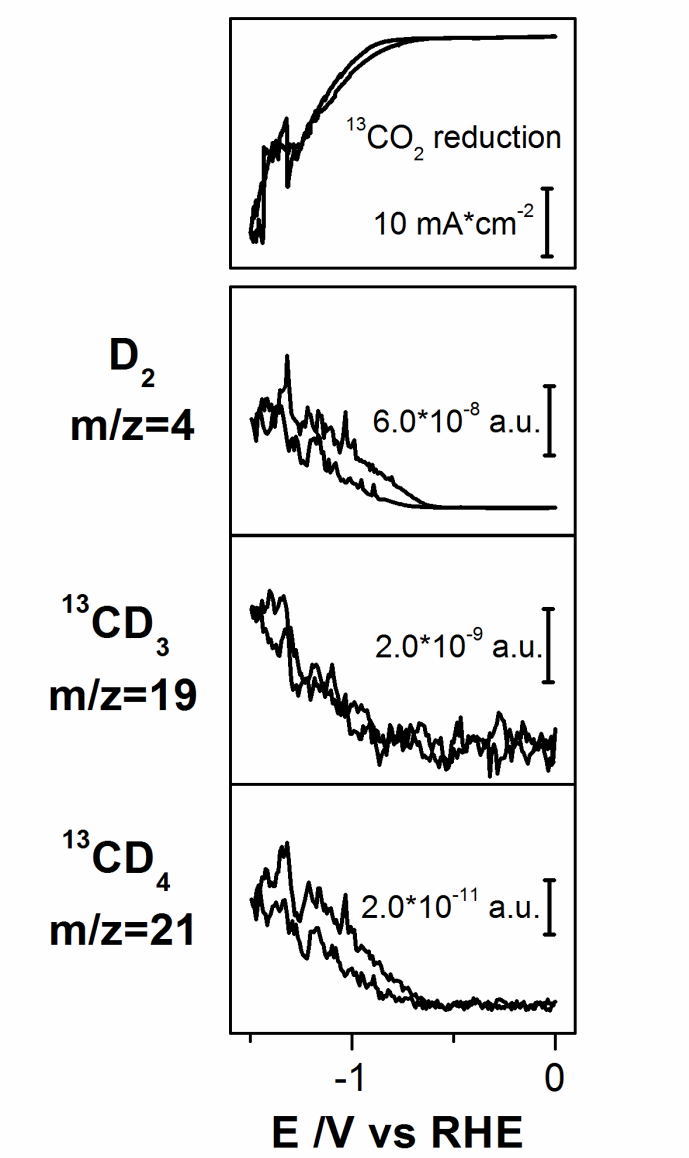

Figure 8. Combined CV-OLEMS measurement of electrochemical reduction of $^{13}CO_2$ on cobalt protoporphyrin modified pyrolytic graphite electrode in 0.1 M $DClO_4$ + D_2O solution, showing the cyclic voltammetry (upper panel) and the hydrogen and methane formation (lower panels). This experiment proves that the catalytic activity of cobalt protoporphyrin and the formation of methane are from dissolved CO_2. m/z=19 corresponds to $^{13}CD_3$; m/z=21 corresponds to $^{13}CD_4$.

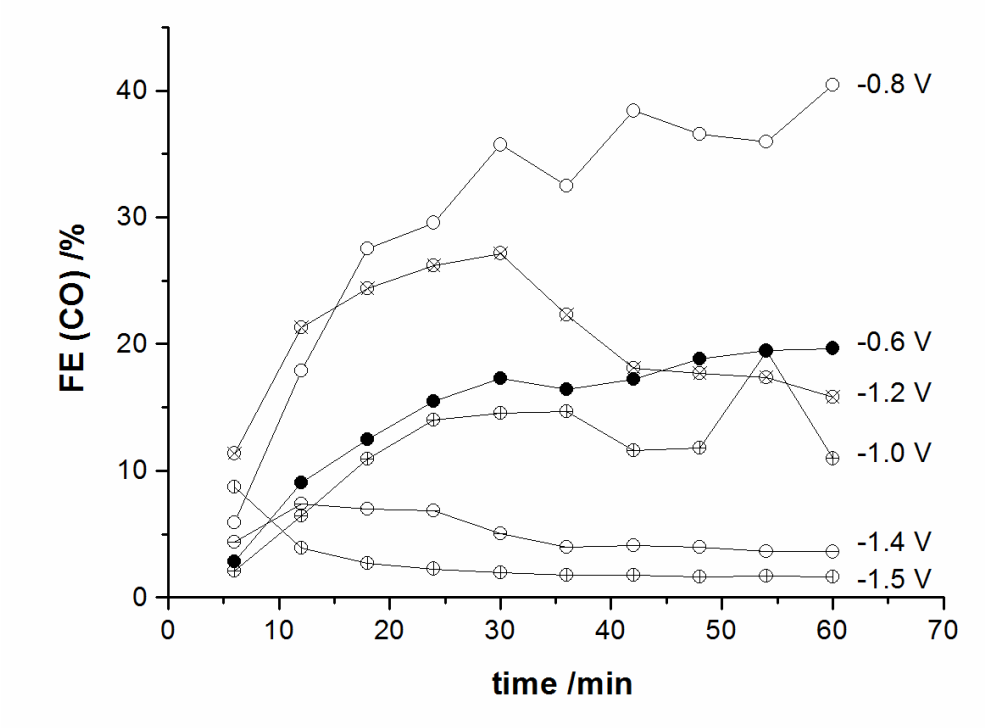

Figure 9. Faradaic efficiency (FE) of CO from controlled potential electrolysis of CO_2 electrochemical reduction on cobalt protoporphyrin modified pyrolytic graphite electrode at different potentials vs RHE as a function of time. Solution: 1 mM $HClO_4$ + 99 mM $NaClO_4$ (pH=3); CO_2 pressure: 1 atm.

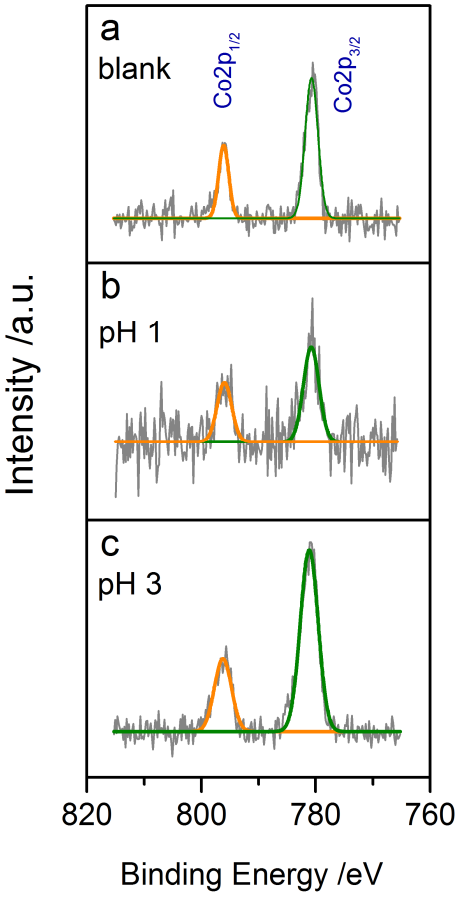

Figure 10. XPS spectra of (a) freshly prepared cobalt protoporphyrin immobilized PG electrode; (b) cobalt protoporphyrin immobilized PG electrode after electrolysis at -1.5 V in 0.1 M $HClO_4$ solution (pH = 1) for 1 hour and (c) cobalt protoporphyrin immobilized PG electrode after electrolysis at -0.8 V in 99 mM $NaClO_4$ + 1 mM $HClO_4$ solution (pH = 3) for 1 hour. Figure (b) and (c) show that the CoPP remains intact on the electrode after electrolysis at very negative potentials. X-ray photoelectron spectroscopy (XPS) spectra were collected on a Quantera SXM (Scanning XPS microprobe) spectrometer equipped with Al Kα (1486.6 eV) X-ray source. The source was operated with a 25 W emission power, beam size of 200 μm and pass energy of 224 eV. The resolution of the spectrometer was 0.2eV and 0.8 eV for high resolution element scan and survey spectra, respectively.

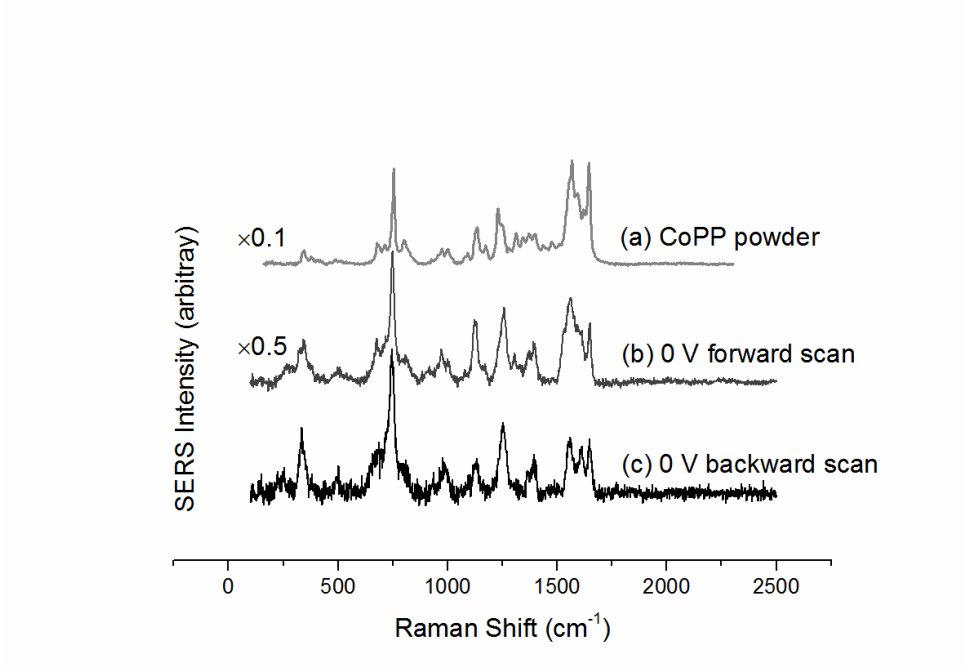

Figure 11. SERS spectra of (a) cobalt protoporphyrin powder; (b) cobalt protoporphyrin immobilized Au electrode at 0 V before scanning and (c) cobalt protoporphyrin immobilized Au electrode at 0 V after voltammetry scanned to negative potentials. Au nano particles were synthesized as in reference[2], which were drop-cast onto a clean Au electrode. The electrode was then dipped into 0.5 mM cobalt protoporphyrin solution to saturate the surface with porphyrin. Cobalt protoporphyrin immobilized electrode was held at different potentials started from 0 V to – 1.5 V vs RHE with 100 mV interval and then back while SERS spectra was collected at each potential.

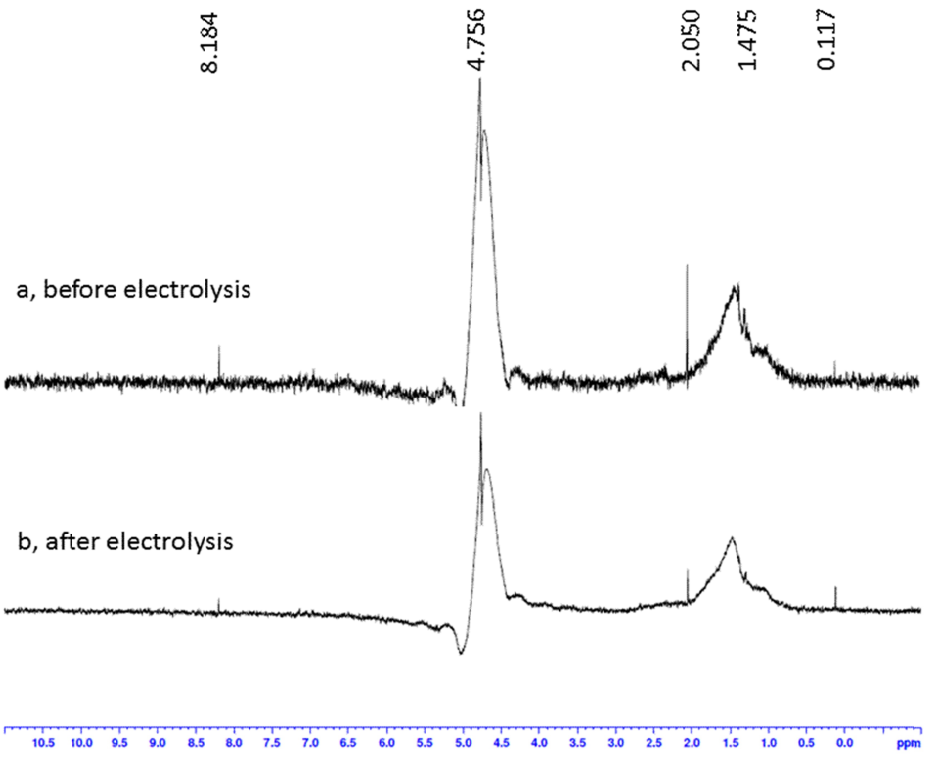

Figure 12. NMR spectra of electrolyte (a) before and (b) after long-term electrolysis in CO_2 saturated 0.1 M $HClO_4$ solution on CoPP immobilized PG electrode. The electrolysis was conducted for 5 hours in a H-cell with 15 mL volume in each compartment. 100 uL solution in working electrode compartment was collected after electrolysis for NMR measurement.

Reference:

1. Kwon Y, Koper M.T.M. Combining Voltammetry with HPLC: Application to Electro-Oxidation of Glycerol. *Anal. Chem.* **2010**, 82(13): 5420-5424.
2. Palomar-Pardavé M, Scharifker BR, Arce EM, Romero-Romo M. Nucleation and diffusion-controlled growth of electroactive centers: Reduction of protons during cobalt electrodeposition. *Electrochim. Acta*. **2005**, 50(24): 4736-4745.

Appendix B: Supplementary Material for Chapter 3

Table 1: Binding energies for low and high spin states and relative energies of the high spin states (vs low spin states) for calculated negatively charged intermediates.

	Low Spin /eV	High Spin /eV	Relative Values /eV*
CoP	-260.03 (1)***	-259.17 (3)	0.86
CoP-CO_2	-282.74 (1)	-281.71 (3)	1.03
CoP-COOH	-285.38 (2)	-284.76 (4)	0.62
CoP-OCHO	-286.18 (2)	-286.58 (4)	-0.4
CoP-CO	-274.74 (1)	-274.70 (3)	0.04
CoP-CHO	-278.13 (2)	-277.11 (4)	1.02
CoP-COH	-276.06 (2)	-275.48 (4)	0.58
CoP-CH_2O	-282.27 (1)	-281.34 (3)	0.93
CoP-CH	-268.49 (2)	-268.26 (4)	0.23
CoP-CH_2	** (1)	-268.54 (3)	**
CoP-CH_3	-278.73 (2)	-278.02 (4)	0.71
CoP-CH_2OH	-285.20 (2)	-284.35 (4)	0.85
CoP-OCH_2O	-287.98 (1)	-287.52 (3)	0.46
CoP-OCH_2	-281.88 (1)	-281.22 (3)	0.66
CoP-OCH_3	-285.81 (2)	-283.42 (4)	2.39
CoP-O	-264.97 (1)	-264.95 (3)	0.02
CoP-OH	-270.20 (2)	-269.88 (4)	0.32
CoP-OCH_2OH	-292.55 (2)	-292.24 (4)	0.31

* Relative values = $E_{\text{high spin}} - E_{\text{low spin}}$

** The close-shell singlet does not converged probably because the lowest singlet configuration is open-shell.

*** The numbers in the brackets are the spin multiplicity.

Table 2: The equilibrium potentials for the formation of the [CoP-COOH] and [CoP-OCHO] intermediates with and without solvation correction.

	E^0 /V_{RHE} Without solvation	E^0 /V_{RHE} With solvation
$[CoP]^0 + CO_2 + H^+ + e^- \longrightarrow [CoP\text{-}COOH]^0$	-0.72	-0.43
$[CoP]^0 + CO_2 + H^+ + e^- \longrightarrow [CoP\text{-}OCHO]^0$	-1.31	-0.92
$[CoP\text{-}CO_2]^- + H^+ + e^- \longrightarrow [CoP\text{-}COOH]^-$	*	-1.01
$[CoP\text{-}CO_2]^- + H^+ + e^- \longrightarrow [CoP\text{-}OCHO]^-$	*	-0.21

* CO_2 cannot bind to CoP without solvation correction, which makes the $[CoP\text{-}CO_2]^-$ is not stable.

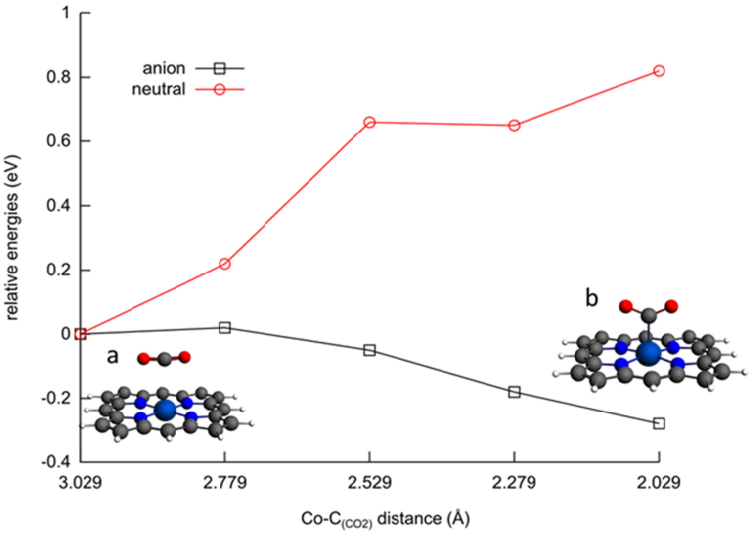

Figure 1. The relative energy of neutral and anionic complexes [Co(P)-(CO_2)] with large Co-$C_{(CO2)}$ distances varies as the CO_2 approaches the metallic center of complex. Inserted Figure (a) is the dissociated CO_2 adduct; inserted Figure (b) is the optimized CO_2 adduct.

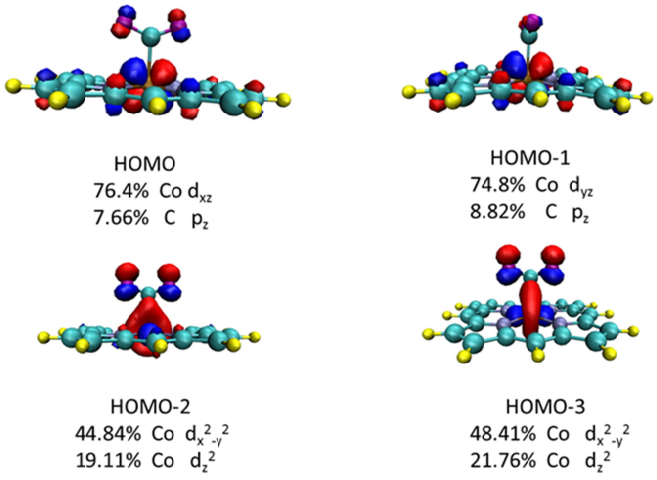

Figure 2. The structures and main contributions of the highest occupied molecular orbitals (HOMO to HOMO-3).

Summary

This thesis discusses the parameters affecting the catalysis for the electrochemical reduction of small molecules, such as carbon dioxide and nitrate, on immobilized metal-porphyrin catalysts. The relatively high overpotentials and the competing hydrogen evolution reaction (HER) are the major bottlenecks in the electrochemical reduction of these two molecules, which reduces their efficiency for the reduction to useful chemicals.

Carbon dioxide is an abundant greenhouse gas in the atmosphere. It would be ideal if we could convert carbon dioxide into valuable chemicals, such as carbon monoxide, methanol, methane and ethylene, by using renewable energy, such as sun light and wind. The electrochemical reduction of carbon dioxide is a promising approach to achieve this goal. Different kinds of catalysts have been studied for the electrochemical reduction of carbon dioxide. Metal electrodes have been divided into different groups based on the products they produce from carbon dioxide reduction. Most metal electrodes form 2-electron transfer products, such as carbon monoxide, formic acid and oxalic acid. Copper is an exceptional electrode, which is able to reduce carbon dioxide to methane and ethylene. Except metal electrodes, metal complexes are also effective catalysts. However, in spite of the extensive investigations, the mechanism of the carbon dioxide reduction is still unclear. The research presented in this thesis is focused on the parameters that influence the carbon dioxide reduction as well as on the insights into the mechanism on metal porphyrin electrode.

Nitrate is commonly used as fertilizer in agriculture and as an explosive. However, the abusive use of nitrate can cause its accumulation into ground water, which is harmful for human health. High concentration of nitrate in drinking water, 10 mg/L, can lead to blue baby syndrome. Previous work from our laboratory has offered detailed studies on the electrochemical reduction of nitric oxide and nitrite on immobilized iron porphyrin. Hydroxylamine was found to be the main product. pH plays an important role in both the

nitric oxide and nitrite reduction. The studies in this thesis are focused on the mechanism of and pH influence on the electrochemical reduction of nitrate on the metal porphyrin catalyst.

The thesis starts in chapter 2 with a study of the electrochemical reduction of carbon dioxide on a cobalt protoporphyrin (PP) modified pyrolytic graphite electrode in aqueous solution. We study the reduction of possible intermediates of the carbon dioxide reduction, such as carbon monoxide, formic acid and formaldehyde, and the influence of pH on the carbon dioxide reduction and the hydrogen evolution reaction. Based on our investigations, we propose a possible mechanism in which a CO_2^- anion initially binds to the complex $[Co(PP)\text{-}(CO_2)]^-$ by an electron transfer. The CO_2 anion acts as an Brønsted base to abstract a proton from water molecule to form a "carboxyhydroxyl" intermediate [Co(PP)-(COOH)]. The [Co(PP)-(CO)] complex is subsequently formed from a [Co(PP)-(COOH)] intermediate, which leads either to the formation of CO or to the further reduction to CH_4 through a series of concerted proton-electron transfer steps.

In chapter 3, we perform a theoretical study using density functional theory (DFT) on the electrochemical reduction of carbon dioxide on a cobalt porphyrin (P) catalyst. Cobalt porphyrin, $[Co^{II}P]$, is reduced to $[Co^{I}P]^-$ to act as the active state for the formation of the $[Co(P)\text{-}(CO_2)]^-$ anion adduct, which is consistent with our experimental observations in Chapter 2. The formation of [Co(P)-(COOH)] intermediate is competing with that of [Co(P)-(OCHO)] intermediate. Our calculations and experiments suggest that the formation of [Co(P)-(COOH)] probably goes through decoupled proton-electron transfer steps, while the formation of [Co(P)-(OCHO)] is through concerted proton-electron transfer steps. This observation can explain the pH dependence of the reduction of carbon dioxide. The formation of methanol as an intermediate is also inferred from our calculations. The electrochemical reduction of methanol on the immobilized cobalt protoporphyrin shows that methanol is indeed reduced to methane.

Various metal protophophyrins are utilized as catalysts for the electrochemical reduction of nitrate in Chapter 4. Among the different metal-centered protophophyrins, cobalt protophophyrin shows the highest selectivity toward hydroxylamine, which makes it

the most interesting catalyst. Besides hydroxylamine, a smaller amounts of ammonia and N_2O are found. The activity for the nitrate reduction is highly affected by pH, because the rate-determining step, the nitrate reduction to nitrite, is highly sensitive to the pH. Interestingly, also the selectivity for hydroxylamine vs. ammonia is very pH sensitive. Two possible mechanisms, a sequential pathway and parallel pathway for the formation of hydroxylamine and ammonia, have been proposed, with the sequential pathway being the most consistent with the observed pH sensitive selectivity.

In summary, this thesis has shown that the metal porphyrin complexes are effective catalysts for both the electrochemical reduction of carbon dioxide and nitrate. The insights into the mechanism for both reactions offer the opportunity for the design of new effective catalysts in the future.

Samenvatting

Dit proefschrift bediscussieert de parameters die de katalyse van de elektrochemische reductie van kleine moleculen zoals kooldioxide en nitraat aan geïmmobiliseerde metaal-porfyrine katalysatoren beïnvloeden. De relatief hoge overpotentialen en concurrerende waterstof evolutie reactie zijn de grootste knelpunten in de elektrochemische reductie van deze twee moleculen, welke het rendement voor de reductie naar bruikbare chemicaliën verlagen.

Kooldioxide is een overvloedig broeikasgas in de atmosfeer. Het zou ideaal zijn als wij kooldioxide zouden kunnen omzetten in waardevolle chemicaliën zoals koolmonoxide, methanol, methaan en ethyleen, door gebruik te maken van hernieuwbare energie zoals zonne- en windenergie. De elektrochemische reductie van kooldioxide is een veelbelovende manier om dit doel te bereiken. Verschillende soorten katalysatoren zijn bestudeerd voor de elektrochemische reductie van kooldioxide. Op basis van de gevormde producten bij de kooldioxide reductie, worden metaalelektroden verdeeld in verschillende groepen. De meeste metaalelektroden vormen 2-elektronoverdracht producten, zoals koolmonoxide, mierenzuur en oxaalzuur. Koper is een unieke elektrode die in staat is kooldioxide te reduceren naar methaan en ethyleen. Naast metaalelektroden zijn ook metaalcomplexen effectieve katalysatoren. Ondanks uitgebreid onderzoek is het mechanisme van de kooldioxide reductie nog steeds niet duidelijk. Het onderzoek in dit proefschrift richt zich op de parameters die de kooldioxide reductie beïnvloeden en inzichten in het mechanisme aan metaal-porfyrine elektroden.

Nitraat wordt veelvuldig gebruikt als kunstmest in de landbouw en als springstof. Onzorgvuldig gebruik van nitraat kan leiden tot ophoping in grondwater, wat een gevaar vormt voor de gezondheid van de mens. Hoge concentraties van nitraat in drinkwater, 10 mg/L, kan het blauwebabysyndroom als gevolg hebben. Eerder onderzoek in onze vakgroep heeft geresulteerd in gedetailleerde studies over de elektrochemische reductie van stikstofoxide en nitriet aan een geïmmobiliseerd ijzer porfyrine. Hydroxylamine bleek het

dominante product te zijn. De pH speelt een belangrijke rol in zowel de stikstofoxide reductie als de nitriet reductie. Het onderzoek in dit proefschrift concentreert zich op het mechanisme van en de invloed van de pH op de elektrochemische reductie van nitraat aan metaal-porfyrine katalysatoren.

Het proefschrift begint in hoofdstuk 2 met een studie van de elektrochemische reductie van kooldioxide aan een met kobalt protoporfyrine (PP) gemodificeerde pyrolytisch grafietelektrode in een waterige oplossing. We bestuderen de reductie van verschillende intermediairen van de kooldioxide reductie, zoals koolmonoxide, mierenzuur en formaldehyde, en de invloed van de pH op de kooldioxide reductie en waterstof evolutie reactie. Op basis van ons onderzoek, suggereren we een mogelijk mechanisme waarin een CO_2^- anion zich in de eerste instantie bindt aan het complex $[Co(PP)\text{-}(CO_2)]^-$ door elektronoverdracht. Het CO_2^- anion gedraagt zich als een Brønsted base door een proton van het water molecuul te onttrekken, waardoor een "carboxyhydroxyl" intermediair [Co(PP)-(COOH)] gevormd wordt. Het [Co(PP)-(CO)] complex wordt vervolgens gevormd uit het [Co(PP)-(COOH)] intermediair, wat leidt tot de vorming van of CO of de verdere reductie tot CH_4 door een serie van gekoppelde proton-elektronoverdacht stappen.

In hoofdstuk 3 voeren we een theoretische studie uit gebruikmakend van dichtheidsfunctionaaltheorie (DFT) aan de elektrochemische reductie van kooldioxide aan een kobalt porfyrine (P) katalysator. Kobalt porfyrine, $[Co^{II}P]$, wordt gereduceerd tot $[Co^{I}P]^-$ en fungeert als de actieve toestand voor de vorming van het $[Co(P)\text{-}(CO_2)]^-$ anion, wat overeenkomt met onze experimentele bevindingen in hoofdstuk 2. De vorming van het [Co(P)-(COOH)] intermediair in competitie met die van het [Co(P)-(OCHO)] intermediair. Onze berekeningen en experimenten suggereren dat de vorming van [Co(P)-(COOH)] waarschijnlijk via ontkoppelde proton-elektronoverdracht stappen verloopt, terwijl de vorming van [Co(P)-(OCHO)] via gekoppelde proton-elektronoverdracht stappen verloopt. Deze waarneming kan de pH afhankelijkheid van de reductie van kooldioxide verklaren. De vorming van methanol als een intermediair is ook afgeleid uit onze berekeningen. De elektrochemische reductie van methanol aan de geïmmobiliseerde protoporfyrine wijst uit dat methanol inderdaad wordt gereduceerd tot methaan.

Verscheidene metaal-protoporfyrines zijn gebruikt als katalysator voor de elektrochemische reductie van nitraat in hoofdstuk 4. Van de verschillende metaal gecentreerde protoporfyrines, vertoont kobalt protoporfyrine de hoogste selectiviteit naar hydroxylamine wat het de meest interessante katalysator maakt. Naast hydroxylamine zijn er kleinere hoeveelheden ammonia en N_2O gevonden. De activiteit van de nitraatreductie wordt sterk beïnvloed door de pH, aangezien de snelheidsbepalende stap, de nitraatreductie naar nitriet, erg pH gevoelig is. Opmerkelijk is dat tevens de selectiviteit van hydroxylamine ten opzichte van ammonia erg pH gevoelig is. Twee mogelijke mechanismen, een sequentieel- en parallel reactiepad voor de vorming van hydroxylamine en ammonia zijn geopperd, waarbij het sequentiële reactiepad het meest overeenkomt met de waargenomen pH gevoelige selectiviteit.

Samenvattend, dit proefschrift laat zien dat metaal-porfyrine complexen effectieve katalysatoren zijn voor de elektrochemische reductie van kooldioxide en nitraat. De inzichten in het mechanisme voor beide reacties kunnen de mogelijkheid bieden voor het ontwerp van nieuwe, effectieve katalysatoren in de toekomst.

List of publications

This thesis is based on the following publications:

Chapter 2

Shen J.; Kortlever R.; Kas R.; Birdja Y. Y.; Diaz-Morales O.; Kwon Y.; Ledezma-Yanez I.; Schouten K. J. P.; Mul G.; Koper M.T. M.

Electrocatalytic reduction of carbon dioxide to carbon monoxide and methane at an immobilized cobalt protoporphyrin

Nature Commun. **2015**, **6**, 8177.

Chapter 3

Shen J.; Kolb M.J.; Göttle A. J.; Koper M.T.M..

DFT Study on the Mechanism of the Electrochemical Reduction of CO2 Catalyzed by Cobalt Porphyrin

J. Phys. Chem.C. Submitted

Chapter 4

Shen J.; Birdja Y.Y.; Koper M.T.M..

Electrocatalytic Nitrate Reduction by a Cobalt Protoporphyrin Immobilized on a Pyrolytic Graphite Electrode

Langmuir, **2015**, 31 (30), pp 8495–8501

Other Publications:

Kortlever R.; Shen J.; Schouten K. J. P.; Calle-Vallejo F.; Koper M. T. M.,

Catalysts and Reaction Pathways for the Electrochemical Reduction of Carbon Dioxide.

J. Phys. Chem. Lett. **2015,** 6, 4073-4082.

Curriculum Vitae

Jing was born in Yueyang, a city in North Hunan Province in China in 1984. After high school, she studied chemistry at Zunyi Normal College, and recieved her bachelor degree in 2007. On July 2008, she started her master degree in University of Science and Technology of China with professor Quanxin Li. The research topic during her master was the synthesis and application of metal oxides. In November 2011, Jing started her PhD at Leiden University (the Netherlands) under the supervision of Prof. Marc T.M. Koper with the project title of "carbon dioxide reduction on electrodes modified with molecular catalysts" sponsored by the Chinese Scholarship Council (CSC), to investigate the activity of molecular catalysts immobilized on (carbon) electrode to convert carbon dioxide to small organic molecules such as carbon monoxide, formic acid, methanol and methane, as well as the mechanistic insights into the carbon dioxide reduction. The results of this work are presented in this thesis. Parts of this work have been presented at several international conferences.